AD-756 926

STATIC CONCRETE CONSTITUTIVE RELATIONS
BASED ON CUBICAL SPECIMENS. VOLUME I.
MODEL DEVELOPMENT AND VERIFICATION

Elton G. Enderbrock, et al

New Mexico State University

Prepared for:

Air Force Weapons Laboratory

December 1972

AD768926

STATIC CONCRETE CONSTITUTIVE RELATIONS BASED ON CUBICAL SPECIMENS

Volume 1

Model Development and Verification

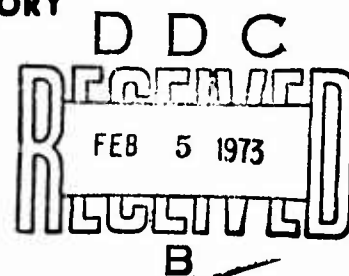Elton G. Endebrock

Leonard A. Traina

New Mexico State University

TECHNICAL REPORT NO. AFWL-TR-72-59, Vol. I

December 1972

AIR FORCE WEAPONS LABORATORY
Air Force Systems Command
Kirtland Air Force Base
New Mexico

DDC

RECEIVED

FEB 5 1973

B

AIR FORCE WEAPONS LABORATORY
Air Force Systems Command
Kirtland Air Force Base
New Mexico 87117

DOCUMENT CONTROL DATA · R & D

(Security classification of title, body of abstract and indexing annotation must be entered when the overall report is classified)

1 ORIGINATING ACTIVITY (Corporate author)	2a. REPORT SECURITY CLASSIFICATION
New Mexico State University Las Cruces, New Mexico 88001	UNCLASSIFIED
	2b. GROUP

3 REPORT TITLE

STATIC CONCRETE CONSTITUTIVE RELATIONS BASED ON CUBICAL SPECIMENS
Volume I
Model Development and Verification

4 DESCRIPTIVE NOTES (Type of report and inclusive dates)

September 1970 through August 1972

5 AUTHOR(S) (First name, middle initial, last name)

Elton G. Endebrock and Leonard A. Traina

6 REPORT DATE	7a. TOTAL NO. OF PAGES	7b. NO. OF REFS
December 1972	~~218~~ 219	32

8a. CONTRACT OR GRANT NO.	9a. ORIGINATOR'S REPORT NUMBER(S)
F29601-71-C-0007	
b. PROJECT NO.	AFWL-TR-72-59, Vol. I
5710	
c. Subtask SC157	9b. OTHER REPORT NO(S) (Any other numbers that may be assigned this report)
d.	

10 DISTRIBUTION STATEMENT

Approved for public release; distribution unlimited.

11 SUPPLEMENTARY NOTES Details of illustrations in this document may be better studied on microfiche.	12. SPONSORING MILITARY ACTIVITY
	AFWL (DEV) Kirtland AFB, NM 87117

13 ABSTRACT

(Distribution Limitation Statement A)

Uniaxial, biaxial, and triaxial tests were performed on three-inch cubes using various combinations of compressive and tensile loads. One nominal concrete strength of 4000 psi was used in the testing. The testing machine and its associated hardware such as load cells, platens, and extensometers were designed as a part of this study. The test information was obtained as stress-strain records for the three principal directions of the cubical test specimens. The tests were run until the largest compressive stress reached 30,000 psi or there was a tensile failure. Whenever possible the test results were compared to those of other investigators. A model to simulate concrete behavior was developed. It consisted of bars connected at nodal points which were located at the points of an octahedron. The bars were assigned stiffnesses such that the load-deformation characteristics of the model were similar to those of the experimental stress-strain curves of concrete. The model solution was programmed for use with a computer utilizing Fortran IV language.

DD FORM 1473 1 NOV 65

I-a

KEY WORDS	LINK A		LINK B		LINK C	
	ROLE	WT	ROLE	WT	ROLE	WT
Concrete						
Concrete testing						
Constitutive relations						
Stress Strain relations						

I-6

STATIC CONCRETE CONSTITUTIVE RELATIONS

BASED ON CUBICAL SPECIMENS

Volume I

Model Development and

Verification

Elton G. Endebrock

Leonard A. Traina

New Mexico State University

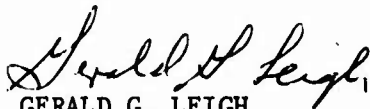TECHNICAL REPORT NO. AFWL-TR-72-59, Vol. I

I-C

FOREWORD

This report was prepared by the New Mexico State University, Las Cruces, New Mexico, under Contract F29601-71-C-0007. The research was performed under Program Element 61102H, Project 5710, Subtask SC157, and was funded by the Defense Nuclear Agency (DNA).

Inclusive dates of research were September 1970 through August 1972. The report was submitted 7 November 1972 by the Air Force Weapons Laboratory Project Officer, Captain Philip G. Stowell (DEV-S).

This technical report has been reviewed and is approved.

PHILIP G. STOWELL
Captain, USAF
Project Officer

GERALD G. LEIGH
Lt Colonel, USAF
Chief, Facilities Survivability
  Branch

WILLIAM B. LIDDICOET
Colonel, USAF
Chief, Civil Engineering Research
  Division

TABLE OF CONTENTS

Preceding page blank

TABLE OF CONTENTS (cont'd)

LIST OF FIGURES

LIST OF TABLES

NOTATION

a,b,c	Bar lengths
A	Compatibility matrix
A^T	Transpose of compatibility matrix
c	A constant incorporated into the stiffness function
E_o	Initial tangent modulus
f	Bar force matrix
F	Force matrix
F_1, F_2, F_3	Forces in the directions of axes of the model
k	Bar stiffness matrix
$k_1, k_2, k_3, k_4, k_5, k_6$	Bar stiffnesses
K_{ij}	Elements of the model stiffness matrix
$\overline{K}$	Model stiffness matrix
n, n_1	Integers used in stiffness functions
u,v,w	Model dimensions
x	Bar displacement matrix

$x_1, x_2, x_3,$

x_4, x_5, x_6 Bar displacements

X Model displacement matrix

X_0, X_1, X_{11} Constants incorporated into stiffness functions

X_1, X_2, X_3 Model displacements

$\varepsilon_1, \varepsilon_2, \varepsilon_3$ Principal strains

$\sigma_1, \sigma_2, \sigma_3$ Principal stresses

σ_1 Largest absolute principal stress

σ_2 Intermediate absolute principal stress

σ_3 Smallest absolute principal stress

σ_o Mean normal stress

σ_r Uniaxial unconfined compressive strength

μ Poisson's Ratio

τ_o Octahedral shear stress

INTRODUCTION AND HISTORICAL REVIEW

1.1 INTRODUCTION

There has been an increased emphasis directed toward refinements in the design of concrete members. For refinements to be possible, a knowledge of the behavior of concrete under combined stresses is a necessity. Past research on concrete behavior under combined stresses has generally been limited to the study of the relationships between the applied stresses at failure. Information on the relationships between the applied stresses and the resulting strains was limited. None of the investigators of concrete behavior reported any attempts to mathematically relate stresses to strains for the combined stress conditions.

This contract was awarded to New Mexico State University to perform an experimental investigation on the behavior of plain concrete under various biaxial and triaxial loadings. Some of the terms of the contract were as follows:

(a) Develop the necessary techniques and perform the necessary tasks to record the strains in the three principal directions of loading.

(b) Construct or obtain a loading device which is capable of producing a maximum compressive stress of 30,000 psi and a tensile stress to failure.

(c) The loading device will be capable of three-dimensional loading.

(d) Concrete with a nominal unconfined compressive strength of 4000 psi will be used in all specimens.

1

(e) The applied loads will range from a tensile load causing failure
to a maximum compressive load producing a stress of 30,000 psi
in the test specimen.

(f) Develop relations which will enable prediction of the state of
stress for a concrete element from a state of strain.

(g) Determine a failure theory that is consistent with observed
failure modes.

(h) Develop a computer program which incorporates the failure theory
and yields a set of stresses for a given set of strains.

1.2 HISTORICAL REVIEW

Many investigators have reported experimental and theoretical
studies on the failure characteristics of concrete subjected to combined
compressive and tensile stresses. Most of the investigators concentrated
on compressive loadings only. All of the publications listed in the List
of References, with the exception of (19), (20), and (24)*, contain in-
formation on concrete behavior studies. Generally an attempt was made to
associate the failure stresses to an existing failure theory or to a
modification of an existing failure theory. Association of the failure
stresses to an existing failure theory was never completely successful.

Failure theories that have been considered are listed below and are
discussed on the basis of their agreement with observed results from
tests on concrete cubes.

(a) Mohr's Failure Theory - The failure mode for this theory is

---

* Number in parenthesis refers to List of References.

2

slippage along a plane inclined with respect to the principal stresses. The observed failure mode was splitting of the cubes such that the fractured surfaces were essentially perpendicular to the direction with the lowest applied stress. In addition, the shear on a slip plane is assumed to be a function of the maximum and minimum stresses only and does not consider the effect of the intermediate stress. Test results indicate that the intermediate stress does effect the failure envelope.

(b) Octahedral Shear Theory - This failure theory assumes that failure occurs whenever the shear stress on planes whose normals possess equal directional cosines with respect to the principal stress axes reaches a specific value. It is impossible to relate the octahedral shear stress to a failure mode and it has not adequately described the experimental results.

(c) Distortion Energy Theory - This theory assumes that failure will occur whenever the energy of distortion exceeds a constant value. The energy of distortion is the difference between the total energy in an element and the energy due to a hydrostatic loading (equal stresses in all three directions). Computation of the energy of distortion is not convenient and it does not agree with experimental results.

(d) Maximum Tensile Strain Theory - Failure occurs whenever the largest tensile strain exceeds a constant value. The failure mode of this theory conforms to that observed from tests; however, there is not agreement between the failure stresses predicted by this theory and experimental results.

(e) Griffith's Theory - This theory predicts a failure mode similar to the experimental results. It considers the existence of microscopic

3

cracks and the propagation of these cracks due to high tensile stresses generated at their tips. It requires an analytical description of the stresses around the cracks; hence, its use is limited and an experimental verification is difficult.

(f) Maximum Compressive Distortion Stress Theory - This theory assumes that failure occurs whenever the compressive stress which produces distortion of an element exceeds a constant value. The distortion stresses are the difference between the stresses acting on an element and the average of all of the stresses acting on the element. This theory does not agree with experimental results.

(g) Maximum Tensile Distortion Stress Theory - This theory assumes that failure occurs whenever the tensile stress of distortion reaches a limiting value. The distortion tensile stress is obtained in the same manner as mentioned for the compressive distortion theory. The theoretical failure mode agrees with the experimental failure mode; however, the failure stresses predicted by this theory do not agree with the experimental results.

(h) Modification of the Maximum Tensile Distortion Stress Theory - Zimmerman (29) proposed an empirical modification of the maximum tensile distortion stress theory. Combining the empirical modification and the tensile distortion stress theory resulted in adequate agreement between the failure stresses whenever compared to experimental results. This agreement was limited to a rather limited range of principal stresses.

A review of the existing failure theories as related to concrete behavior leads to the conclusion that they cannot be used directly to describe the failure characteristics of concrete.

4

A review of publications on concrete behavior under combined stresses revealed that only a few of the investigators reported the results of strain measurements. In no case was there reported any attempt to obtain relationships between stresses and strains.

1.3 SCOPE OF PRESENT STUDY

The present study was designed to determine experimental stresses and corresponding strains for combined stress conditions. The combined stress conditions included both compressive and tensile stresses as well as all combinations of compressive and tensile stresses acting together. This also includes uniaxial, biaxial, and triaxial states of stress. Presently, dynamic codes calculate a stress matrix from a given strain matrix. Therefore, this effort will consist of the formulation of constitutive relationships such that a set of stresses can be determined from a given set of strains. In experimental considerations the strains would be measured and the stresses computed from the measured strains.

1.4 STATE-OF-THE-ART IN CONCRETE TESTING AND MODELING

A review of the published results indicate that several different approaches have been taken in the testing of concrete subjected to multiaxial loadings. Multiaxial tests were conducted using hollow and solid cylinders, cubes and square slab-type specimens.

Hollow cylinders have been used in specimens for biaxial compression, biaxial tension-compression and biaxial tension tests. For biaxial compression tests using the hollow cylinders, a triaxial state of stress is suspected and the reported strengths are considered to be too high.

5

Solid cylinders have been used as specimens for biaxial and triaxial compression tests. This type of specimen has a disadvantage since it is not possible to independently control the applied stress in three directions.

Cubes have been used primarily for biaxial and triaxial compression test specimens. When this type specimen was used, with no provision made for the reduction of friction between the specimen and the loading platen, the reported results are considered to be too high.

Several investigations have been conducted using square slab-type specimens. Biaxial compression, biaxial tension-compression and biaxial tension type tests have been conducted using this type of specimen. This type of specimen seems to develop a reasonably unconfined biaxial stress state. This type of specimen, however, does not seem to be suitable for a triaxial test specimen.

There are very few published results in connection with the modeling of concrete behavior for concrete subjected to multiaxial loading.

Anson (23) used a model to simulate the behavior of concrete. His model consisted of nodal points connected by bars of different stiffnesses. The nodal points are located at the points of an octahedron. Bars of a constant stiffness ratio were used. The model was used to simulate stress-strain curves of concrete in uniaxial tension and compression and the failure envelope of concrete subjected to biaxial loading and triaxial loading. The author concluded that his model should only be used for qualitative examination of concrete behavior.

The results of an experimental and analytical investigation, of simplified models of concrete to study the strength and deformational

6

behavior of plain concrete subjected to short term compressive loads was reported by Buyukoztush, Nilson and Slate (32). The study was limited to uniaxial and biaxial states of stress. Thin square plates of mortar with round stone inclusions of uniform size were loaded in-plane. The experimental results were compared to a finite element analysis. The model used had a disadvantage in that the solution involved 428 triangular finite elements to model the behavior of a 5 x 5 inch specimen.

The model did not predict the nonlinear load-deformation curves very accurately. The authors acknowledged that the two-dimensional representation of the material adopted for their study was not entirely satisfactory even for the two-dimensional stress state considered.

SECTION II

MATERIALS AND MIXING PROCEDURES

2.1 CONCRETE MATERIALS

The water used in mixing the concrete was taken from the water system
supplying New Mexico State University. Type I cement was used and was pur-
chased locally. No control was exercised over the quality of the water or
the cement.

The fine aggregate (sand) and the coarse aggregate (gravel) were
both purchased locally and from the same supplier. The sand was taken
from the supplier's stock and delivered to the laboratory and placed in a
weather-protected storage bin.

The gravel required for this project (maximum size of aggregate was
limited to 1/2 inch) was not stocked by any local supplier; therefore, it
had to be specially produced. Approximately five cubic yards of the gravel
were processed and delivered to the laboratory. The gravel was stored out-
side the laboratory and was exposed to the weather.

The results of sieve analyses on the sand and gravel are shown in
Figure 1. The variation in the sieve analyses is indicated along with
the average of all the sieve analyses.

All results from sieve analyses of the sand fell within the ASTM
grading limits. There was variation from test to test; however, this is
mostly due to the difficulty in obtaining representative samples to be
used in the sieve analyses. The sand was removed from the bottom of the

8
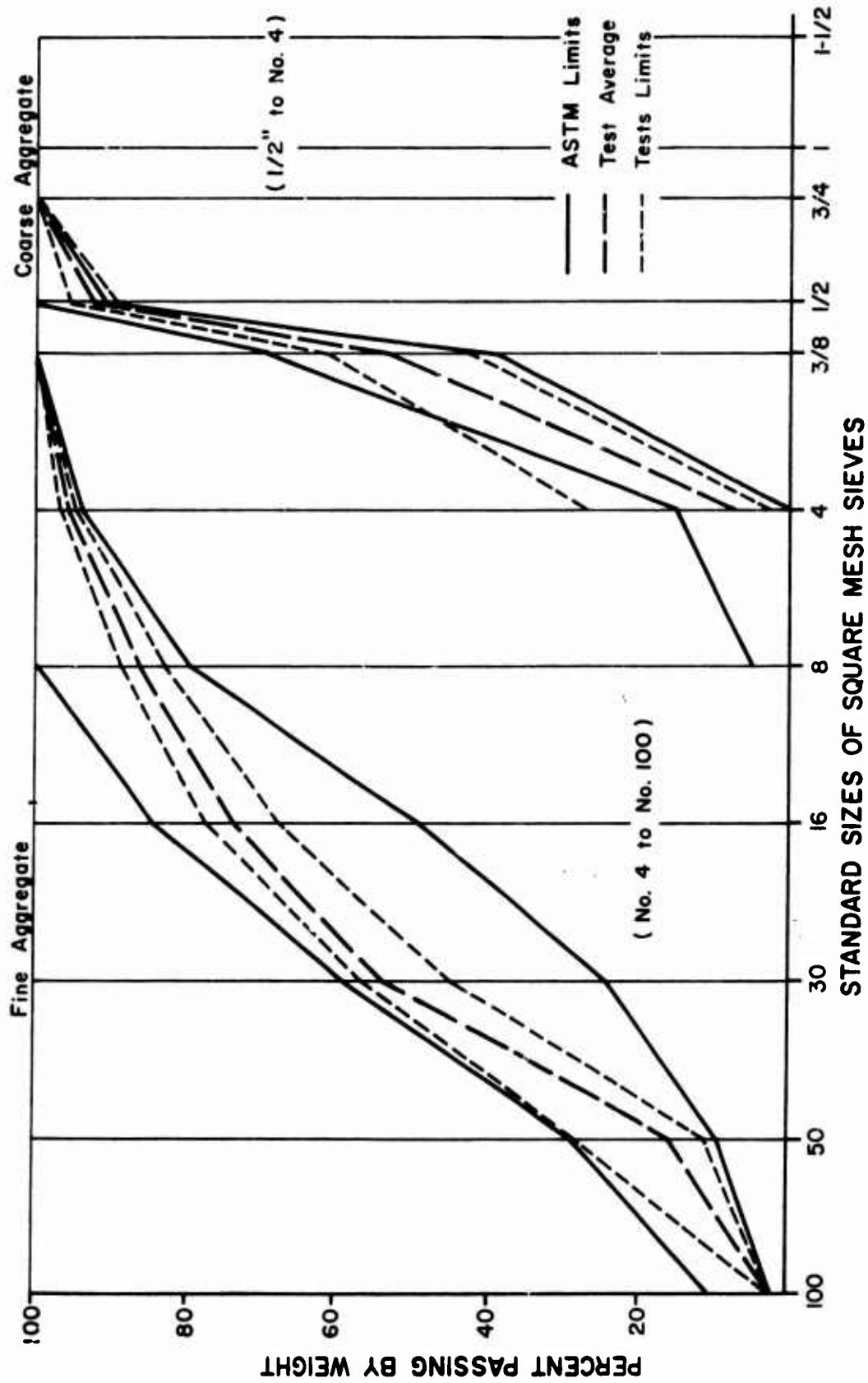
Figure 1. Results of Sieve Analysis

storage bin. Some segregation of the sand sizes no doubt occurred at the time the sand was dumped into the storage bin. The larger particle sizes roll to the outside of the sand column and the fines tend to concentrate in the center of the sand column. The sand sample was obtained by taking two or three shovelsful of the sand and reducing the amount with the aid of a sand splitter. The sample weights ranged from 935 to 1710 grams.

The Fineness Modulus of the sand was also computed for each sieve analysis. The average Fineness Modulus was 2.69 and the range was 2.55 to 2.92. The entire range was within the recommended Fineness Modulus limits of 2.3 to 3.1. The Fineness Moduli for the various samples are listed below.

Sample	Fineness Modulus
1	2.65
2	2.55
3	2.77
4	2.66
5	2.74
6	2.59
7	2.74
8	2.63
9	2.68
10	2.92
11	2.64

In two of 13 tests, the sieve analysis results for the gravel exceeded the ASTM grading limits for the No. 4 size. The average of all the test results did fall within the ASTM grading limits. It was intended that no

10

batch falling outside the ASTM grading limits be used. Obtaining representative samples of the gravel for sieve analysis was far more difficult than in the case of the sand.

Samples of gravel to be used in the sieve analyses were obtained by taking two or three shovelsful from a batch and reducing the sample size by using the sand splitter. The gravel would pass through the sand splitter. Gravel sample weights ranged from 840 to 1805 grams.

The gravel contained more than the specified maximum percentage of flat and elongated particles. Twenty percent maximum was originally specified, however, the gravel contained approximately twenty-five percent flat and elongated particles. The gravel consisted of crushed stone. It appears that the flat and elongated particles resulted from the crushing operation.

2.2 CONCRETE MIX DESIGN CRITERIA

The concrete used in forming the cube test specimens was designed on the basis of a 28-day strength of 4000 psi and a slump of 3-4 inches. The rather large slump was required to form the relatively small cube test specimens. Good workability was also important. One side of the cube specimens had to be manually smoothed with a trowel.

2.3 TRIAL CONCRETE MIXES

The first trial concrete mix was proportioned on the basis of the absolute volume method recommended by the Portland Cement Association (PCA). The material quantities for the first trial mix was estimated using charts and graphs published by the PCA. The design mix was based upon a cubic yard of plastic concrete; hence, the quantities were scaled

11

down for use in the laboratory. The estimated quantities were then mixed and the properties of the fresh (slump and workability) and hardened concrete (strength) observed. The first trial mix did not yield the desired properties of slump, workability, nor strength. Adjustments were made in the water-cement ratio and in the relative proportions of the sand and gravel. The water-cement ratio adjusted the strength and the ratio of sand to gravel affected the slump and workability.

After five or six trial mixes and adjustments, a concrete mix was obtained that produced the desired slump, workability, and strength. The relative proportions by weight of the final concrete mix before free moisture or absorption adjustments were:

<div align="center">

Water-cement ratio   0.56

Cement-sand-gravel   1 - 2.36 - 2.45

</div>

This concrete mix had a rather large ratio of sand to gravel. The gravel was angular shaped and therefore required a greater amount of sand to obtain the desired workability.

2.4 MIXING PROCEDURE

The water, cement, sand, and gravel were mixed in a power-driven revolving drum mixer that had a capacity of approximately two cubic feet. Prior to mixing, a mortar composed of equal parts of cement and sand was placed in the mixer. The mixer was then run for a few minutes until the mortar had covered the entire wall of the mixer. The excess was then discarded. The mortar adhering to the mixer was intended to compensate for loss of mortar from the batch.

The ingredients were weighed to the nearest one-tenth of a pound. The gravel, sand and cement were placed in the mixer in the order mentioned. The water was slowly added while the mixer was running. The mixing continued for approximately five minutes after all the water had been added.

A slump test was made immediately after mixing. The slump tests were conducted according to ASTM standards. The results of all tests are shown in Table 1. The desired slump was 3-4 inches. This range was not always obtained as noted from Table 1. The slump was quite sensitive to slight changes in relative percentages of different particle sizes and to humidity and temperature in the laboratory.

After the slump test had been completed, the concrete was placed in the cylinder and cube molds. The cylinders were the standard 6 x 12 inch test cylinders and were used for quality control. The cube molds were made of aluminum plate 1/2 inch thick. A mold is shown in Figure 2. There were six cube molds per unit. The nominal inside mold dimensions were 3 inches on each side. The concrete cylinders were cast according to ASTM standards.

Consolidation of the concrete in the cube molds was accomplished by vibrating the molds while the concrete was being placed in the molds. The concrete was placed in the molds in approximately three equal layers. Vibration was continued only long enough to obtain a relatively smooth surface of the concrete. Different methods of consolidating the concrete in the cube molds had been attempted. Tamping with different size rods

13

TABLE 1

SLUMPS FOR CONCRETE MIXES

Date	Slump (in)
1-28-71	5.75
2-1-71	4.00
2-2-71	2.75
2-3-71	3.24
2-4-71	3.24
2-8-71	2.50
2-9-71	3.25
2-11-71	3.00
2-16-71	3.25
2-24-71	3.00
2-25-71	3.50
3-2-71	3.75
3-8-71	3.75
3-10-71	4.00
3-11-71	4.00
3-15-71	5.00
3-17-71	5.00
3-22-71	5.50
3-29-71	3.75
3-31-71	3.50
4-7-71	3.50-3.00
4-12-71	4.00-2.75
4-14-71	3.75-6.00
4-19-71	3.50-4.50
4-21-71	3.75-4.00
4-26-71	2.75-3.25
4-28-71	3.50-3.50
4-29-71	3.75-3.75
5-3-71	4.00-5.75
5-5-71	4.50-5.00
5-6-71	4.50-4.50
5-10-71	3.50-3.75
5-12-71	4.50-4.50
5-19-71	4.00-3.75

Figure 2. Cube Molds

15

was attempted. Also tapping the mold and tamping simultaneously was attempted. The effectiveness of the different methods of consolidation was determined by sawing the cubes into halves and visually noting the number and size of voids in the hardened concrete. The method described above yielded the smallest number and smallest sized voids.

The cylinder molds were coated with oil and the cube molds were coated with wheel bearing grease prior to pouring of the concrete. This was to prevent the concrete from sticking to the walls of the molds. A thin layer of the grease was used.

The specimens were allowed to set in the molds for about 24 hours. After 24 hours, the specimens were removed from the molds and placed in a curing room for 28 days. The curing room conditions were 100 percent humidity and approximately 75 degrees F.

The cylinders were tested for compressive strength at 7 days and at 28 days. The results of these tests are shown in Table 2. A noticeable increase in cylinder strength occurred in the cylinders cast on March 8 and thereafter. This increase in strength was thought to have been due to the use of a new cement. The new cement was of the same type as the cement used previously.

A typical strength curve in which the strength is plotted versus curing time is shown in Figure 3. This curve was obtained by casting 14 cylinders using the same mix and testing 3 cylinders at 7, 14, and 28 days. Two cylinders were tested at 35 days of curing. All cylinders including the ones tested at 35 days were moist cured until the day of testing.

TABLE 2

CYLINDER STRENGTHS

Date Mixed	7-day strength		28-day strength	
	lbs.	Psi	lbs.	Psi
2-2-71	90,500	3200	118,000	4173
2-3-71	83,500	2953	122,000	4314
2-4-71	94,000	3324	122,500	4332
2-8-71	98,500	3483	128,000	4527
2-9-71	91,500	3236	125,000	4420
2-11-71	78,000	2758	113,000 (35 day)	3996 (35 day)
2-16-71	90,000	3183	122,500	4332
2-24-71	80,000	2829	118,000	4173
2-25-71	80,000	2829	116,000	4102
3-2-71	73,500	2599	114,500	4049
3-8-71	92,500	3271	136,500	4827
3-10-71	95,000	3359	136,000	4810
3-11-71	87,500	3094	136,000	4810
3-15-71	91,000	3218	132,500	4686
3-17-71	96,000	3395	140,500	4969
3-22-71	90,000	3183	134,000	4739
3-29-71	95,500	3377	130,000	4597
3-31-71	89,000	3147	131,000	4633
4-7-71	100,500	3554	137,000	4845
4-12-71	94,000	3324	140,000	4951
4-14-71	101,000	3572	143,000	5057
4-19-71	96,000	3392	129,500	4580
4-21-71	89,000	3147	129,500	4580
4-26-71	77,000	2723	118,500	4191
4-28-71	75,500	2670	117,000	4138
4-29-71	88,500	3130	144,500	5110
5-3-71	90,500	3200	141,500	5004
5-5-71	89,000	3147	114,500	4058
5-6-71	93,500	3306	143,000	5057
5-10-71	90,500	3200	139,000	4916
5-12-71	92,500	3271	128,500	4544
5-19-71	88,500	3130	120,000	4244
5-24-71	104,000	3678	142,000	5013
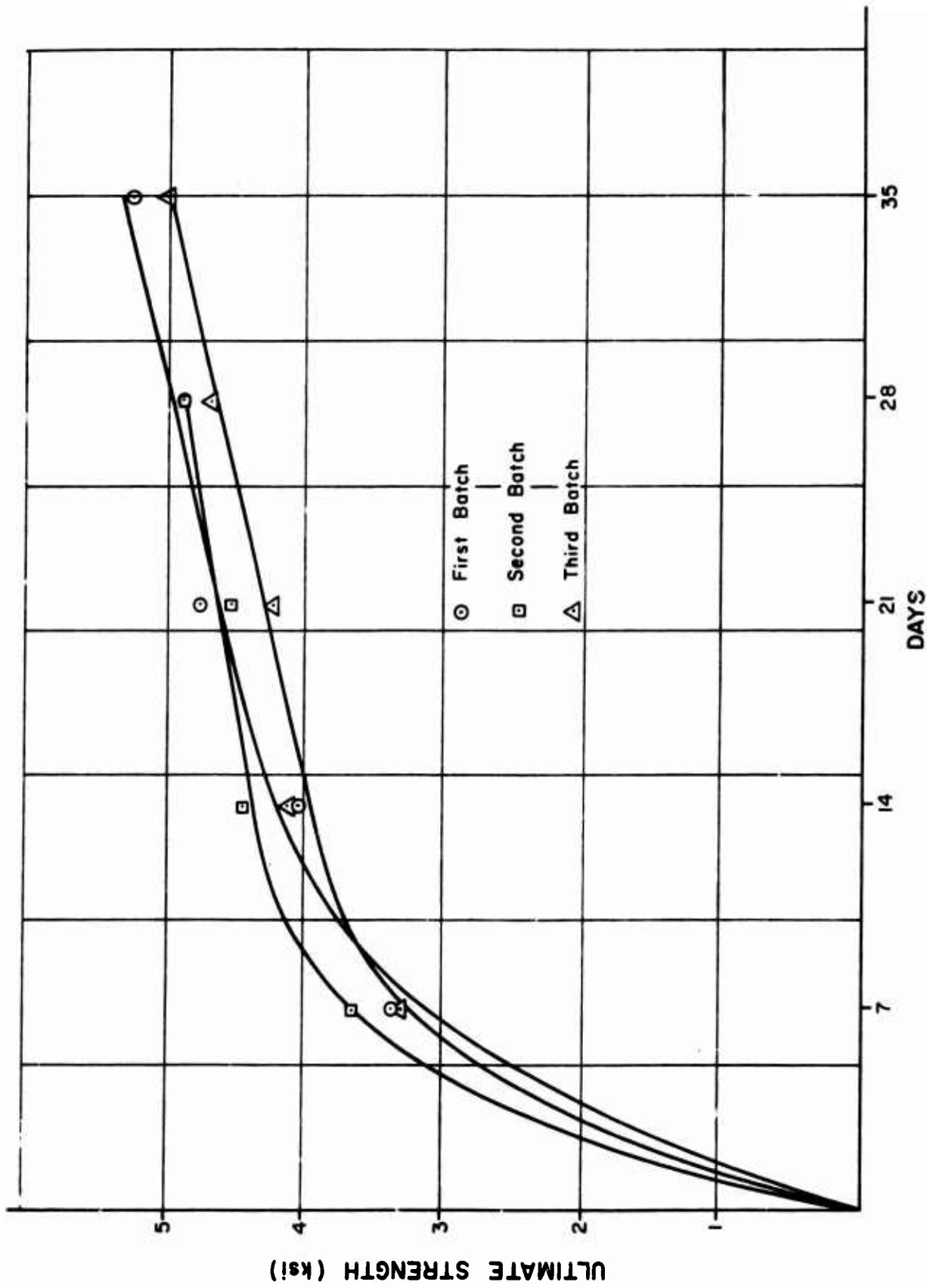
Figure 3. Strength Curve for Concrete

18

SECTION III

DESCRIPTION OF EQUIPMENT

3.1 TESTING MACHINE

The triaxial testing machine was designed and constructed as a part
of the research program. The testing machine design was based upon the
following criteria:

a. Loads could be applied in three orthogonal directions.

b. The loading in each direction would be independently controlled.

c. The loading capacity of the testing machine would be such that
a maximum stress of 30,000 psi could be applied triaxially to
a three-inch cube.

d. The measurement of the applied load and the accompanying deforma-
tions would be possible.

e. The frame would deform symmetrically under an applied load.

f. The loads could be applied in compression or tension.

3.2 TESTING FRAME

The frame of the testing machine was dimensioned such that there
was sufficient space for the hardware such as the jacks, compression
platens, load cells, and extensometers to be installed.

The testing frame was designed to be flexible and to deform sym-
metrically such that the test specimen would remain in a fixed position
as the loads were applied. Upon checking the performance of the machine,
it was noted that a slight shift of the test specimen occurred as the
loads were applied. The shift was in a direction away from the active

19

jacks. A shift in the test cube would not affect the uniaxial tests. It would introduce friction forces between the test cube and the loading platens in biaxial and triaxial tests. Friction reducing methods were utilized in the testing program; hence, the magnitude of the induced friction forces was probably small.

The main members of the testing frame consisted of wide-flanged steel sections. The sections were selected according to AISC specifications for A36 steel. A load factor of two was also applied in the structural design.

All connections on the testing frames were welded. The spans were short and the possible loads high; hence, a large number of shear stiffener plates were required. Web stiffners were also used beneath the jacks and the bearing plates to prevent buckling of the webs.

The testing machine was composed of two frames, one being suspended horizontally within the other as shown in Figure 4. The horizontal frame was suspended from the vertical frame by two cable hoists. Two jacks were attached to the horizontal frame and one to the vertical frame. The horizontal frame was adjustable in both the horizontal and vertical directions.

The loads were applied by means of manually operated hydraulic jacks with capacities of 150 tons. The jacks were equipped with spherical heads which were self aligning. The jacks were also double-acting. This was necessary in order that tensile loads could be applied.

The compression platens were machined from high strength steel (75 ksi). The bearing surface dimensions were 2.75 inches by 2.75 inches.

20
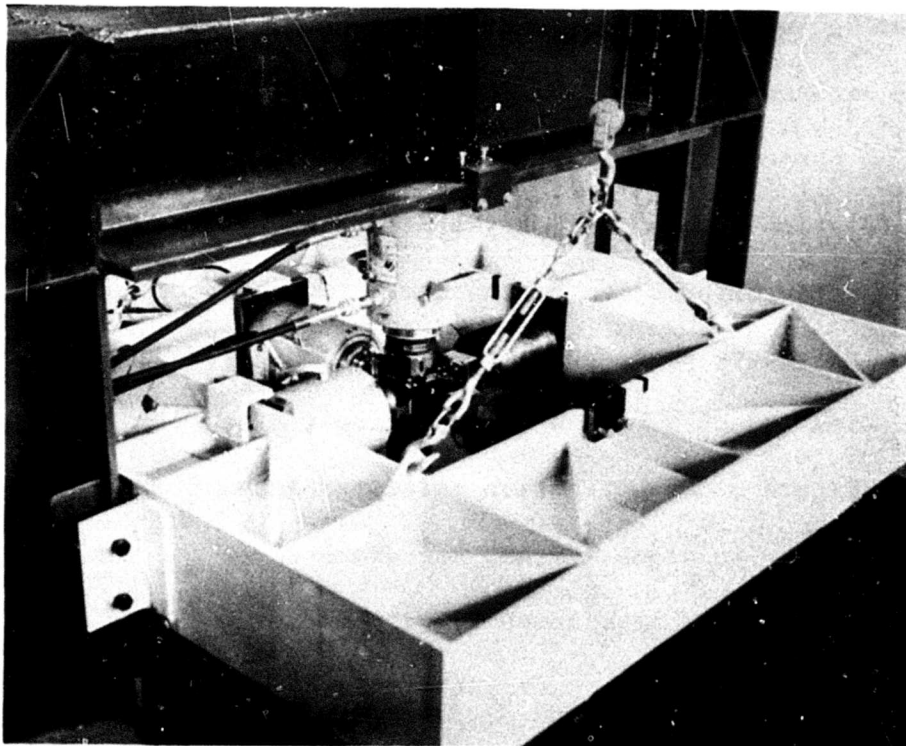
Figure 4. Testing Frame

21

The area of the platens were necessarily smaller than the test specimens to prevent the platens from contacting against each other during a test. The compression platens had a slot milled in them to accomodate the extensometer arms. In addition, a hole was drilled into the center of the bearing surface to accomodate a flange pin as shown in Figures 5 and 6. The extensometer arm was placed in the slot and on the one end of the pin. The purpose of the pin was to remove deformations arising from the use of friction pads such that the deformation detected by the extensometers was the deformation at the center of the test cube only. Whenever friction pads were used, polythelene washers of the same thickness as the friction reducing pads were placed behind the flange of the pins as shown in Figure 6. The friction reducing pads had a hole, which was slightly larger in diameter than the diameter of the pin flange, punched in their centers. This allowed the pin flange to directly contact the surface of the test cube; hence, the only deformation detected was that of the center of the cubes.

A pair of tension heads are shown in Figure 7. The tension heads are connected to the test specimen with an epoxy glue and to the load cells by means of ball joints. All of the tension heads had a 1/4 inch hole drilled at their centers to accomodate steel pins. The extensometer arms were then connected to these pins. The contact area of the tension heads was three inches square.

3.3 LOAD CELLS

The load cells used in the testing program were constructed and

22

Figure 5. Compression Platen

23
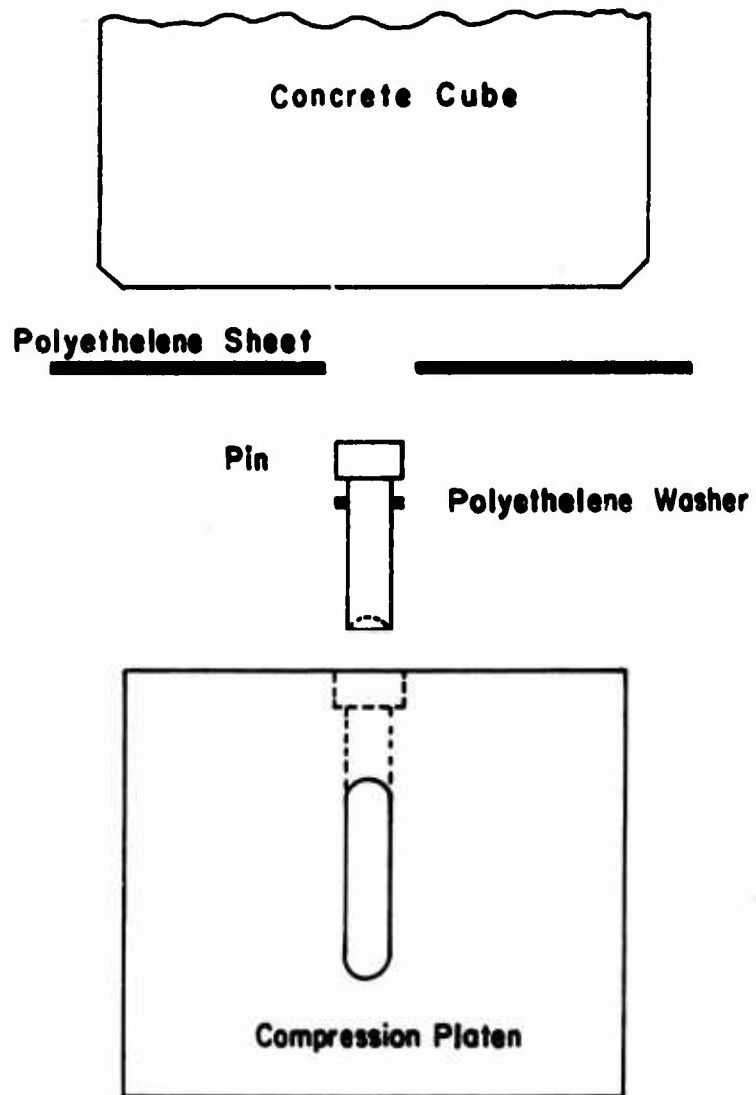
Figure 6. Arrangement of Platen, Pin, Polyethelene Sheets, and Cube

Figure 7. Tension Heads

calibrated at NMSU. The cells consisted of columns five inches in length, made of steel or aluminum. Four electrical resistance strain gages were mounted at mid-height of the columns. The strain gages were arranged and wired in a manner such that only axial strains were detected.

Three different types of load cells were used for the entire testing program. Two types were used in compression testing and a third type was used in tension testing. The three types of load cells are shown in Figure 8. One type of compression load cells had circular cross-sections and was made of aluminum. Their capacity was 120,000 pounds. The second type of compression load cells had three-inch square cross-sections and were made of high-strength steel. Their capacity was 300,000 pounds. The aluminum load cells were used in the biaxial tests and the steel cells in the triaxial tests. Two types of compression load cells were used to obtain better accuracy at the lower load levels.

The tension load cells had circular cross-sections and were made of steel. Their capacity was controlled by the one-half inch attaching bolts whose capacity was approximately 5,000 pounds.

The load cells were calibrated with the aid of a universal testing machine located in the Materials Testing Laboratory at NMSU. The maximum capacity available was 200,000 pounds. This exceeded the capacity of the aluminum compression load cells and the tension load cells, but was less than the capacity of the steel compression load cells. The 300,000 pound cells were, therefore, calibrated by loading up to 200,000 pounds.
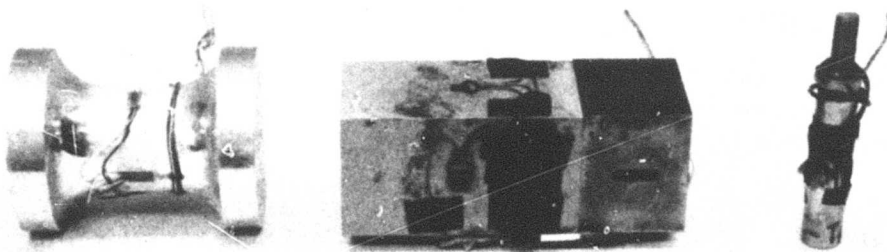
Figure 8.   Load Cells

It was assumed that the load-strain relationship was valid up to 300,000 pounds.

The same calibration procedure was followed for each type of load cell. The cells were loaded incrementally with load and strain readings taken after each increment. About ten readings were taken between no load and maximum load. The cells were then unloaded incrementally and readings taken again after each unloading increment. This procedure was repeated until readings were taken for five loading and unloading cycles. All of the load and strain readings were then taken and a straight line relationship was fitted using the method of least squares. The calibration constants for the load cells are given below:

LOAD CELLS	CELL NUMBERS Units (lbs/micro in. per inch)		
	No. 1	No. 2	No. 3
Aluminum	15.790	15.295	15.920
Steel (Compression)	89.430	88.060	89.510
Steel (Tension)	6.270	6.803	7.076

3.4 EXTENSOMETERS

The extensometers consist of an aluminum bar attached to two steel clamps shaped as shown in Figure 9. The elbows of the steel clamps are necessary to hold the extensometer away from the loading platens on the other loading axes. An extensometer in position for testing is shown in Figure 10. Four electrical resistance strain gages were
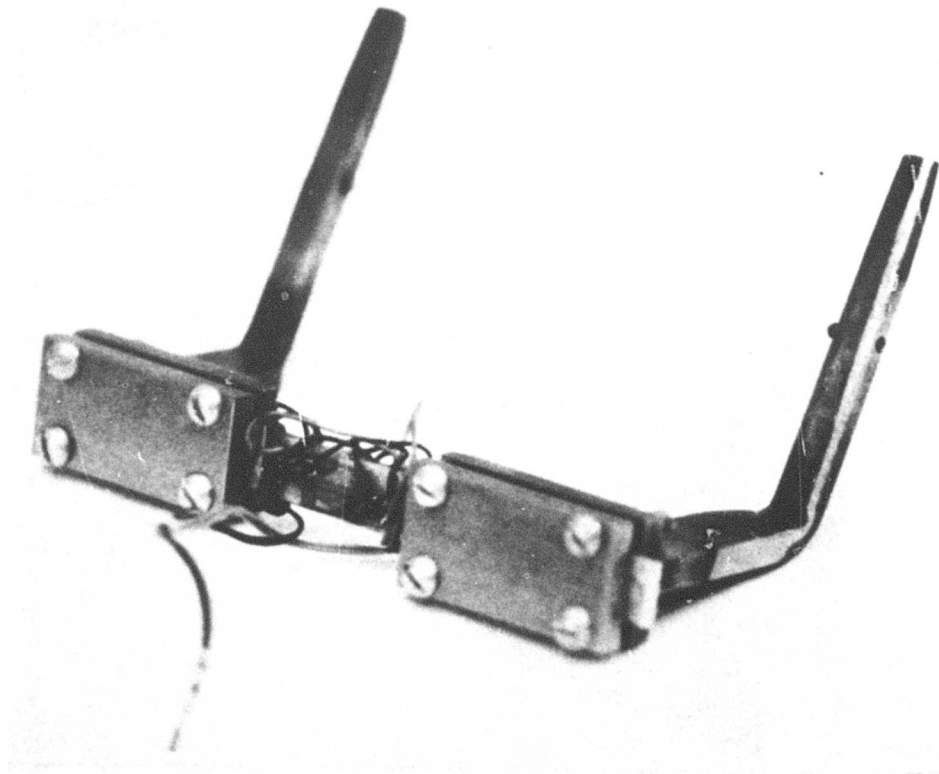
Figure 9. Extensometer
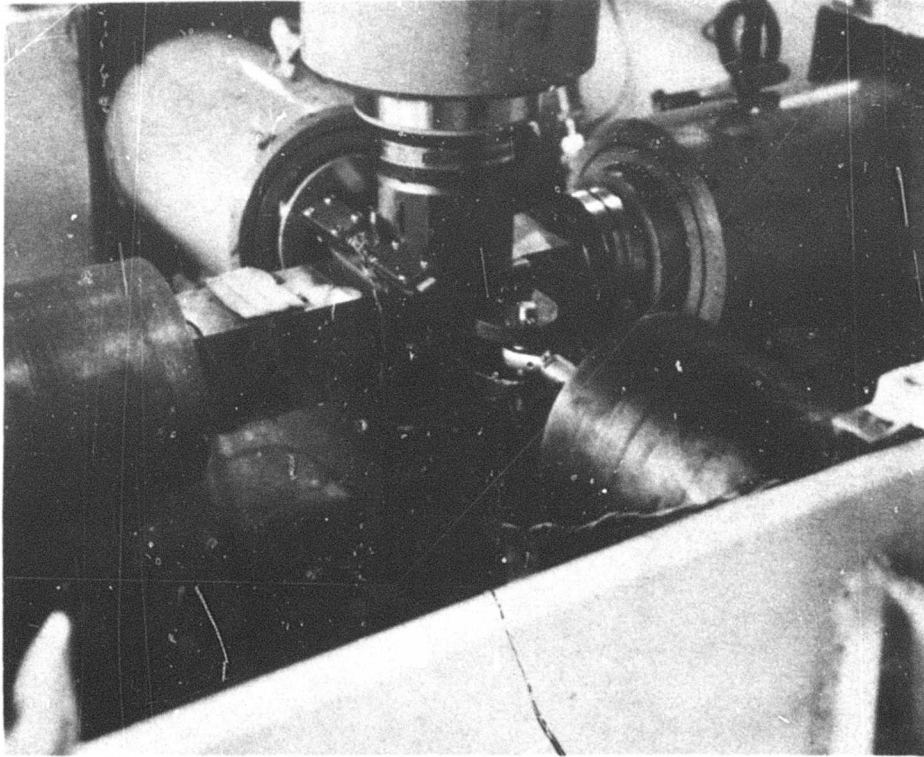
Figure 10.   View of Extensometers in Place

attached to the aluminum bar. They were arranged and wired in a manner such that only flexural strains were detected.

The extensometers were calibrated in the testing frame and in the same position as used in testing. This was found to be necessary when it was discovered that a different calibration constant resulted if a given extensometer was used in different positions and on different axes.

Calibration of the extensometers was achieved with the aid of a hexagonal shaped aluminum bar. The bar was three inches in length and had two electrical resistance strain gages mounted at its mid-height. The strain gages were wired to detect axial strains only. The aluminum bar was placed into the testing machine between two compression platens of a particular axis. The strain gages were wired into an X-Y recorder. The extensometer strain gages were wired into the other axis of the X-Y recorder. A load was then applied to the aluminum bar. The result indicated on the X-Y recorder graph is the strain indicated by the aluminum bar versus the strain output of the extensometer. The aluminum bar was three inches in length, the same as the nominal length of the concrete test specimens; hence, it was assumed that the strains indicated by the aluminum bar would be comparable to the strains in the test specimens. The calibration constant was obtained by taking the average slope of the plot obtained on the X-Y recorder. A typical record of this type is shown in Figure 11. The load was applied and released a number of times to get an indication of the extensometers ability to duplicate strains. This is indicated by the width of the band. The extensometers were removed and replaced during calibration to determine if this changed the constant. Removing and replacing the extensometers

31
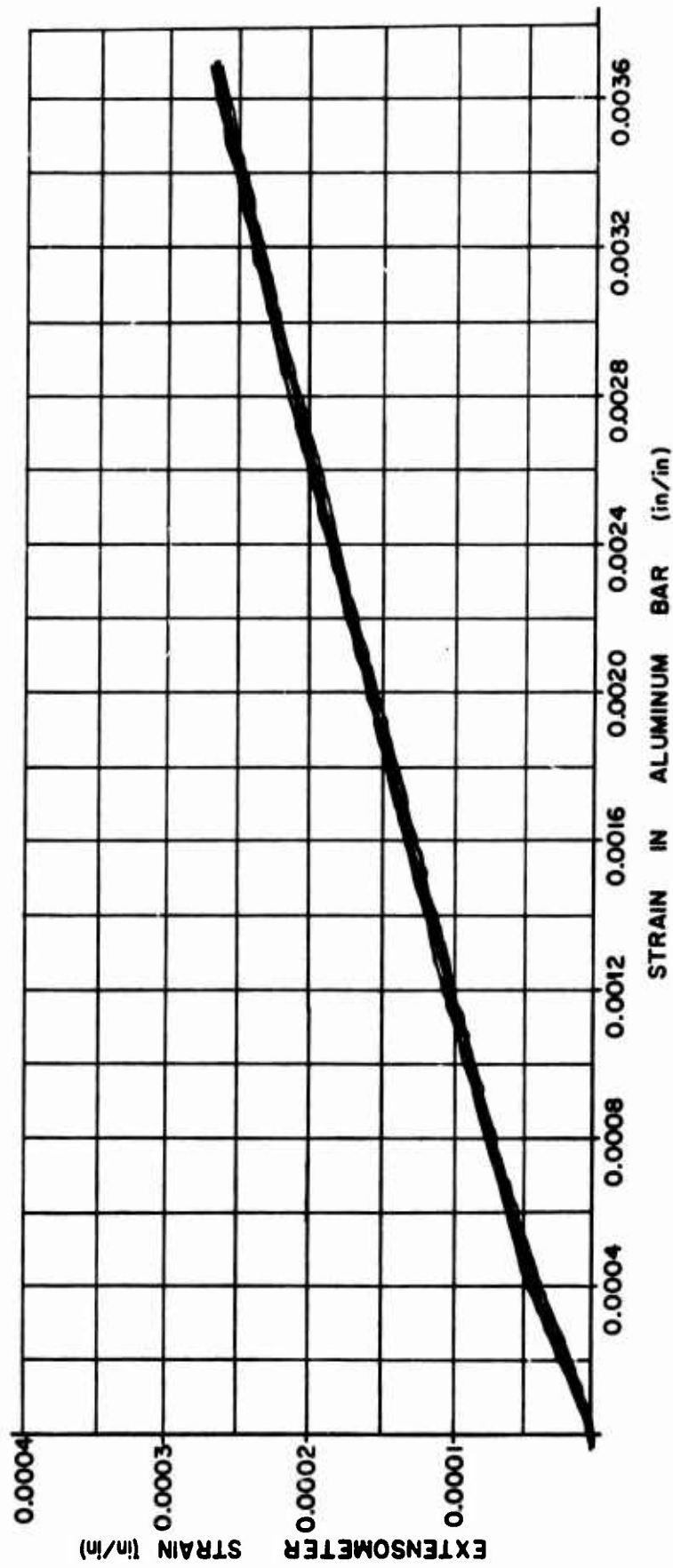
FIGURE 11 Extensometer Calibration Record

did not appear to change the calibration constant as did a change of
axis and position.

The extensometers were recalibrated whenever any hardware such as
load cells or platens were changed. A change in hardware did usually
result in a slight change in the calibration constant.

3.5 RECORDING EQUIPMENT

The load and deformation were monitored for each of the three axes.
The deformation was measured at the center of the concrete cube. This
information was recorded with the use of X-Y recorders. To accomplish
this, amplifiers were used to obtain the desired accuracy and flexibility
in changing scales for the different tests. The loads and deformations
were scaled such that the recorded information was the stress-strain
curve for the given axis. The loads were detected using load cells and
the deformations were detected using special extensometers.

The X-Y recorders used were manufactured by Instron, Mosley, and
EAI. The amplifiers were manufactured by Instron, Hallmark, and Newport.
The arrangement of the instrumentation is shown in Figure 12.

Both the vertical and horizontal axes of the recorders were cali-
brated using a precision fixed resistor of known value. The resistor
most often used produced a strain of 518 μ in/in when placed across one
arm of a four-arm bridge.

3.6 COMMENTS REGARDING THE TESTING MACHINE

An attempt was made to evaluate the performance of the testing
machine. Six electrical resistance strain gages were mounted (three

33
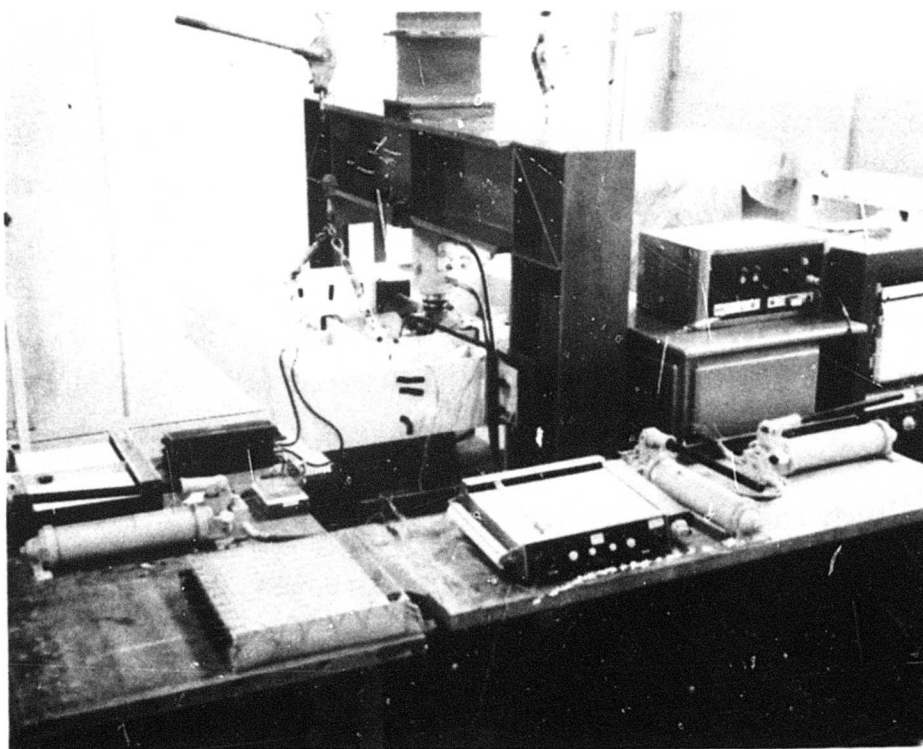
Figure 12. Test Equipment

34

parallel to each other on two opposite sides) on a three-inch aluminum cube. The aluminum cube was then placed in the testing machine and loaded uniaxially. The load was applied parallel and perpendicular to the directions of the strain gages. A calibrated load cell was used to determine the magnitude of the applied load and a calibrated extensometer was used to determine the deformation of the center of the cube. One purpose of the test was to determine if the extensometer could be used to determine strain in the cube.

Strain readings were taken to determine the distribution of strains throughout the cube. A uniform strain distribution proved difficult to obtain. A slight eccentricity would cause rather large differences in strain from side to side. Finally, a transit was used to align the jack, compression platens, cube and load cell. Even when aligned with the transit, rather large variations in strain were obtained. The strain readings were also compared to the readings obtained with the extensometer. It was noted that the average of the strain readings taken from the gages mounted on the aluminum cube compared quite favorably with the values obtained with the extensometer. It was, therefore, concluded that the extensometers could be used in determining strains in concrete cubes. This was also verified after uniaxial test results on concrete became available. The stress-strain curves obtained from the tests were comparable to those published in various journals.

TESTING PROCEDURES

4.1 INTRODUCTION

The procedures utilized during the testing, the problems encountered during testing, and the problem solutions or compromises are reviewed in this section.

4.2 TEST SPECIMENS

4.2.1 Compression Tests

The three inch cubical concrete test specimens were cast in aluminum molds as described in Section II. Five of the six sides of the cubes were formed by the sides of the molds. The sixth side was trowelled after the concrete had been consolidated in the molds; hence, it was not nearly so smooth nor as plane as the other sides of the cubes. The trowelled sides were later trimmed with a diamond saw blade and then sanded on a disc sander to make it smoother. This surface will be referred to as the shaped surface.

Various surface treatment methods were considered. They are listed below. The maximum difference in cube dimensions from point to point for the different methods considered are also indicated below.

	Dimensional Variation (inches)	
Surface Treatment	Formed Surfaces	Shaped Surface
No treatment	0.008	0.020
Lightly sanded	0.011	0.013
Well sanded	0.015	0.018

The above values do not give an indication of flatness or planeness of the surfaces. The flatness was more critical than the difference in dimensions since adjustable heads were used on the jacks.

Unconfined compression tests (uniaxial) were conducted to determine any effects due to the different surface treatments. The results are indicated below. The listed strength values were obtained by averaging results from three tests.

Surface Treatment	Avg. Uniaxial Strength
(a) Formed surfaces lightly sanded, shaped surface trimmed and sanded, loaded on shaped surface.	4270 psi
(b) Formed surfaces lightly sanded, shaped surface trimmed and sanded, loaded on sanded surface.	3850 psi
(c) All surfaces trimmed and sanded, loaded on shaped surface.	3780 psi
(d) All surfaces trimmed and sanded, loaded on sanded surfaces	3840 psi

From the above results it was concluded that the surfaces could be lightly sanded and loaded on the sanded surfaces. This treatment was the simplest. Treatments (b), (c), and (d) were not considered to be significantly different. At that point in time it had not been recognized that the difference in strengths obtained from loading on the sanded and

shaped surfaces was not necessarily due to surface treatment, but due to the anisotropic cubes resulting from the casting operations.

The uniaxial and biaxial tests were conducted on cubes that were lightly sanded on the formed sides and trimmed on the trowelled sides. Loads for these tests were applied to the sanded surfaces and not to the trowelled surfaces.

Later for some of the triaxial tests, the trowelled sides were trimmed with the diamond blade and then placed into a surface grinding machine. The finished surface was then quite smooth and plane. The maximum dimensional variation was usually less than 0.003 inch whenever the surface grinder was used.

Uniaxial tests on cubes whose trowelled side was finished in the surface grinder indicated that the difference in strengths from test to test was smaller than for the cases where the trowelled surface was not planed.

4.2.2 Tension Tests

No special surface treatment was required in the case of cubes subjected to tensile loads. Tension heads were attached to the cubes by means of an epoxy resin layer which was approximately 1/8 inch in thickness. The tensile strength of the epoxy resin was much larger than the tensile strength of the concrete. The modulus of elasticity of most unfilled epoxies (no fillers) ranges from 50,000 psi to 500,000 psi as compared to a modulus of elasticity of 3-6 million psi for concrete. The low modulus of elasticity of the epoxy coupled with the 1/8 inch lay would provide little restraint at the tension heads.

4.3 UNIAXIAL COMPRESSIVE TESTS

Uniaxial test results were frequently used to normalize results obtained from biaxial and triaxial tests; hence, a reliable uniaxial strength value was desired. Only 18 cube molds were available; hence, a rather large number of batches of concrete was required to obtain a sufficient number of test cubes. There was batch to batch variation in ultimate strengths. This made it necessary to perform uniaxial tests for each batch.

The uniaxial tests were conducted in the triaxial testing machine. The compression platens on the testing machine were smaller in area than the area of the cubes. In addition the cubes were beveled along their edges. This also reduced the cross-sectional area. The length to width ratio for cubes is unity; hence, friction effects between the compression platens and cubes would greatly affect the uniaxial test results.

4.3.1 Friction

Several uniaxial tests were performed using friction reducing pads and several tests without friction reducers. The friction reducing pads consisted of two polyethelene sheets four mils thick with grease between the sheets as suggested by Mills (25). Other friction reducing methods were tried; however, the method mentioned above yielded the lowest uniaxial strengths. The results of these tests are shown below.

No Friction Reducer	Friction Reducer
5760 psi	3530 psi
4990 psi	3830 psi
5080 psi	3660 psi
Avg. 5280 psi	Avg. 3670 psi

The results shown on the previous page clearly indicate that friction effects are considerable in uniaxial tests of cubes. As a result the friction reducing pads consisting of the two polyethelene (a thermoplastic synthetic resin) sheets and grease were used in all tests.

4.3.2 Beveling

The concrete test cubes were beveled along their edges. This was performed to reduce the contact area of the cubes to approximately the same area as the compression platens. Beveling also reduced the cross-sectional area of the cubes. Uniaxial tests were conducted to determine the effects due to beveling. Beveled and unbeveled cubes were tested in a universal testing machine. Friction reducing pads were used in these tests. The results of these tests were compared to the results obtained by stacking four cubes and testing uniaxially in a universal testing machine. This comparison was considered of interest since in the stacked cube tests, friction effects are essentially eliminated as a result of the larger height to width ratio and not by the use of friction reducing pads. The results of the tests are shown below. In all cases the stresses were computed on the basis of a three-inch square cross section.

Cubes	Batch No. 1	Batch No. 2
Stacking Four Cubes	4720 psi	4390 psi
Cubes Not Beveled	4600 psi	4570 psi
Cubes Beveled	4040 psi	4010 psi

40

The percentage difference between the beveled and unbeveled cubes for the two batches was -12.2 and -12.4, respectively. The difference between results of the stacked cubes and the unbeveled cubes was not considered to be significant. The differences were no more than the test to test variation.

4.3.3 Testing

Whenever conducting uniaxial tests in the triaxial testing machine, care was taken to ensure that no lateral confinement would occur until at least the maximum stress had been obtained. The slightest lateral pressure would greatly affect the test results. The compressive platens were placed adjacent to the unconfined sides of the test cube. This was necessary whenever lateral strains were measured. The load cells were activated in the directions of the unconfined sides. Any pressure that developed could therefore be detected. A spacer was used to prevent contact initially with the platens located near the unconfined sides to prevent lateral pressure from developing during a test.

4.4 UNIAXIAL TENSION TESTS

There were no significant problems involved with the uniaxial tension tests. The tension heads which were glued to the cubes with an epoxy resin were connected to the load cell and jack head by means of ball joints. The ball joints allowed the cube to align itself as the tensile load was applied. Special hardware was required to protect the extensometers whenever separation of the cubes occurred. Strains were small in the uniaxial tension tests; hence, the accuracy of the recorded

41

strains may be questionable. The extensometers were designed to detect large strains.

During the uniaxial tension test, it was discovered that different strength values could be obtained depending upon the direction the tensile load was applied. Higher strength values were obtained whenever the load was applied to the formed sides of the cubes. The results of four uniaxial tension tests are shown below.

Load Applied to Shaped Surface	Load Applied to Formed Surfaces
237 psi	364 psi
287 psi	322 psi
Avg. 262 psi	Avg. 343 psi

The cubes were all from the same batch. The percentage differences between the average values is 31. This indicates that the concrete cubes were not isotropic. The properties are essentially the same in the directions of the cubes formed by the sides of the molds, but are somewhat different in the direction of casting.

4.5 BIAXIAL TESTS

4.5.1 Compressive Tests

Biaxial tests were conducted to determine the effect of using friction pads. As in the case of the uniaxial tests, the test results without the use of the friction reducing pads indicated higher strengths. In addition, the tests without friction pads indicated a more ductile material than did the tests where friction reducing pads were used;

therefore, all biaxial tests were conducted using friction reducing pads.

Biaxial test results were also greatly affected by the presence of a slight lateral pressure on the unconfined axis; therefore, a small space was left between the cube and the compression platens. The load cell in that direction was activated; hence, the presence of any lateral pressure was easily detected.

The biaxial tests were conducted using the jacks on the horizontal frame of the triaxial testing machine. The test cubes were always placed into the testing machine in the same manner, that is, the orientation was the same as in the casting operation. The shaped surface faced upward. No load was applied to the shaped surface in the biaxial test series until late in the testing program. In one test the major load was applied to the shaped surface. The strength values were larger than had been previously obtained. A test series was then initiated to determine if the orientation of loading affected the test results. The test results are shown below. The values shown are averages of two tests. Equal loads were applied in the two directions.

(a) Load Applied to Formed Surfaces   4040 psi

(b) Loads Applied to Two Formed Surfaces
    and the Shaped Surface   5300 psi

There is a rather large difference between the strengths resulting from applying the loads to the formed surfaces or to the shaped surface. Fortunately all of the cubes were loaded the same way in the biaxial tests.

The first few biaxial tests were performed by applying the minor load and then applying the major load until failure occurred. This loading procedure was abandoned after only a few tests. It was very difficult to control the minor load at a constant value during the time the major load was being applied.

Proportional loading (load in each direction applied simultaneously and in a fixed proportion) was used for the majority of the biaxial tests. The loads were easier to control whenever proportional loading was used. In addition, the results from a proportional loading test were easier to interpret.

Incremental loading was used on a few biaxial tests for the purpose of studying the interaction between the two loaded axes.

The time required to fail a cube subjected to proportion biaxial loads was less than two minutes.

Once a maximum stress had been reached, it was impossible to maintain the same proportions between the applied load; hence, the loading proportions listed on any of the stress-strain records was valid only up to the maximum stress on the major axis.

Some difficulty was encountered in conducting tests in which the ratio of the major axis load to the minor axis load was greater than 10. The application of the major load would produce a load in the minor axis that was greater than the intended value. This required a release of pressure in the jack applying the minor load. Releasing the pressure and maintaining a constant load level was difficult.

4.5.2 Tension-Tension and Compressive-Tension Tests

The greatest difficulty encountered in the biaxial tension and com-pressive-tension tests was the elimination of bending stresses induced durin; testing. This problem was never resolved. An initially per-fectly aligned test specimen would deform as the loads were applied such that bending stresses were induced into the test specimen. In the case of compressive-tension tests, the larger the compressive force in rela-tion to the tensile force, the greater the induced bending stresses. It is believed that the indicated maximum stresses in this loading region are less than the actual concrete strength. The error intro-duced by the addition of bending is difficult to estimate. The magni-tude of the bending is dependent upon the stiffness of the testing frame, bearing blocks, load cell-, and loading platens, as well as the stiffness of the concrete test cube. Comparison of test results in the compression-tension region with other investigators (Section VI) indicates that the induced bending error may not be 'arge.

Bending stresses were no doubt also induced in the biaxial tension test specimens; however, their magnitude would be considerably less than in the compressive-tension tests. Bending stresses could be elim-inated by using a testing machine designed such that the loading axes could be adjusted during a test.

4.6 TRIAXIAL TESTS

4.6.1 Compression Tests

All of the triaxial tests were conducted using friction reducing pads.

Many of the problems encountered during the uniaxial testing and the biaxial testing were not applicable to triaxial testing. All sides were confined, therefore, no problem arose in preventing confinement.

The effect of loading on the different cube surfaces was not discovered until after the triaxial test series had been completed. The test records indicate that the minor load was not always applied to the shaped surface; hence, it was concluded that some of the scatter in the test results was due to cube orientation in the testing machine. The minor load should have always been applied to the shaped surface.

The compressive capacity of the testing machine was reached before the test cube failed whenever the ratio of the minor load (lowest absolute load) to the major load (largest absolute load) was 0.3 or larger. At the higher stress levels, it became difficult to operate the pumps supplying pressure to the jacks.

As in the biaxial tests, once the maximum stress had been obtained on the major axis (axis on which the largest absolute load was applied), the original loading proportions could not be maintained. It was impossible to decrease the load on the minor axis once the peak stress had been reached on the major axis. The test cube expanded rapidly in the direction of the minor axis.

4.6.2 <u>Triaxial Tension Tests and Combined Compression-Tension Tests</u>

The elimination of bending stresses induced during the test was the greatest problem associated with triaxial testing where at least one of the loads was applied in tension. This problem was not resolved in the case of triaxial testing either.

The triaxial tension test specimens were difficult to obtain. The tension heads had to be glued to the faces of the cubes. Four of the tension heads could be glued in place in one operation; however, the remaining two had to be put in place at a later time. Proper alignment of the last two tension heads was difficult. Alignment was important to reduce bending stresses.

RESULTS OF TESTS

5.1 INTRODUCTION

Most of the tests conducted in this testing program were biaxial and triaxial compression tests. Some tension-compression and tension-tension type biaxial tests were also conducted. In the triaxial series of tests, some tension-compression-compression, tension-tension-compression and tension-tension-tension type testing was conducted.

The strain data is presented primarily in Section VIII in connection with the model predicted results and in Appendix II. Some strain data is also presented in Section VI where comparisons are ma e with other published strain data.

5.2 BIAXIAL STRENGTH OF CONCRETE

All data on the strength of concrete subjected to a biaxial state of stress are presented in normalized form. The results show the ratio of the maximum stress observed to the uniaxial unconfined compression strength, σ_r, for various principal stress ratios, σ_1/σ_2. A value of σ_r was obtained for each batch of 18 cubes by taking the average uniaxial unconfined compression strength of 3 cubes which were randomly selected from the batch. Thus, in each batch of test cubes, 15 cubes were available for the various multiaxial tests.

The relationship between principal stresses, σ_1/σ_r and σ_2/σ_r, at failure is shown in Figure 13. In this figure, the average biaxial
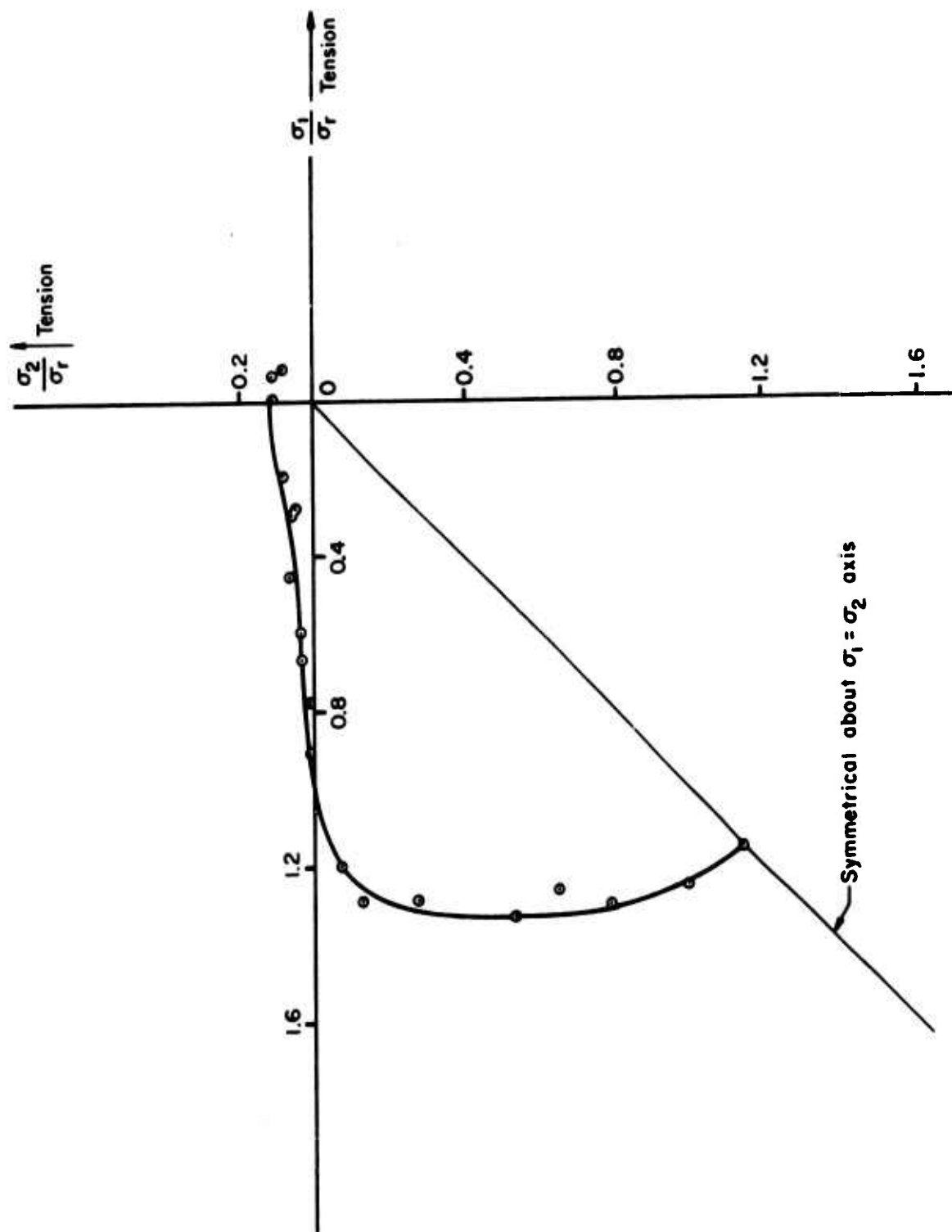
Figure 13. Biaxial Strength of Concrete

49

strength curve is shown based on the biaxial tests which were conducted. Based on the tests in the biaxial compression region, a strength of 1.15 σ_r was observed for the case of equal compression in both principal directions. The highest relative strength was observed at a stress ratio of $\sigma_1/\sigma_2 = 2.5$ where $\sigma_1/\sigma_r = 1.33$. The curve is relatively flat in this region with a sharp rise from the value of σ_r for a very small amount of stress in the σ_2 direction.

The data points which are the basis for the biaxial compression curve shown in Figure 13 are plotted in Figure 14 and tabulated in Table 8. In Figure 14 it can be seen that most of the data are close to the average curve. The experimental scatter which is observed occurred as a result of the batch to batch variation of the concrete and to some extent on the dimensional variation from cube to cube.

The biaxial tension-compression strength curve is also shown in Figure 13. The data points and curve to a larger scale are plotted in Figure 15. The biaxial tension-tension strength curve is also shown in Figures 13 and 15. The ratio of the uniaxial tension to the unconfined compression strength, σ_r, was approximately 0.11 for the batch of cubes used in this series of tests. In the biaxial tension region the strength curve was found to be relatively flat for a range in principal stress ratio $\sigma_1/\sigma_2 = 0$ to $1/2$. For equal tension in both principal directions, a strength of 0.083 σ_r was observed.

5.3 TRIAXIAL STRENGTH OF CONCRETE

The triaxial compression testing made up the largest part of the

50
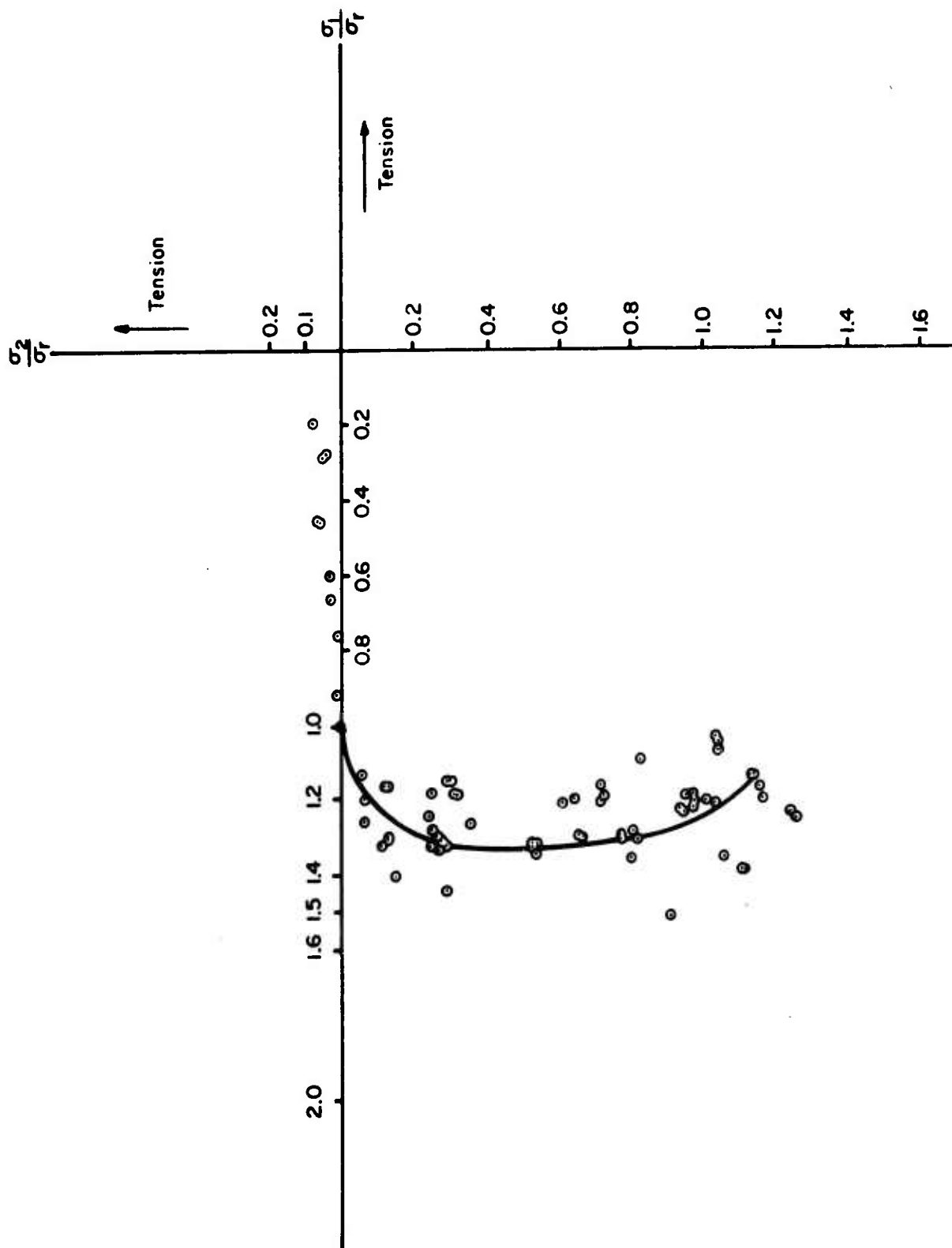
Figure 14. Biaxial Strength Data
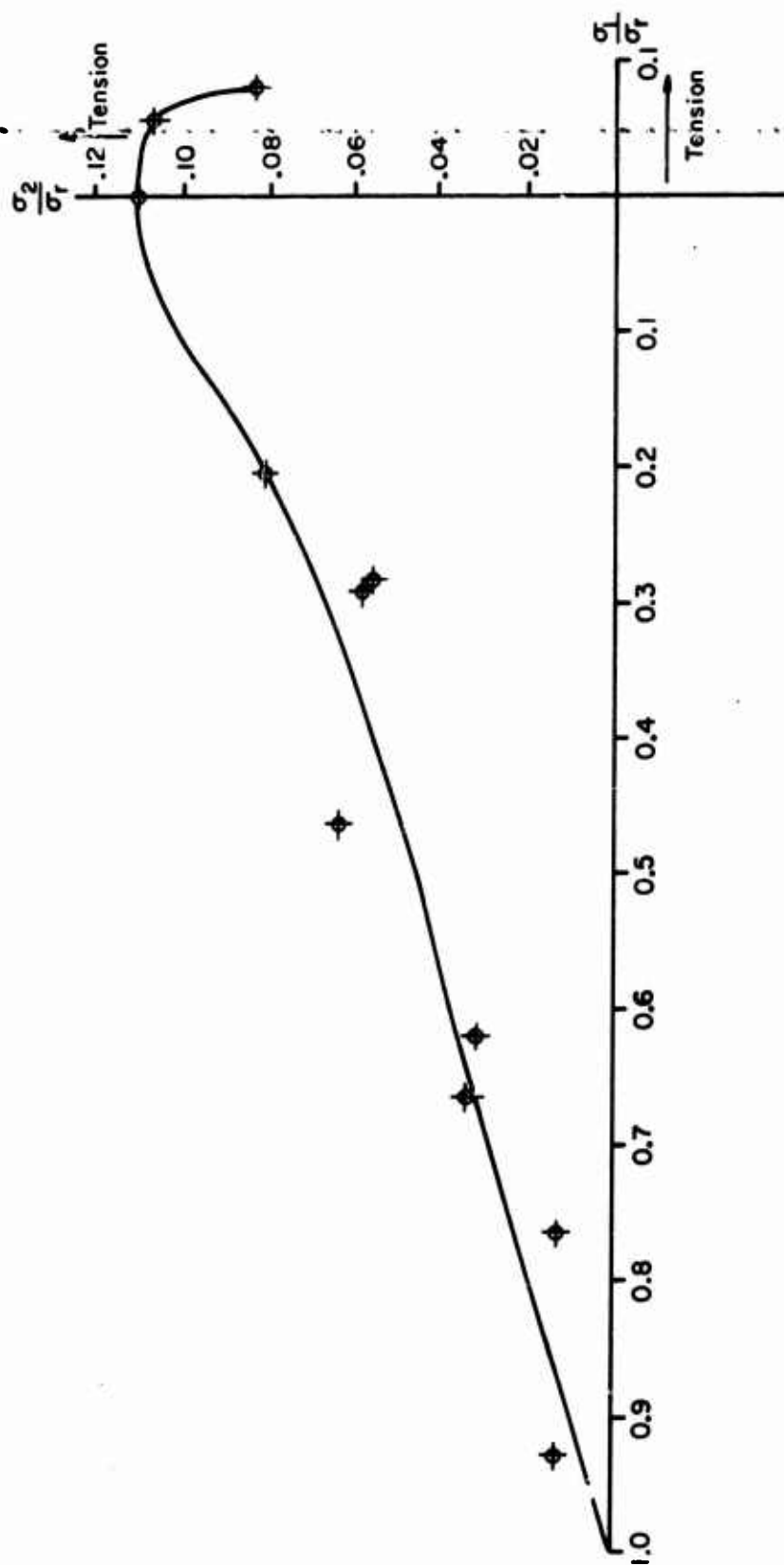
Figure 15. Biaxial Tension and Tension-Compression Strength Data

52

triaxial test program. Most of the triaxial tests were conducted with a ratio of the smallest compressive stress, σ_3, equal to 10% and 20% of the largest compressive stress, σ_1. For these ratios of smallest to largest stress, σ_3/σ_1, various ratios of intermediate stress, σ_2 to largest stress, σ_1, were used. The results of the triaxial compression tests are presented in tabular form and graphical form.

In Table 3 the average maximum values of stress observed for tests with various nominal stress ratios $\sigma_1/\sigma_2/\sigma_3$ are shown. The normalized results based on the uniaxial unconfined compression strength, σ_r, are also tabulated. The triaxial compression curves for $\sigma_3 = 0.2\ \sigma_1$ and $\sigma_3 = 0.1\sigma_1$ are shown in Figure 16. The triaxial compression strength data are also plotted in Figure 16. The curves are a representation of the three-dimensional strength of concrete observed in this test series. The largest compressive stress, σ_1, is plotted against the intermediate compressive stress, σ_2. The increase in the maximum principal stress, σ_1, is primarily a function of the ratio of minimum principal stress, σ_3, to maximum principal stress, σ_1. Thus all points with a constant ratio σ_3/σ_1 will fall on a curve. Each curve determined in this manner will be a line on the three-dimensional concrete strength envelope.

The data plotted in Figure 16 are tabulated in Table 9. The triaxial compression strength data are also listed in normalized form in Table 9. The normalized strength data listed in Table 9 are plotted in Figure 17. The biaxial strength curve, $\sigma_3 = 0$, is also shown in Figure 17 and is seen as a special case of the triaxial strength curves.

53

TABLE 3

AVERAGE TRIAXIAL COMPRESSION STRENGTH DATA

Nominal Ratio $\sigma_1-\sigma_2-\sigma_3$	σ_1 (psi)	σ_2 (psi)	σ_3 (psi)	σ_1/σ_r	σ_2/σ_r	σ_3/σ_r
10-1-1	10,360	1,307	1,120	3.103	0.391	0.335
10-2-1	12,650	2,590	1,140	3.569	0.730	0.394
10-3-1	13,070	4,070	1,330	3.920	1.220	0.400
10-4-1	10,125	4,150	1,000	2.965	1.213	0.293
10-8-1	12,800	10,280	1,280	3.647	2.930	0.366
10-10-1	10,730	10,660	1,050	2.883	2.871	0.281
10-2-2	19,220	4,170	4,000	5.842	1.265	1.215
10-3-2	22,130	6,950	4,500	6.641	2.075	1.350
10-5-2	23,720	11,820	4,690	7.304	3.640	1.444
10-8-2	24,200	19,550	4,810	7.442	6.012	1.479
10-10-2	20,660	20,380	4,175	5.703	5.623	1.155
10-10-1/2	8,283	8,250	447	2.104	2.097	0.112
10-10-3/2	15,560	15,500	2,285	4.059	4.045	0.595

FIGURE 16. TRIAXIAL COMPRESSION DATA

55

FIGURE 17. NORMALIZED TRIAXIAL COMPRESSION DATA

For the case of equal principal stresses in two directions, the effect of a variation of the third principal stress is summarized in Table 4. The effect of a very small amount of triaxial confinement is clearly seen here. For the case of $\sigma_3 = 0.05 \, \sigma_1$, the triaxial strength is almost double the biaxial strength in the direction of σ_1. For the case of $\sigma_3 = 0.20 \, \sigma_1$, the triaxial strength is approximately five times as great as the biaxial strength.

The results of the testing indicate that for a constant stress ratio, σ_3/σ_1, the highest stress occurs approximately at a stress ratio of $\sigma_2 = 0.5 \, \sigma_1$. In order to establish this ratio more exactly it would be necessary to do more testing in this region than was done on this project. It would also be desirable to use all specimens from the same batch of concrete. Based on the test results obtained, it appears that the stress increase in the region $\sigma_2 = 0.5 \, \sigma_1$ is occurring at a somewhat faster rate than the stress increase in the region $\sigma_2 = \sigma_1$ as the third principal stress σ_3 is increased.

Triaxial tests in the tension-compression region were also conducted. The results of the tests are tabulated in Table 10 (Appendix II). Since the preparation of test specimens of this type was very difficult, there was no attempt made to duplicate results for a given principal stress ratio. Individual tests were conducted for various principal stress ratios. The stress ratios selected were varied to cover as much of this region as possible and to have at least some information over a fairly large range of stress ratios.

TABLE 4

Nominal Ratio $\sigma_1 - \sigma_2 - \sigma_3$	σ_1/σ_r	σ_2/σ_r	σ_3/σ_r
10-10-0	1.15	1.14	0
10-10-1/2	2.10	2.10	0.112
10-10-1	2.88	2.87	0.281
10-10-3/2	4.06	4.05	0.595
10-10-2	5.70	5.62	1.155

58

The data tabulated in Table 10 include the biaxial tension-compression data also. These data are a special case of the triaxial tension-compression region. For biaxial tension-compression data, the intermediate stress, σ_2, is zero and the principal stress, σ_1, is compressive with the principal stress, σ_3, being the tensile stress. For the triaxial tension-compression data, the intermediate stress, σ_2, is either compressive or tensile. The data are presented in normalized form with the ratios of the principal stress to the absolute value of σ_r listed. Thus each data point has the same sign as the corresponding principal stress, in each case.

The data in Table 10 are presented in groups which have approximately the same principal stress ratio, σ_3/σ_1. Within these groups it is possible to observe strength trends as the intermediate principal stress, σ_2, is varied from the case $\sigma_2 = \sigma_1$ to the other limiting case $\sigma_2 = 0$. As in the triaxial compression region, the most significant strength parameter is the ratio of minimum principal stress, σ_3, to maximum principal stress, σ_1. The variation of the intermediate principal stress, σ_2, for a constant stress ratio, σ_3/σ_1, has a secondary effect.

As might be expected, an increase in stress ratio, σ_3/σ_1, causes a decrease in maximum compressive strength σ_1. In other words, a principal tension stress increase in one axis causes a principal compressive stress decrease on another axis. For the case of an approximately equal stress ratio, σ_3/σ_1, an intermediate principal stress variation from $\sigma_2 = 0$ to $\sigma_2 = \sigma_1$ causes a reduction in the maximum principal stress, σ_1.

59

A graphical representation of the data tabulated in Table 10 is shown in Figure 18. Figure 18 is a direct plot of the values σ_1/σ_r against the values σ_2/σ_r. The number shown next to each plotted data point is the ratio σ_3/σ_1. The biaxial compression strength curve is shown in order to establish a reference base since it represents one boundary for the region under consideration. The curves shown should give interpolated values of concrete strength in this region which are associated with the data points through which the curves pass. Each curve, therefore, contains all points on the strength envelope for this region which have a constant ratio of σ_3/σ_1.

Table 5 shows the triaxial tension data for the case of three approximately equal principal tensile stresses. Only one test was conducted in this region since the region is very small compared to other regions considered. It was not expected that a significant variation in strength would occur for various principal tensile stress ratios. The result in Table 5 indicates a slight strength reduction compared to the uniaxial tension strength of approximately 0.11 σ_r.

TABLE 5

TRIAXIAL TENSION DATA

σ_1/σ_r	σ_2/σ_r	σ_3/σ_r
+0.102	+0.100	+0.098
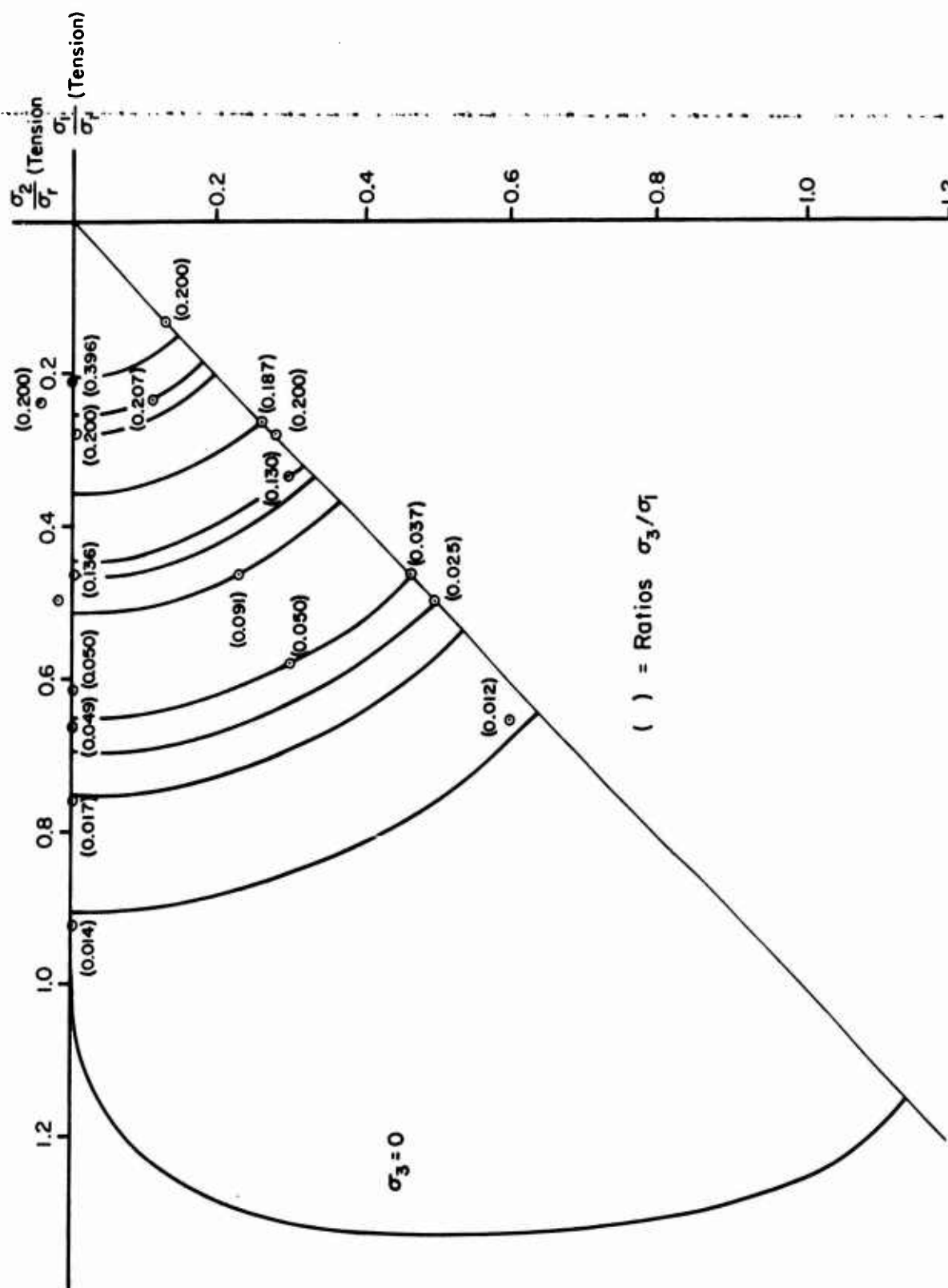
Figure 18. Triaxial Tension-Compression Strength

A final presentation of the variation in triaxial strength of concrete is shown in Figure 19. Two curves showing the relative concrete strength for various triaxial states of stress are presented. The curves show how the ratio of minimum compressive stress σ_3 to maximum compressive stress σ_1 affect the maximum strength obtained during a test. The two cases included are the cases where the intermediate compressive stress $\sigma_2 = \sigma_1$ and $\sigma_2 = 0.5\,\sigma_1$. For both cases, the curves show the decrease in σ_1 for a decrease in the ratio σ_3/σ_1 in the triaxial compression region. In the triaxial tension-compression region, there is a continued decrease in σ_1 as the ratio of tensile stress σ_3 to compressive stress σ_1 increases. The points on the curve where $\sigma_3/\sigma_1 = 0$ are points on the biaxial compression curve.

5.4 FAILURE MODES

The crack patterns observed in the specimens after failure (after the ultimate strength had been obtained) were similar to those reported by previous investigators.

Numerous cracks in a direction parallel to the applied loads were observed in cubes subjected to uniaxial compression. Several examples of failures of this type are shown in Figure 20. The top side of the cube, as seen in Figure 20, was the loaded surface. The crack pattern on the loaded surface is random.

In cubes subjected to equal biaxial compression, the cracking occurred on planes parallel to the unloaded surface. This type of crack pattern develops since the cube is expanding uniformly in the direction in which there is no confinement. Failure occurs when this

62
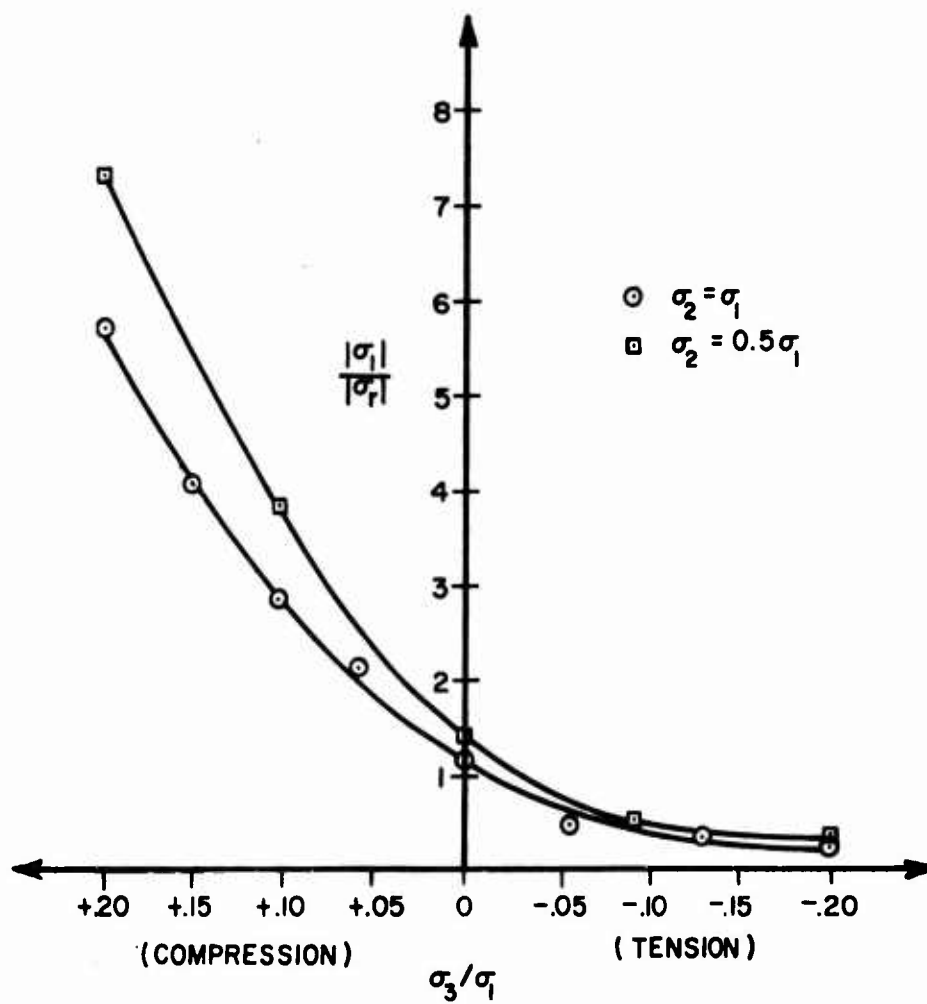
Figure 19. Triaxial Concrete Strength

for Various Ratios $\dfrac{\sigma_3}{\sigma_1}$

63

$$\sigma_1 > \sigma_2 = \sigma_3 = \bigcirc$$

Figure 20. Uniaxial Type Failures

expansion becomes excessive. In Figure 21 cubes with this type of failure pattern are shown. The top surface of the cubes was the free surface. The cracks on the loaded surfaces are numerous and in general parallel to each other. Cubes loaded in unequal biaxial compression are shown in Figure 22. The cracking observed here was somewhat different from the cracking observed in the cubes subjected to equal biaxial compression. As the stress state changes from close to equal to unequal biaxial compression, the cracking changes from numerous parallel failure planes to a few major nonparallel failure planes. The angle between the failure planes increases as the stresses become more unequal. The cracks on the surface with the higher stress are essentially parallel, with the nonparallel cracks occurring on the surface with the lower stress.

Cubes which were subjected to high triaxial compression are shown in Figure 23. The cubes were unloaded carefully after the maximum strength had been attained for the given loading ratios. Large dimensional changes have occurred. Numerous random microcracks exist in all directions. The cubes will crumble if they are not handled carefully. The observed failure modes for cubes subjected to small triaxial compressive stresses fall into three categories. For the case where the two smaller principal stresses are equal, the failure is as shown in Figure 20. For the case where the two larger principal stresses are equal, the failure is of the type shown in Figure 21. For the case where the three principal stresses are all different, the failure was by splitting in the direction of the minor principal stress similar to that shown in Figure 22.

65

$$\sigma_1 = \sigma_2 > \sigma_3 = 0$$
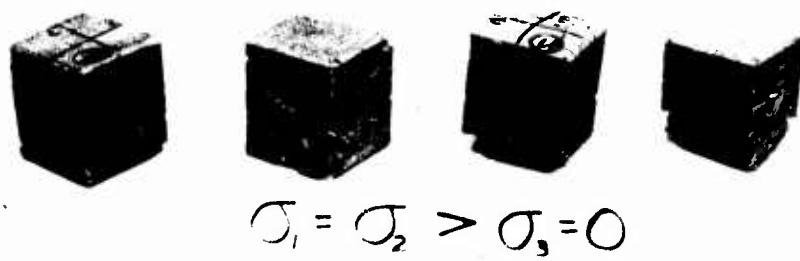
Figure 21. Equal Biaxial Type Failures

Figure 22. Unequal Biaxial Type Failures

TRIAXIAL

Figure 23. Triaxial Type Failures

68

Failure in the cubes subjected to uniaxial tension was due to
a major crack through the specimen which was essentially parallel to
the loaded surfaces. The orientation of the failure plane in biaxial
tension varied from 0-45 degrees with the horizontal as the tensile
stresses varied from the uniaxial case to the equal biaxial stress
case. In the cubes subjected to triaxial tension, the failure was
due to a single major crack with no preferred direction.

5.5 CUBE VERSUS CYLINDER STRENGTHS

A tabulation of the unconfined compression strength, σ_r, and the
7- and 28-day cylinder strengths is given in Table 6. The cylinder
tests were used as initial control on each batch. Once a strength
curve was determined, it was possible to predict whether the batch
would conform to the specified strength based on the 7-day tests.
The 28-day strengths were taken 4 weeks after the casting date while
the values of σ_r were taken at the test date. It was initially
assumed that there would not be an appreciable strength increase in
the concrete after 28 days since all specimens were removed from the
curing room and stored in a dry condition until tested. Tests on
two control cylinders which were broken at the time that the uniaxial
cube strengths were determined indicated a 14% to 20% increase in the
strength of the batch. Since the cubes were tested approximately
four months after the cylinders in each case, a direct strength com-
parison cannot be obtained. Another factor which makes a direct
strength comparison difficult is that the cube strength is based on
a cube with beveled edges in each case. This gives an apparent cube

69

TABLE 6

UNIAXIAL TEST RESULTS

Date Tested	Date Cast	Cube σ_r (psi)	6" x 12" Cylinder Strength	
			7-day (psi)	28-day (psi)
5-20-71	2-3-71	3,620	2,953	4,314
5-18-71	2-2-71	3,412	3,200	4,173
6-29-71	2-9-71	3,756	3,236	4,420
6-7-71	2-8-71	3,930	3,483	4,527
6-16-71	2-4-71	3,340	3,324	4,314
7-2-71	2-11-71	3,333	2,758	3,996
7-2-71	3-2-71	3,327	2,599	4,029
7-12-71	2-16-71	3,500	3,183	4,332
7-20-71	3-8-71	3,307	3,271	4,827
7-28-71	3-11-71	4,337	3,094	4,810
8-3-71	3-10-71	3,161	3,359	4,810
8-10-71	4-7-71	2,597	3,554	4,845
8-19-71	4-12-71	2,977	3,324	4,951

strength which is too low. It is felt that a 10% to 12% increase
in the cube strength would give a better comparison basis.

In general the cube strength falls between the 7-day and 28-day
cylinder strengths. For the last three batches shown in Table 6,
the cube strengths were lower than the 7-day cylinder strengths.
This inconsistency could be due to any number of factors such as
difference in compaction, segregation of material or curing method.
Since the cube strength in each case was used as the strength basis,
the inconsistency noted here is not of great importance.

5.6 PLATEN SHEARING EFFECT

It was necessary to use a loading platen which was smaller than
the cube in order to allow for deformation of the specimen during a
test. In order to obtain a better stress distribution, the cubes were
beveled along the edges. For the 4000 psi concrete mix used in this
testing program and for cubes tested using friction reduction pads,
a shearing effect along the edge of the platen was not observed to be
a significant problem in this test program. If shearing was signif-
icant, thin plates of concrete would have broken off on all sides
during a uniaxial test. Typical uniaxial type failures are shown in
Figure 20. The type of failure described above did not occur.

SECTION VI

COMPARISON OF DATA WITH OTHER INVESTIGATORS

6.1 INTRODUCTION

A comparison of published data with the data obtained from this
testing program can be accomplished generally for strength comparisons
only. In only one case, Hilsdorf (4), are there strains published that
can be compared. This is for the biaxial case only. Mills (25) has a
few stress-strain curves for the triaxial case, but not enough to be
able to compare completely.

In comparing the ultimate strengths from the various multiloading
test results published, difficulty is encountered in that different
authors present their results differently. Some use normalized results
whereas others do not. Still another complication arises since different
types of test specimens were used and the stresses or loads were applied
differently. In some cases cylindrical specimens were used, in other
cases slabs were used, and in others cubes were used. Hollow as well
as solid cylinders were used. Hollow cylinders were generally loaded
axially along with a torsion or fluid pressure. Solid cylinuers were
generally tested in a solid type triaxial testing machine. Slabs were
tested biaxially only. Only those using cube specimens could indepen-
ently control the applied load in three directions. Usually only the
ultimate strengths were reported. Measuring of strains was difficult
or impossible in many of the different types of test setups.

72

6.2 BIAXIAL COMPRESSION STRENGTH COMPARISON

A comparison of the biaxial strength of concrete determined from this test program with the results obtained by other investigators has been made. In Figure 24, the results of the biaxial compression investigators were determined as accurately as possible from the available reports. In some cases the published data was very limited but the curves in general show the reported trends.

Rosenthal-Glucklich (22), Campbell-Allen (14) and Bellamy (11) used hollow cylinders subjected to axial compression and external hydraulic pressure. For the case of equal biaxial compression, the range of values for σ_1/σ_r was 2.24 to 2.69. A triaxial state of stress is suspected in this type of test and the determined strength increase is considered to be too high.

Iyengar et al. (5) used 4-in. and 6-in. cubes with solid bearing platens and no friction reduction attempted between the specimen and the platens. Using this type of testing procedure, the friction between specimen and platen has a confining effect on the concrete and will result in an overestimate of strength increase. For the case of equal biaxial compression, these tests resulted in a ratio $\sigma_1/\sigma_r = 3.6$. This estimate of the biaxial compression strength is not as good as that obtained using hollow cylinder test specimens.

Tests using square slab-type specimens subjected to in-plane loading were conducted by Vile (26) and Robinson (3). Both investigators used 10 x 10 x 4-inch specimens and solid bearing platens with a special concrete curing compound used as packing to reduce the friction effects

73
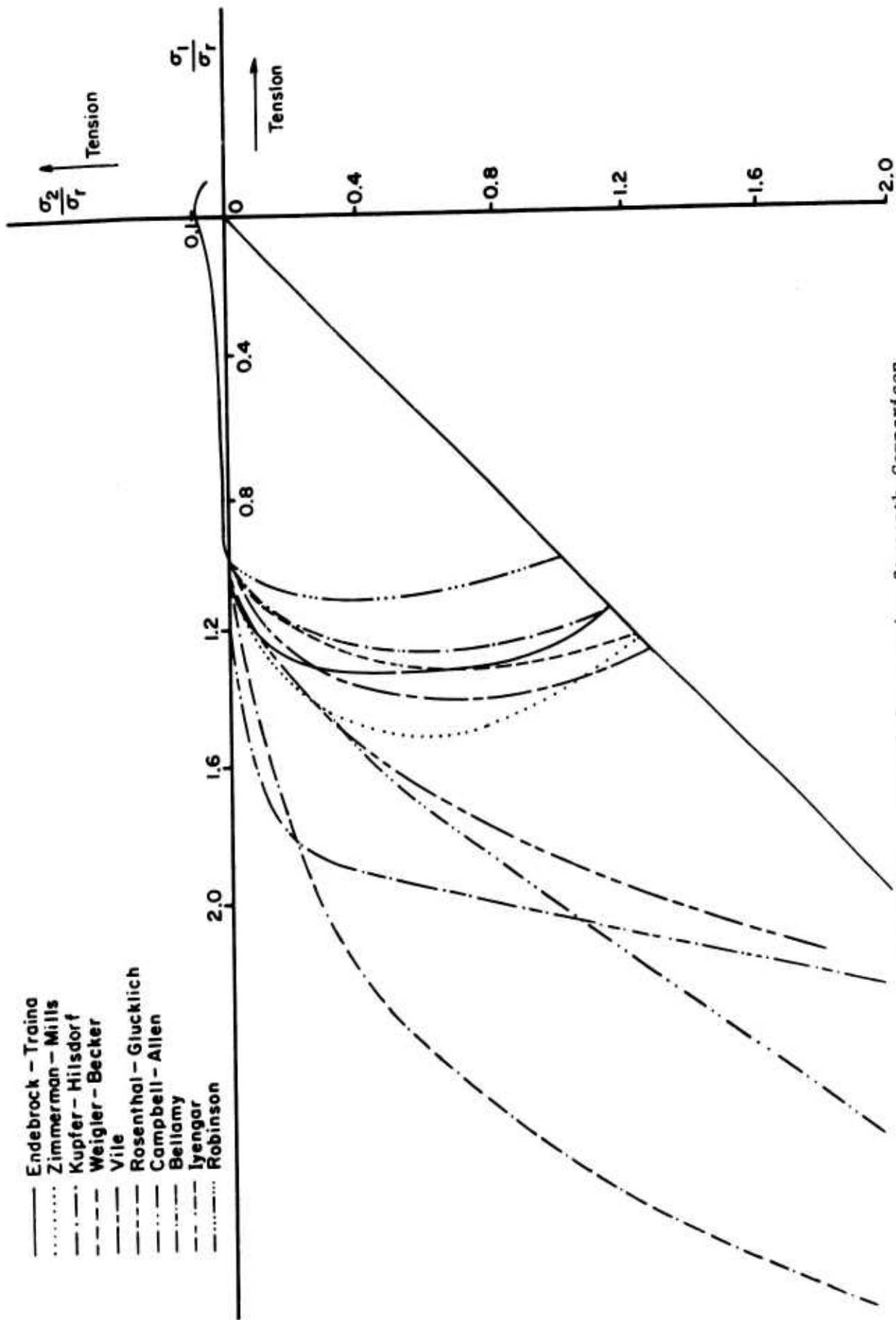
Figure 24. Biaxial Compressive Strength Comparison

Legend:
— Endebrock–Traina
⋯ Zimmerman–Mills
—·— Kupfer–Hilsdorf
——— Weigler–Becker
—— Vile
—··— Rosenthal–Glucklich
—·—· Campbell–Allen
—··— Bellamy
—·— Iyengar
⋯ Robinson

74

between the specimen and the platens. For the case of equal biaxial compression, a ratio σ_1/σ_r of 1.10 was obtained by Robinson, and 1.25 to 1.45 was obtained by Vile. Some of the difference in results observed by these two investigators was probably due to the different concrete mixes which were used.

Weigler and Becker (27) used 10 x 10 x 2.5-cm slabs with solid bearing platens and no friction reduction material. Their investigations yielded a ratio of σ_1/σ_r of 1.10 to 1.20 for the case of equal biaxial compression.

Another investigation using a slab type test specimen was conducted by Kupfer, Hilsdorf and Rusch (4). A 20 x 20 x 5-cm specimen was used. This research made use of a brush type bearing platen in an attempt to load the test specimen without end restraint. A ratio of $\sigma_1/\sigma_r = 1.16$ was found for the case of equal biaxial compression.

Mills and Zimmerman (21) used a 2 1/4-inch cube for a test specimen. In order to eliminate end constraint, a system using two polyethylene pads with grease between the pads was used. The biaxial tests, in this investigation, were conducted using a sequential loading. The case of equal biaxial loading was not quite achieved using this loading method. Three different mixes were used with average values of σ_r of 3,340, 3,910 and 5,235 psi, respectively. The biaxial tests for the two higher strength mixes were too few to achieve reliable results. For the lower strength mix, a value of σ_1/σ_r for the case of equal biaxial compression is approximately 1.24.

From the previous discussion it can be concluded that all of the previous biaxial compression studies did not use a test set-up which developed unconfined biaxial state of stress. The hollow cylinder and cube specimens with solid bearing platens and no friction reduction between the concrete cube and the bearing platen fall into this class.

The investigations using slab type specimens with solid and brush type bearing platens seem to develop a reasonably unconfined biaxial stress state. The results of these investigations are comparable to the results obtained from this testing program using a cube type test specimen with greased pads to eliminate platen restraint. The biaxial compression strength curve obtained using the slab type specimens are all within 10% of the results obtained during the present investigation. This appears to be a reasonable variation since the concrete mixes used in all the investigations were different. In fact, during the present investigation, a different batch of concrete using the same mix was found to vary almost as much.

The results obtained using the brush type bearing platen with slab type specimen compare best to the results obtained in this test program. This is not unexpected since of all other systems studied it probably achieves the most unconfined biaxial compression state of stress.

6.3 BIAXIAL TENSION-COMPRESSION STRENGTH COMPARISON

Previous investigations of the biaxial tension-compression strength of concrete were conducted on two different types of specimens.

76

Hollow cylinders loaded axially along with a fluid pressure was used by Rosenthal-Glucklich (22), McHenry-Karni (8) and Tsuboi-Suenaga (18).

Kupfer, Hilsdorf, and Rusch (4) used a slab type specimen 20 x 20 x 5-cm subjected to an in-plane loading. Brush type loading platens were used to reduce end restraint with the specimen glued to the loading platen for application of the tensile stress.

A typical strength curve from each of the above test programs is compared with the results obtained from the present investigation in Figure 25. The results in Figure 25 are in normalized form in order to make a direct comparison. The stresses are normalized by taking the ratio of each stress to the unconfined uniaxial compressive stress of concrete, σ_r. In all of the above test programs, tests on different concrete mixes were conducted. The curves using different mixes with the same test set-up have the same general shape. Another trend which was observed is that the ratio of uniaxial tension to uniaxial compression decreases with an increase in compression strength for various mixes. The range of values observed during the previous test programs for the ratio of uniaxial tension to the absolute value of uniaxial compression was 0.07 to 0.13. This compares to a value of 0.11 obtained during this investigation. This value appears to be reasonable since the compressive strength of the mix used was within the range of compressive strengths used by the previous investigators. In the region where the ratio of compression to tension is high, the

77
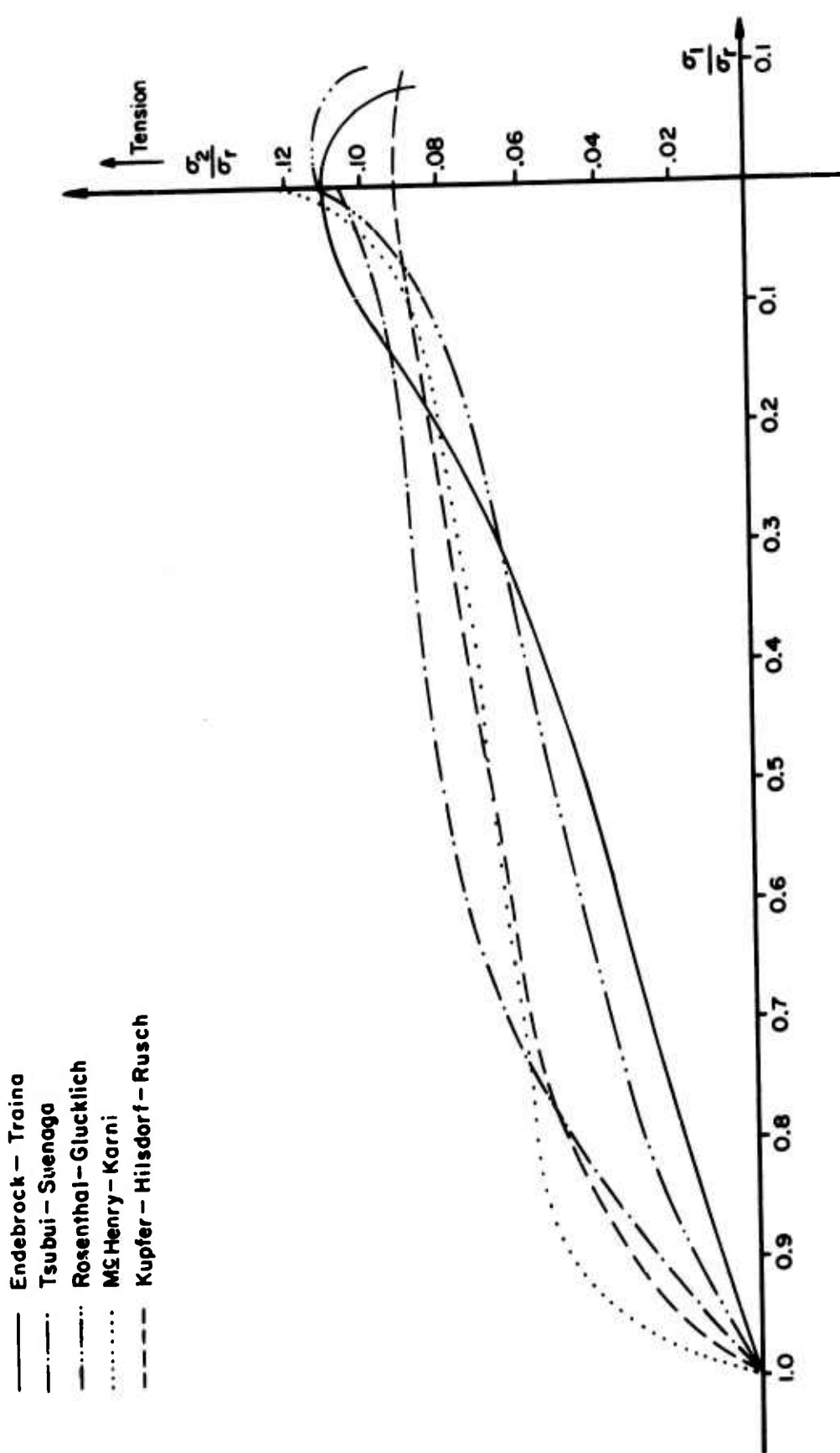
Figure 25. Biaxial Tension and Tension-Compression Strength Comparison

Endebrock — Troina

Tsubui — Suenaga

Rosenthal — Glucklich

M℃ Henry — Karni

Kupfer — Hilsdorf — Rusch

strength curve obtained is lower than other reported results. However, in general there is not too much difference between these results and those of Rosenthal (22). This is encouraging since of all the cylinder type testing the diameter ratio in that test program was closest to thin wall assumptions which were used in all the hollow cylinder test programs.

6.4 BIAXIAL TENSION STRENGTH COMPARISONS

Biaxial tension strength testing was previously conducted by Kupfer, Hilsdorf and Rusch (4). They used the same test set-up here as for the tension-compression testing except that the specimen was glued to the platens on both sides in order to apply a tension stress in orthogonal directions. A very flat biaxial tension curve was reported using this testing method. Figure 25 shows the biaxial tension comparison curves. It was reported that the biaxial tensile strength is approximately equal to its uniaxial strength.

Rosenthal and Glucklich (22) conducted biaxial tension tests by loading hollow cylinders with axial tension and internal fluid pressure. The resulting biaxial tension strength shows a small decrease in the biaxial tension strength compared to its uniaxial tension strength.

6.5 TRIAXIAL STRENGTH COMPARISONS

A comparison of the triaxial strength of concrete can be made in the triaxial compression region only. There have been no other published test results for the triaxial tension-compression region. In

79

the triaxial compression region, it is difficult to get a direct strength comparison since there are so many different loading combinations which are possible. Most of the testing which was performed by others used loading combinations which were different from those used in this test program. There was also a difference in types of specimens used, concrete mixtures, end conditions and the uniaxial unconfined compression strength. Any of these factors could cause some difference in the results obtained by the other investigators.

The specimens used by other investigators include cubes, solid cylinders and hollow cylinders. A summary of other investigations including specimen type, maximum aggregate size and end conditions is shown in Table 7.

TABLE 7

SUMMARY OF PREVIOUS TRIAXIAL COMPRESSION INVESTIGATORS

Investigators	Specimen Type	Maximum Size Aggregate	End Condition
Balmer (13)	6"x12" Solid Cylinders	1 1/2 in.	Steel Plates
Bellamy (11)	6"x12" Hollow Cylinders	Sand	Not Specified
Gardner (2)	3"x6" Solid Cylinders	3/4 in.	Not Specified
Krishnaswamy (1)	4" Cube	3/4 in.	No Capping
Krishnaswamy (1)	4" Cube	3/4 in.	Plastic Sheet
Krishnaswamy (1)	4" Cube	3/4 in.	Plastic & Grease
Mills & Zimmerman (21)	2 1/4" Cube	3/8 in.	Plastic & Grease

The data obtained from these testing programs are limited to a very small portion of the triaxial compression region. The results of tests using cylinders is shown in Figure 26.

80
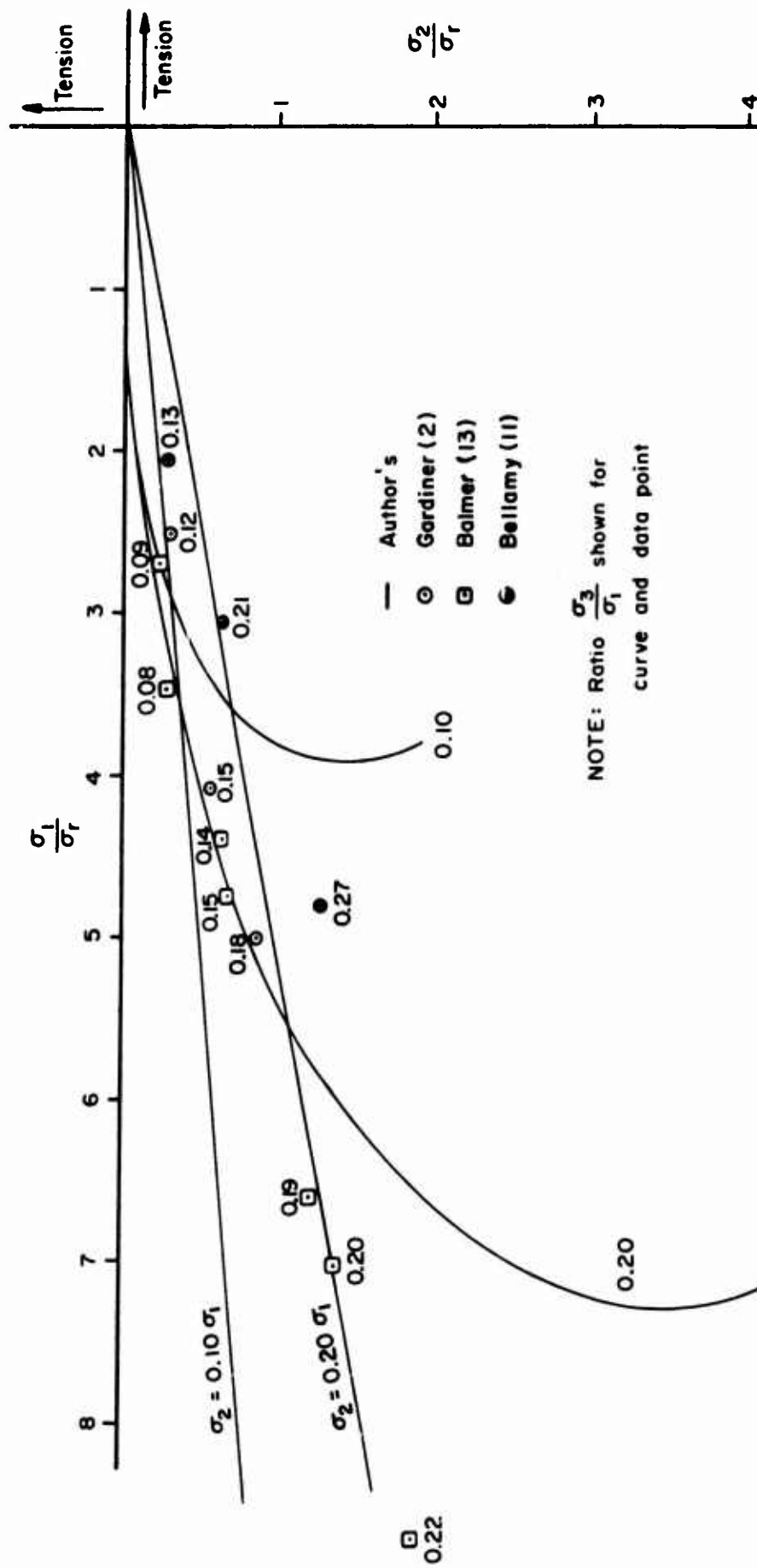
Figure 26. Triaxial Compression Strength Comparisons

The triaxial compression curve obtained during this investigation is also shown in Figure 26 so that a comparison can be shown.

For all cylinder tests, $\sigma_2 = \sigma_3$ due to the nature of the test program. Since the maximum axial strength, σ_1, increases very rapidly for small confining pressures, σ_2 and σ_3, the system becomes self-limiting to a relatively small region. The highest ratio shown in Figure 26 is $\sigma_3/\sigma_1 = 0.27$. Based on the triaxial compression curves obtained during the present investigation, the increase in the maximum compressive strength, σ_1 reported by Bellamy (11) appears to be too low for all reported results. The results reported by Gardner are somewhat low for the ratio $\sigma_3/\sigma_1 = 0.12$ but seem to compare quite well for the other two data points. The results reported by Balmer (13) are a bit high for all reported data.

The comparison of results for tests which used a cube test specimen are shown in Figure 27. Using a cube test specimen all three principal stresses can be varied. It is thus possible to obtain test data over a larger portion of the triaxial compression region. Test results reported by other investigators is limited to the lower portion of the region due to loading limitations of the test set-up which was used. The results are limited to a principal stress ratio, σ_3/σ_1, of approximately 0.13.

Based on the triaxial compression curves obtained during the present investigation, a comparison can be made with the results obtained by Mills and Zimmerman (21) for a stress ratio, σ_3/σ_1 of approximately

82
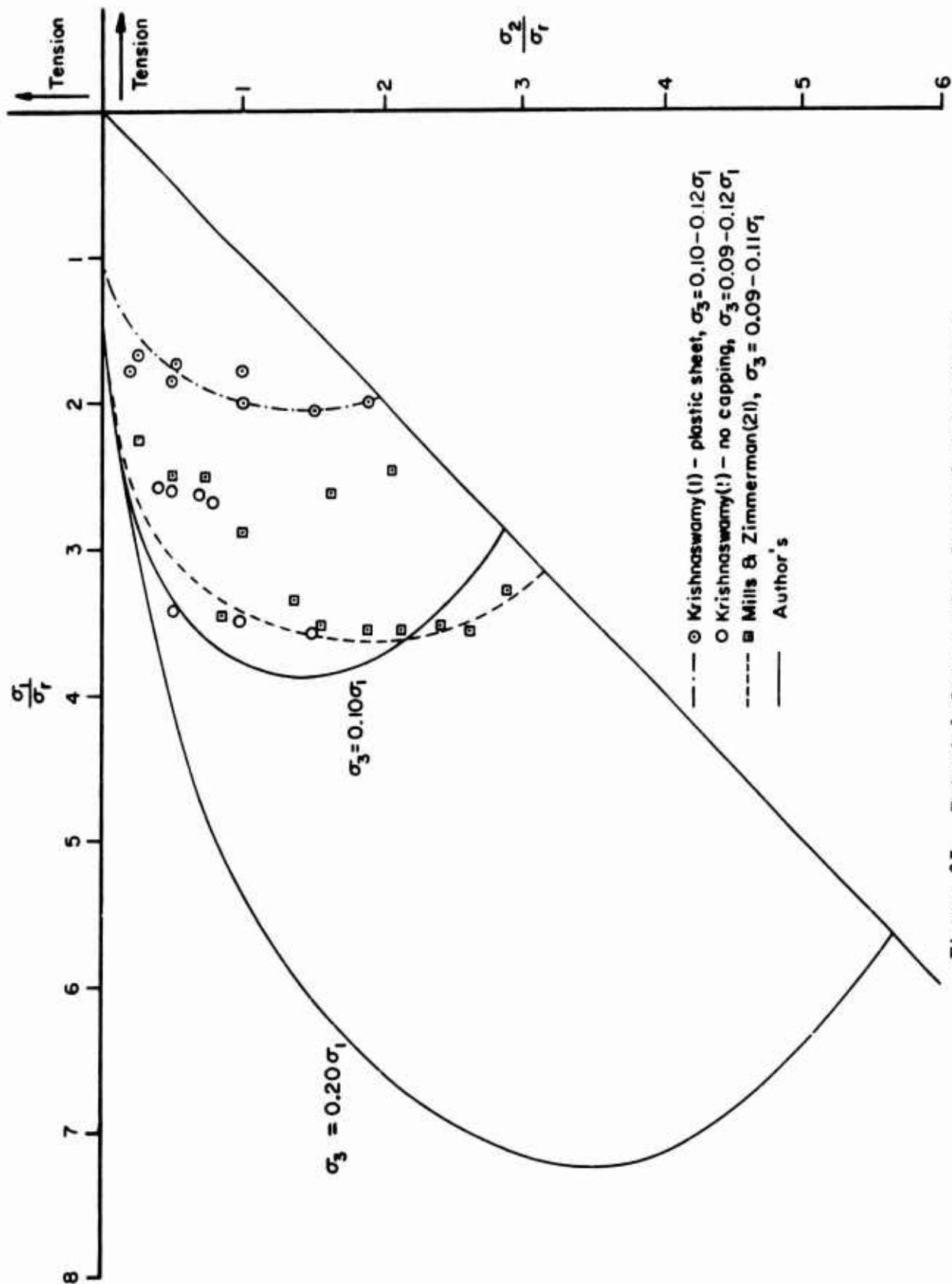
Figure 27. Triaxial Compression Strength Comparisons

0.10. The data reported by them seem to fall on two curves. One curve is quite a bit lower than the other. The upper curve shown in Figure 27 compares quite well with the results of the present investigation.

The results reported by Krishnaswamy (1) were based on tests with end conditions which resulted in various degrees of constraint of the cube by the loading platens. The various conditions were two plastic sheets and grease, one plastic sheet and no capping. His reported results of tests using a stress ratio, σ_3/σ_1, of approximately 0.10 are shown in Figure 27. Using either one plastic sheet or two plastic sheets with grease between the sheets did not produce a significant difference in results. The results reported indicate a much lower strength increase for this type of test than for the tests where no capping was used. For the case where no capping was used the strength increase indicated was somewhat less than that found during the present investigation.

A comparison of the strength increase for the triaxial stress case where $\sigma_1 = \sigma_2$ was attempted. There was not a sufficient amount of published data to make such a comparison. It was also not possible to make any comparisons of triaxial compression strength for the curve where $\sigma_3 = 0.20\ \sigma_1$ in the region between $\sigma_2 = 0.20\ \sigma_1$ and $\sigma_2 = \sigma_1$.

It was also not possible to make any comparisons in the triaxial tension and triaxial tension-compression region since no data of this type has been reported by other investigators.

84

6.6 COMPARISON OF STRESS-STRAIN CURVES

A comparison of stress-strain curves with Hilsdorf et al. (4) was possible. Different strength concretes were involved, hence, stresses are plotted on a comparable basis. These curves are shown in Figure 28. For the uniaxial compression case, the stress-strain curves from these tests and those of Hilsdorf et al. (4) were quite similar in the lower stress range but departed at the higher stress levels. This can be explained by the time element involved in the testing procedure. Hilsdorf et al. required about 20 minutes for a test; whereas, these required about one minute. The larger strains obtained by Hilsdorf et al. can be explained by creep effects which are more pronounced at the higher stress levels. The lateral strains also compare favorably at the lower stress levels, but again depart at the higher stress levels. In the case of the lateral strains, the results of Hilsdorf are smaller than these. This could possibly be explained by the different types of test specimens used. Hilsdorf used square slabs whose thickness was much smaller than the other dimensions. There were probably fewer cracks forming near failure, hence a smaller apparent lateral strain was detected. In the cube specimens, the lateral strain in one unloaded direction always exceeded the lateral strain in the other unloaded direction. Failure first occurred in the direction with the greatest lateral strain.

In the case of biaxial compression with the two applied stresses being equal, again the results of Hilsdorf and the author's compare favorably at the lower stress levels and depart at the higher stress
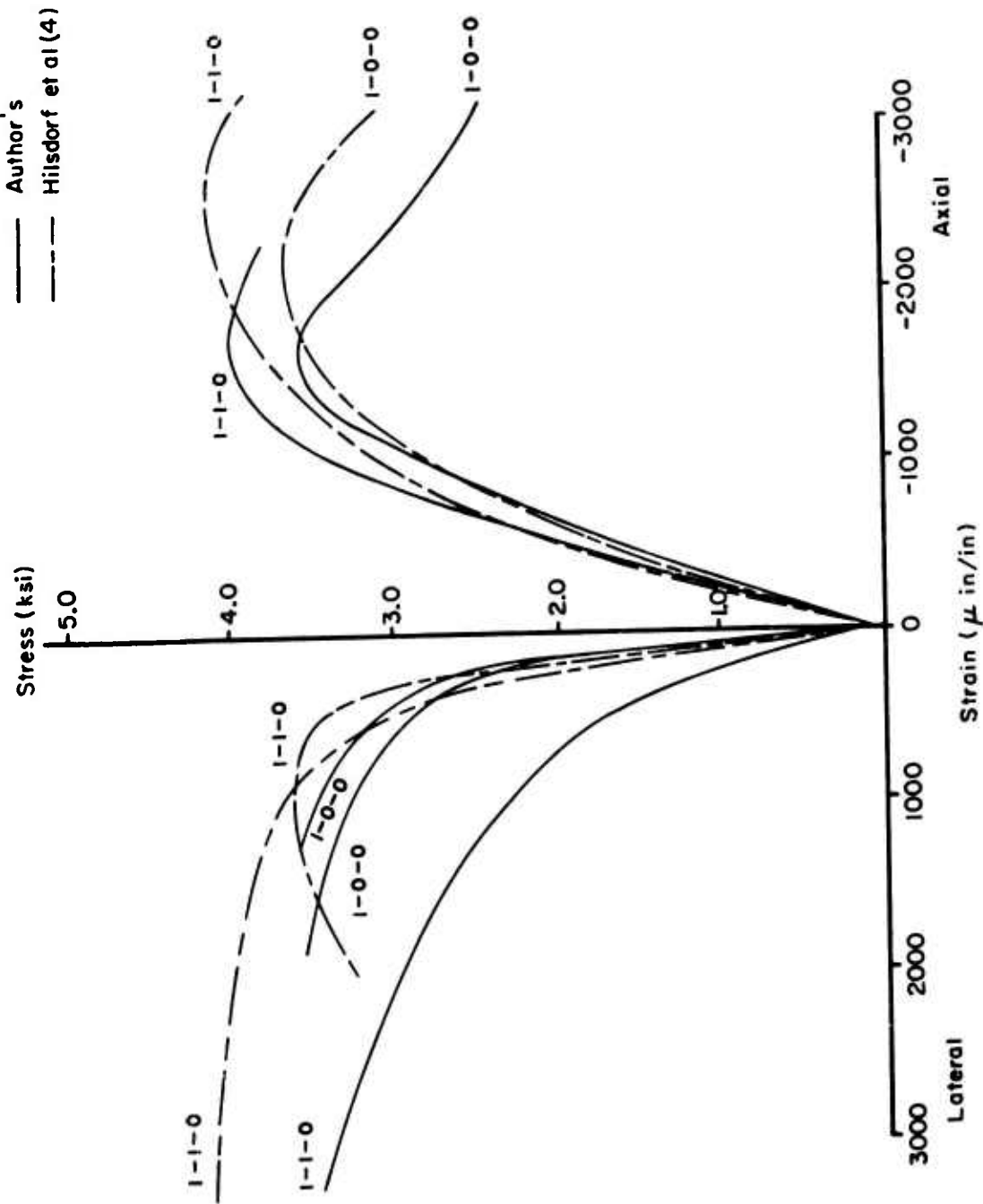
Figure 28. Uniaxial and Biaxial Compression Stress-Strain Curves

levels. The same trends are observed as in the case of uniaxial tests for both lateral and axial strains, however, the difference is more pronounced. The lateral strain in these tests departs even at the lower loads. This is believed to be due to the different types of test specimen used.

In Figure 29 a comparison is made for the case of uniaxial tension. Again the results are quite comparable. The stress-strain curve has the same shape with slightly smaller strains obtained by these. Figure 29 also contains typical biaxial tension-compression stress-strain curves. There is not much difference in the initial portion of the compression axis curve. On the tension axis however, the curves depart at a low stress level. A comparison with Hilsdorf et al. (4) is difficult since different ratios of tension to compression were used.

For the case of biaxial tension, the stress-strain curves obtained during the present investigation are shown in Figure 30. The strain on each loaded axis for the stress ratios $\sigma_1/\sigma_2 = 1$ and 2 are shown.

6.7 OTHER COMPARISONS

Nearly all of the published results, whether biaxial or triaxial could be compared simultaneously by plotting the mean normal stress (σ_0) versus the octahedral shear stress (σ_0) at failure where:

$$\sigma_0 = \frac{1}{3} (\sigma_1 + \sigma_2 + \sigma_3)$$

and
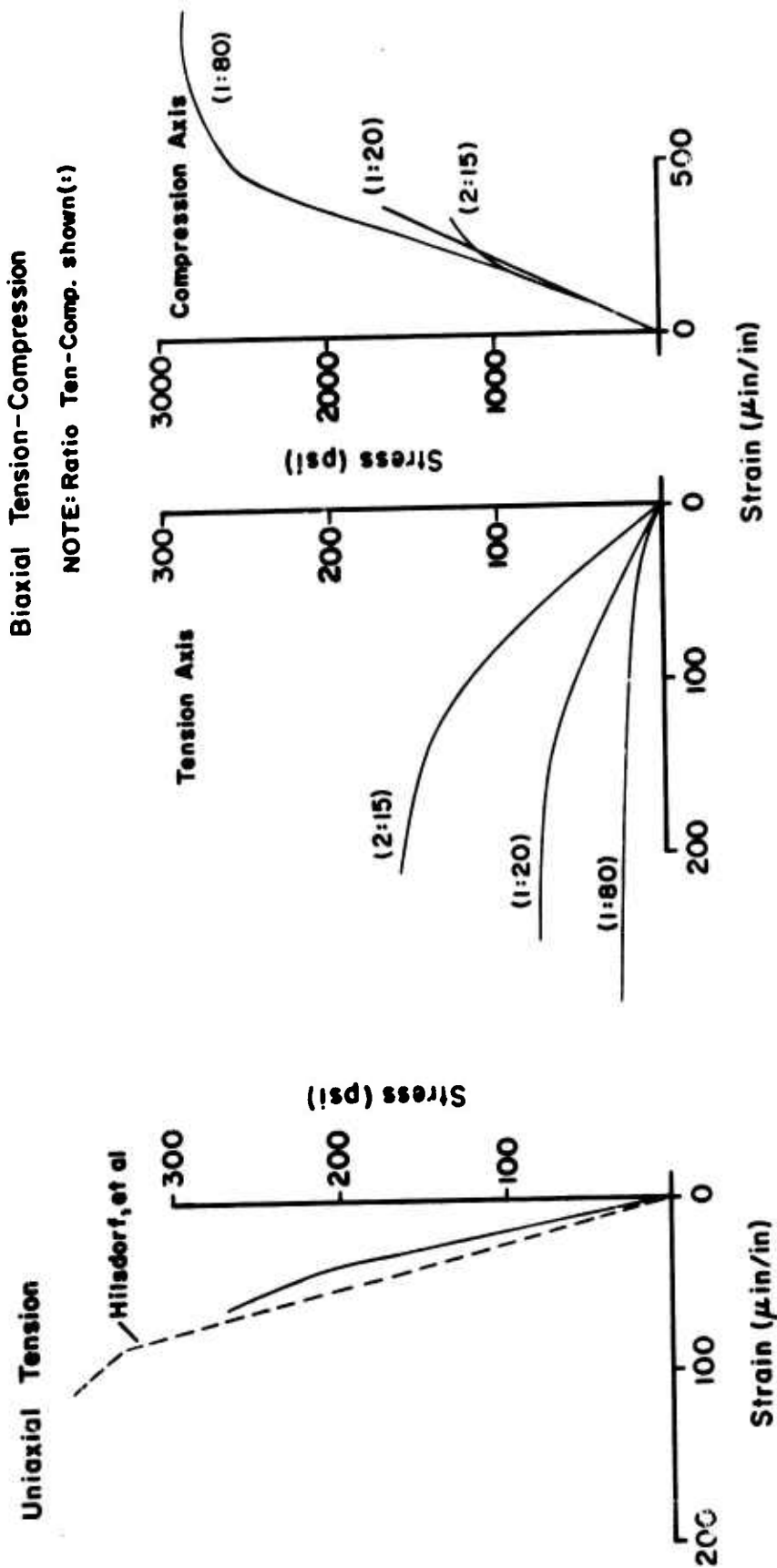
Figure 29. Uniaxial Tension and Biaxial Tension-Compression Stress-Strain Curves

88
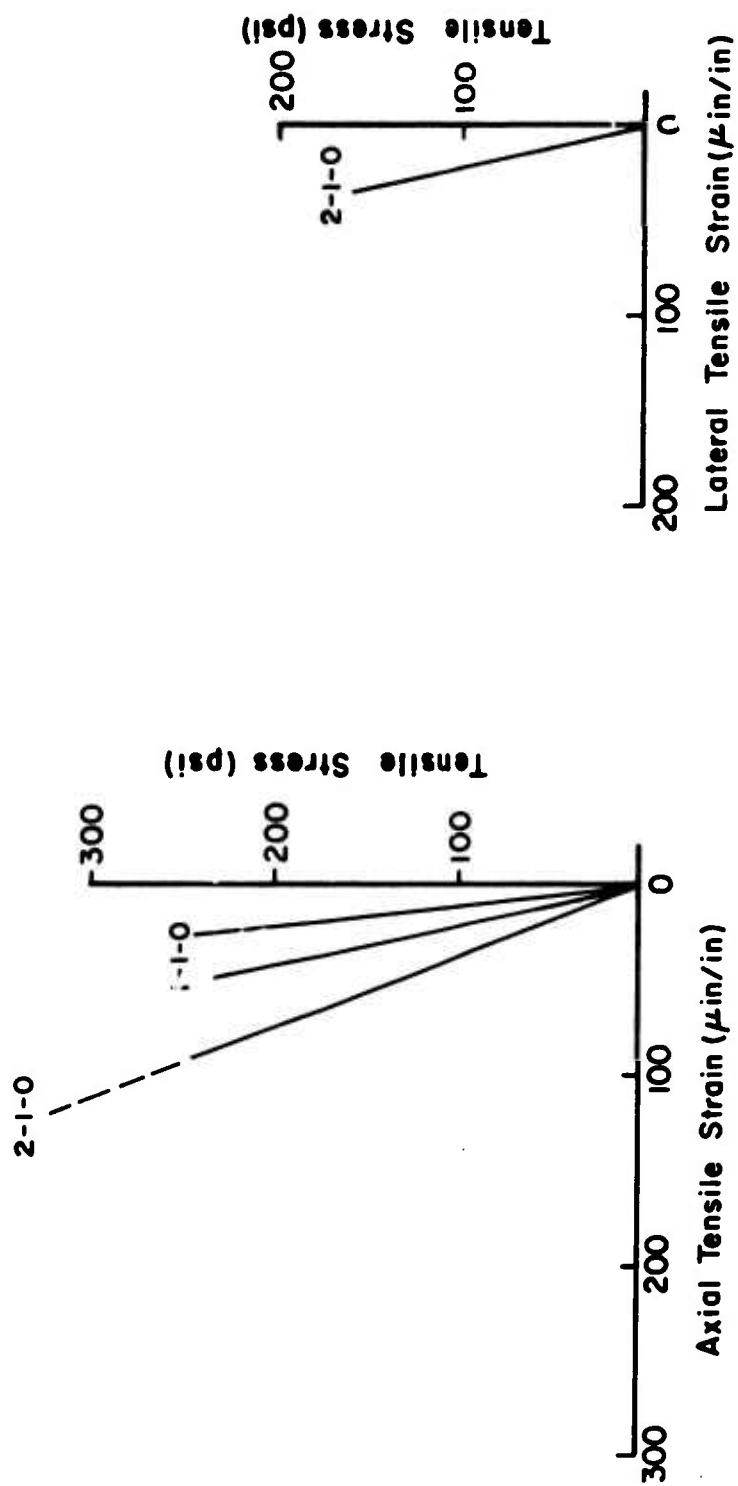
Figure 30. Biaxial Tension Stress-Strain Curves

$$\tau_o = \frac{1}{3} \left[(\sigma_1 - \sigma_2)^2 + (\sigma_2 - \sigma_3)^2 + (\sigma_1 - \sigma_3)^2 \right]^{\frac{1}{2}}$$

This was done and some of the published results are shown in Figure 31. A rather large scatter is observed and the results of the present testing program fall within the range of all published results. Only test results designated as Type I ($\sigma_1 > \sigma_1 = \sigma_3$) and Type II ($\sigma_1 = \sigma_2 > \sigma_3$) are compared. Tests with the intermediate principal stress, σ_2, different from σ_1 or σ_3 will fall between the two curves shown in Figure 31.

A comparison of mean normal stress, σ_m, versus volumetric strain, $\Delta v/v$, is possible. Curves of this type have been plotted in Figures 32 and 33. In Figure 32 the results of some typical biaxial compression tests are shown. In Figure 33 the results of some triaxial compression tests are shown along with a typical biaxial and uniaxial test for comparison.

90
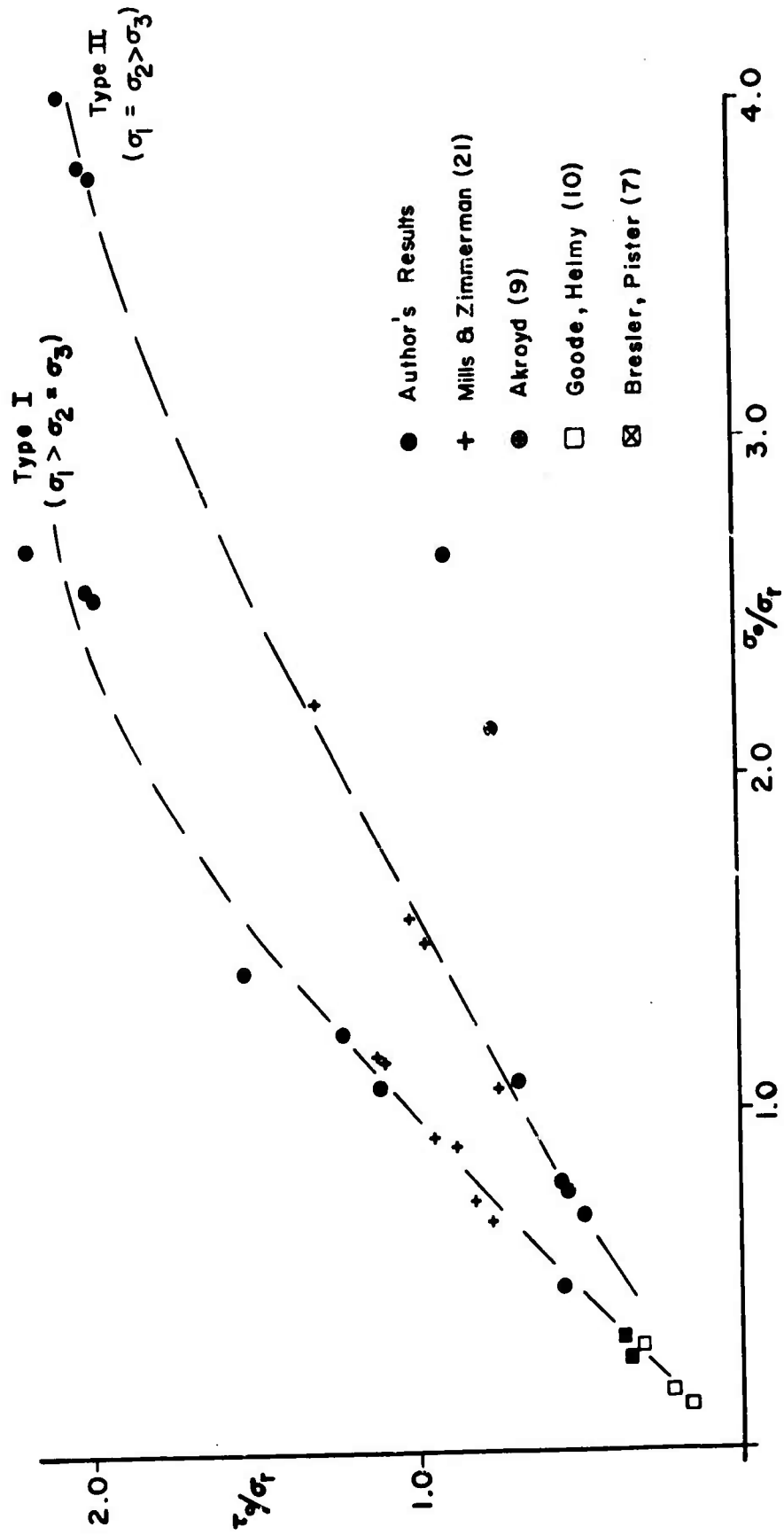
Figure 31. Octahedral Shear versus Octahedral Normal Stress
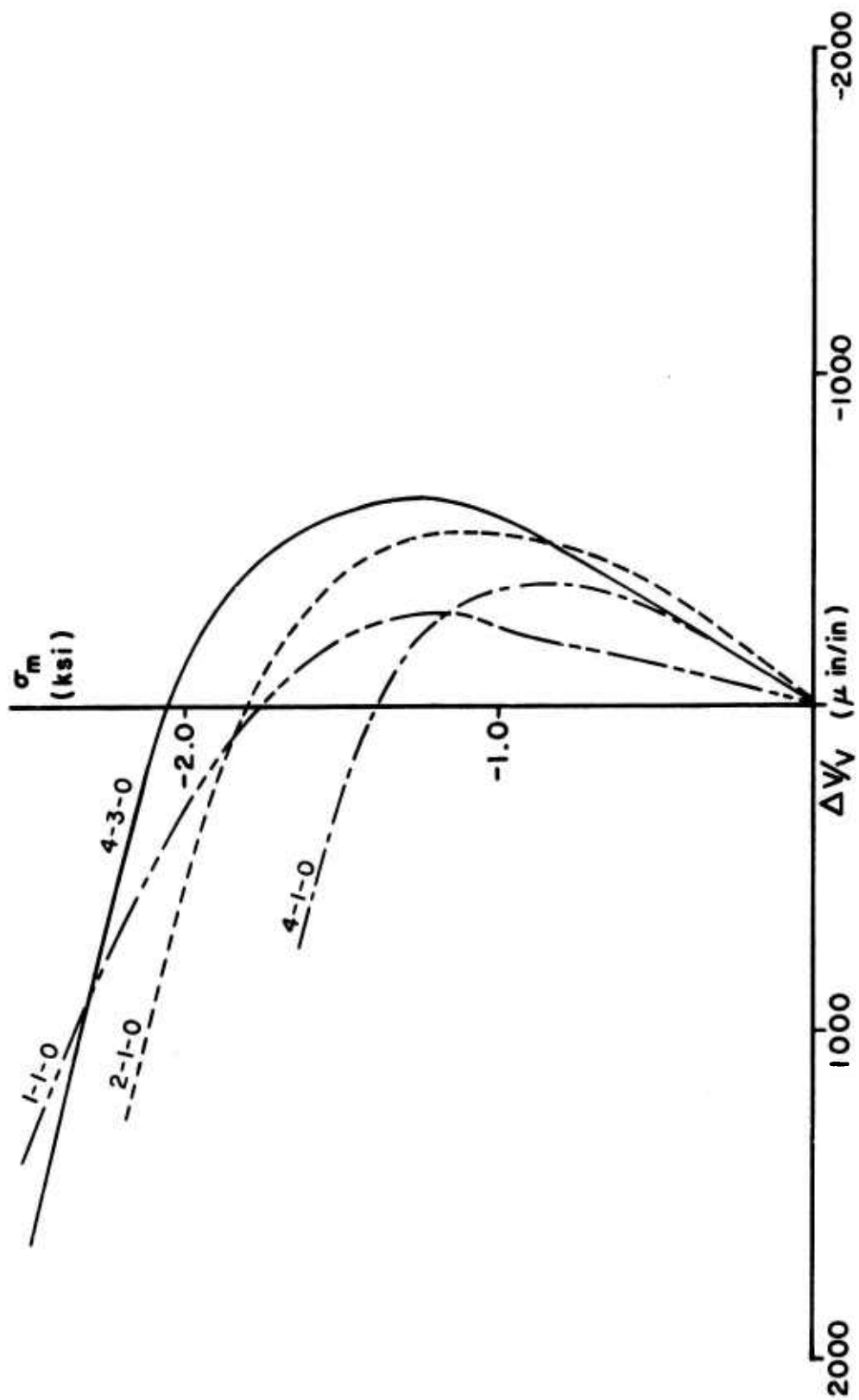
Figure 32. Mean Normal Stress versus Volumetric Strain for Biaxial Compression
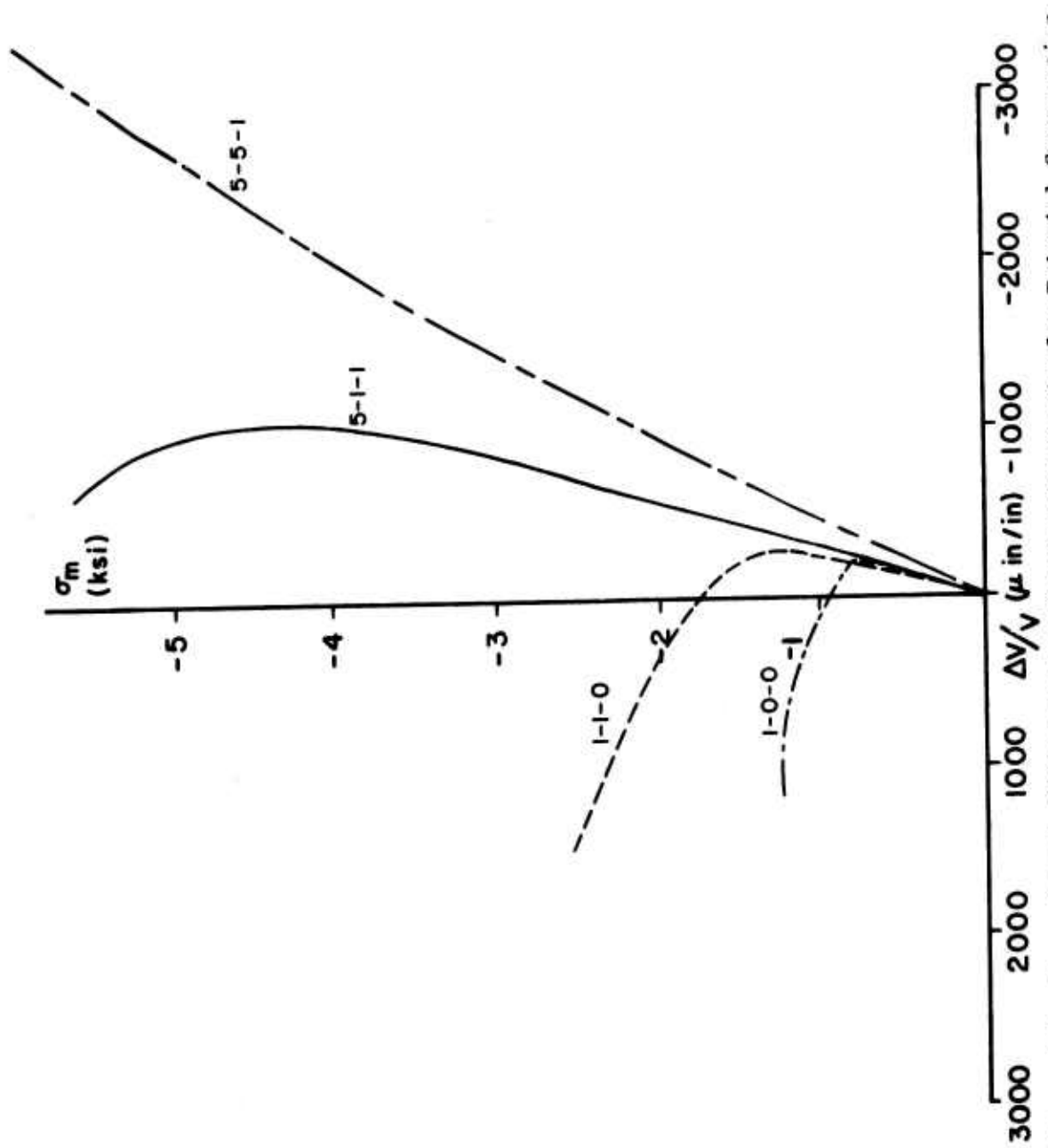
Figure 33. Mean Normal Stress versus Volumetric Strain for Triaxial Compression

93

SECTION VII

THE MODEL

7.1 INTRODUCTION

Several attempts were made at formulating constitutive relationships for concrete subjected to a general loading during this investigation. The earliest attempt utilized the linear constitutive relationships of the theory of elasticity with nonlinearities introduced by considering the modulus of elasticity and Poisson's ratio as functions of the stresses and strains instead of as constants. The slightest degree of success was never achieved using this approach; hence, it was abandoned.

A model to simulate concrete behavior under triaxial loads was then considered. The model consisted of nodal points located at the corners of a cube along with "bars" or "springs" connecting the nodal points. Any number of these cubical model elements could be stacked to form a more sophisticated model. This model could handle shear stresses and strains in addition to the normal stresses and strains. It could be used to simulate a cubical test specimen and would be useful for studying friction effects and failure modes provided that strains were determined from the stresses. Considering the simpliest version of this model, there are eight nodes with three possible displacements at each node; hence, a total of twenty-four possible displacements. A maximum of six strain values exist at a point. Conversion of six known strains to twenty-four displacements was considered an impossible task. It was concluded that this model could not be used to determine stresses whenever strains were given; hence, it was abandoned.

The proposed model for simulating concrete behavior also consists of nodal points connected by "bars." The nodal points are located at the points of an octahedron. The arrangement of the nodal points and bars is shown in Figure 34. This arrangement was patterned after the model used by Anson (23) in his study of the failure mechanism for concrete. The behavior of Anson's model and the one described herein is quite different. This model cannot handle shear stresses or strains; hence, it will be developed with reference to principal stress coordinates.

7.2 DEVELOPMENT OF THE MODEL

The nomenclature used in conjunction with the nodal points, bars, axes, and dimensions for the model are indicated in Figure 34. The bar stiffnesses are shown below. The bars are indicated by the nodal points at the ends of the bars.

Bars (Between Nodal Points)	Stiffness
1-1	k_2
1-2	k_1
1-3	k_6
2-2	k_4
2-3	k_3
3-3	k_5

The model was developed using forces and displacements instead of stresses and strains. The forces and displacements are related to the stresses and strains, respectively, as follows:
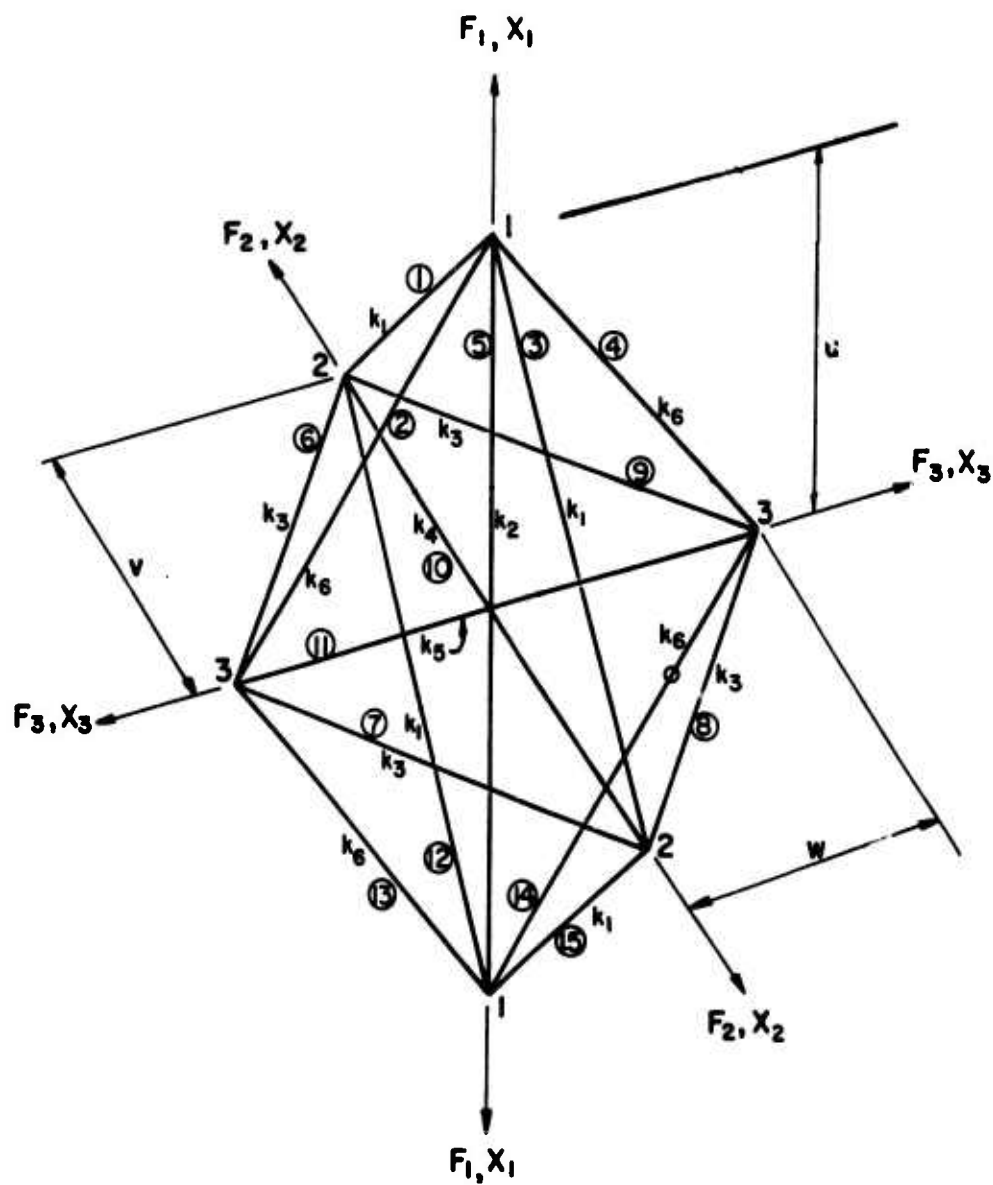
Figure 34. Diagram of Model

96

$$\sigma_1 = \frac{F_1}{2vw} \; ; \quad \sigma_2 = \frac{F_2}{2uw} \; ; \quad \sigma_3 = \frac{F_3}{2uv} \tag{7.1}$$

$$\varepsilon_1 = \frac{X_1}{u} \; ; \quad \varepsilon_2 = \frac{X_2}{v} \; ; \quad \varepsilon_3 = \frac{X_3}{w} \tag{7.2}$$

where the Fs are forces, the Xs are displacements, u, v, and w are the model dimensions, the σs are stresses, and the εs are strains.

The mathematical solution was formulated using the stiffness method of structural analysis.

The relations between the forces and displacements in the individual members (bars) of the model are expressed in matrix notation as

$$\{f\}_{15x1} = [k]_{15x15} \; \{x\}_{15x1} \tag{7.3}$$

where

{f}   is the bar column matrix

{x}   is the bar displacement column matrix, and

[k]   is the diagonal element stiffness matrix.

Matrix [k] is shown below.

$$[k] = \begin{bmatrix} k_1 & & & & & & & & & & & & & & \\ & k_6 & & & & & & & & & & & & & \\ & & k_1 & & & & & & & & & & & & \\ & & & k_6 & & & & & & & & & & & \\ & & & & k_2 & & & & & & & & & & \\ & & & & & k_3 & & & & & & & & & \\ & & & & & & k_3 & & & & & & & & \\ & & & & & & & k_3 & & & & & & & \\ & & & & & & & & k_3 & & & & & & \\ & & & & & & & & & k_4 & & & & & \\ & & & & & & & & & & k_5 & & & & \\ & & & & & & & & & & & k_1 & & & \\ & & & & & & & & & & & & k_6 & & \\ & & & & & & & & & & & & & k_1 & \\ & & & & & & & & & & & & & & k_6 \end{bmatrix} \qquad (7.4)$$

The relations between the bar displacements and the nodal displacements are expressed as

$$\{x\}_{15\times1} = [A]_{15\times3} \ \{X\}_{3\times1} \qquad (7.5)$$

where

$\{X\}$ is the nodal displacement column matrix, and

$[A]$ is the rectangular compatibility matrix.

The compatibility matrix in terms of the model dimensions u, v, and w is

$$[A] = \begin{bmatrix} u/a & v/a & 0 \\ u/b & 0 & w/b \\ u/a & v/a & 0 \\ u/b & 0 & w/b \\ 2 & 0 & 0 \\ 0 & v/c & w/c \\ 0 & v/c & w/c \\ 0 & v/c & w/c \\ 0 & v/c & w/c \\ 0 & 2 & 0 \\ 0 & 0 & 2 \\ u/a & v/a & 0 \\ u/b & 0 & w/b \\ u/a & v/a & 0 \\ u/b & 0 & w/b \end{bmatrix} \qquad (7.6)$$

where

$$a = \sqrt{u^2 + v^2}$$

$$b = \sqrt{u^2 + w^2} \qquad (7.7)$$

$$c = \sqrt{w^2 + v^2}$$

99

The relations between the nodal forces and the bar forces is expressed as

$$\{F\}_{3x1} = [B]_{3x15} \ \{f\}_{15x1} = [A^T]_{3x15} \ \{f\}_{15x1} \tag{7.8}$$

where

$\{F\}$ is the nodal force column matrix

$[B]$ is the rectangular equilibrium matrix, and

$[A^T]$ is the transpose of A, the capability matrix.

The equilibrium matrix is easily obtained by taking the transpose of the compatibility matrix.

Substituting Equation 7.5 into Equation 7.3 yields

$$\{f\} = [k][A]\{X\} \tag{7.9}$$

Substituting Equation 7.9 into Equation 7.8 yields

$$\{F\} = [A^T][k][A]\{X\} = [\bar{K}]\{X\} \tag{7.10}$$

where

$[\bar{K}]$ is the square 3x3 model stiffness matrix.

100

Now

$$[\bar{K}] = [A^T][k][A] \qquad (7.11)$$

hence

$$[\bar{K}] = \begin{bmatrix} 4k_1(\frac{u}{a})^2 + 4k_6(\frac{u}{b})^2 + 4k_2 & 4k_1 \frac{uv}{a^2} & 4k_6 \frac{uw}{b^2} \\ \\ 4k_1 \frac{uv}{b^2} & 4k_1(\frac{v}{a})^2 + 4k_3(\frac{v}{c})^2 + 4k_4 & 4k_3 \frac{vw}{c^2} \\ \\ 4k_6 \frac{uw}{b^2} & 4k_3 \frac{vw}{c^2} & 4k_6(\frac{w}{b})^2 + 4k_3(\frac{w}{c})^2 + 4k_5 \end{bmatrix}$$

$$(7.12)$$

For the model to yield isotropic results, the following conditions
were necessary:

1. The model dimensions u, v, and w, had to be equal to each other.

2. The bar stiffnesses k_1, k_3, and k_6 had to be equal to each other
   initially.

3. The bar stiffnesses k_2, k_4, and k_5 had to be equal to each other
   initially.

The stiffnesses were selected such that the stress-strain results
yielded by the model correspond to the stress-strain results obtained
from tests. This is explained in more detail later. The only requirements
on the model dimensions u, v, and w were that they be equal. This was
required for isotropic results as mentioned earlier. An arbitrary and

101

convenient value of 10 units was therefore assigned to each of the model dimensions. As a result

$$a = b = c = \sqrt{200} = 10\sqrt{2} \qquad (7.13)$$

The dimensional ratios then became

$$\left(\frac{u}{a}\right)^2 = \left(\frac{v}{c}\right)^2 = \left(\frac{w}{c}\right)^2 = \frac{uv}{a^2} = \frac{uw}{b^2} = \frac{1}{2} \qquad (7.14)$$

The force-stress and displacement-strain relationships can then be simplified and become

$$\sigma_1 = \frac{F_1}{200}; \quad \sigma_2 = \frac{F_2}{200}; \quad \sigma_3 = \frac{F_3}{200}$$

$$\qquad (7.15)$$

$$\epsilon_1 = \frac{X_1}{10}; \quad \epsilon_2 = \frac{X_2}{10}; \quad \epsilon_3 = \frac{X_3}{10}$$

The model stiffness matrix $\overline{K}$ can be simplified by substituting the relations 7.14 into matrix 7.12. Note that one cannot in general use conditions 2 and 3 for isotropic behavior to further simplify matrix 7.12. The member stiffnesses are related initially as required for isotropic behavior; however, they change in value dependent upon the displacements and may not remain equal to each other. The member stiffness functions are presented in the next section.

Substitution of relations 7.14 into matrix 7.12 yields

102

$$[\underline{K}] = \begin{bmatrix} 2k_1 + 2k_6 + 4k_2 & 2k_1 & 2k_6 \\ \\ 2k_1 & 2k_1 + 2k_3 + 4k_4 & 2k_3 \\ \\ 2k_6 & 2k_3 & 2k_3 + 2k_6 + 4k_5 \end{bmatrix}$$

$$(7.16)$$

7.3 MEMBER STIFFNESS FUNCTIONS

The stiffnesses of the individual members of the model were selected such that it was possible to simulate concrete behavior. The general shape of a stress-strain curve for a compressively loaded axis as observed from the testing program is shown in Figure 35(a).

The stiffness of a member is represented by the slope to the stress-strain curve. The slope of the stress-strain curve of Figure 35(a) has the general shape as shown in Figure 35(b).

The stiffness function (Figure 35(b)) possesses a negative region; hence, it could not be used as a stiffness function for a member in tension. The negative stiffness region produces a decrease in stress. A stress-strain curve for concrete in tension does not possess a region of decreasing stress, but fractures suddenly.

The exterior members of the model produce the lateral displacement and therefore, for most loading combinations it was not always necessary nor desirable for the exterior members to fail in compression. The exterior members could not possess a negative stiffness. A negative stiffness would result in a sudden change in the direction of the lateral displacements. No such sudden changes in lateral strains were observed during the testing

103
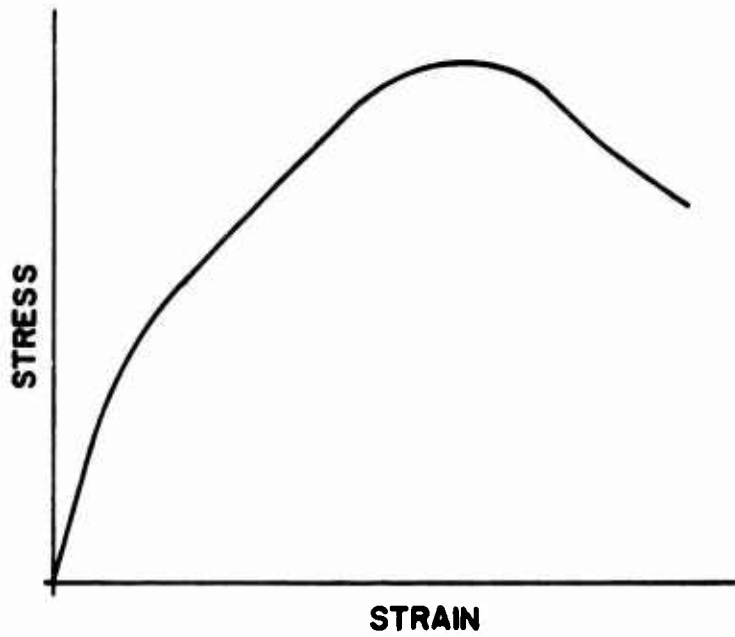
Figure 35(a)   Typical Stress-Strain Curve
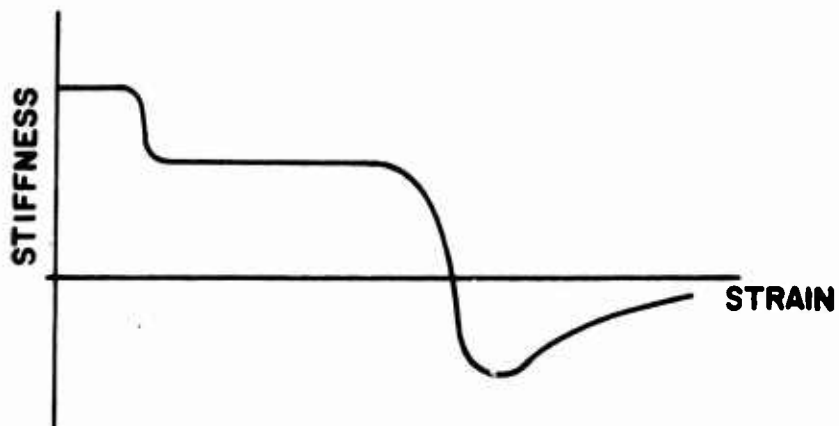
Figure 35(b)   Derivative (Slope) to Stress-Strain Curve

104

program; hence, the stiffness function shown in Figure 35(b) was not used for the members in tension or the exterior members in compression.

Generally stresses are determined from known strains; hence, it was convenient to take the member stiffnesses to be functions of the strains. The mathematical expression for the stiffness functions (Figure 35(b)) for the interior members (1-1, 2-2, 3-3) in compression are of the form

$$k = \frac{(1 + d)k_2}{\left[1 + \left(\frac{g(x)}{X_0}\right)^n\right]^{1+1/n}} + \frac{dk_2(1 + (1 - cn_1)\left(\frac{g(x)}{X_1}\right)^{n_1})}{\left[1 + \left(\frac{g(x)}{X_1}\right)^{n_1}\right]^2} \qquad (7.17)$$

where

k_2 is the initial stiffness of the member

d   is a constant which determines the influence of the individual terms upon the stiffness k

c   is a constant which affects the stress drop-off portion of the stress-strain curves once the peak stress has been reached

n, n_1 are integers which determine the rate at which the stiffness changes

X_0, X_1 are values of the variables at which the stiffness k changes to a different value

$g(x), f(x)$ are functions of the model displacements. They are listed later.

The general shape of the above stiffness function is shown below.

105
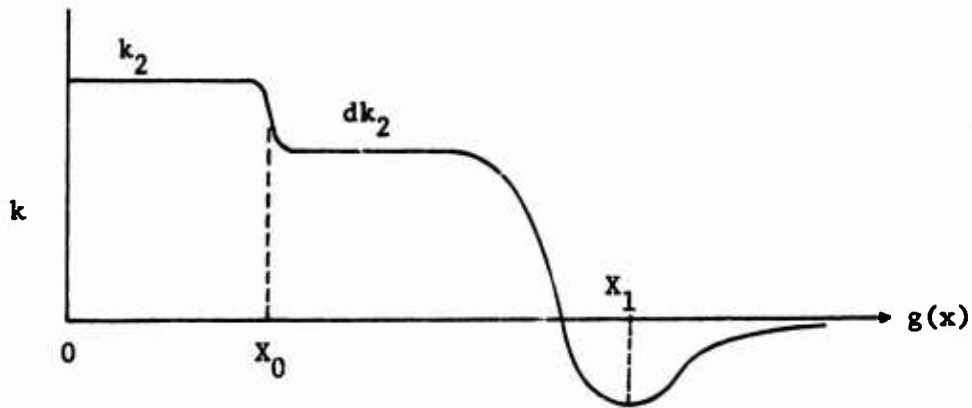
The stiffness functions for the exterior members in compression and of all members in tension is of the form

$$k = \frac{k_1}{\left[1 + \left(\frac{h(x)}{X_{11}}\right)^n\right]^{1+1/n}} \qquad (7.18)$$

where

k_1 is the initial member stiffness

n is an integer influencing the rate of change of k

$h(x)$ is a function of the displacements

X_{11} is the value of $h(x)$ at which the stiffness k changes value.

The general shape of this function is shown below.
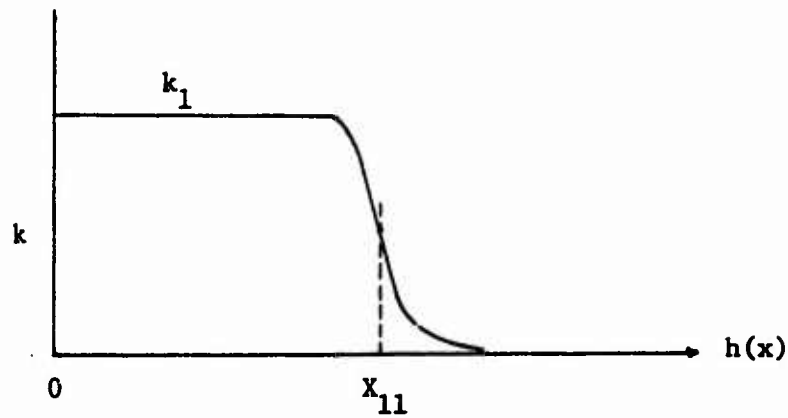
The functions $g(x)$ and $h(x)$ for the different elements in compression are given below. The stiffness functions require that these variables be positive; hence, the absolute values are shown.

Member Stiffness	$h(x)$
k_1	$\lvert X_1 + X_2 - 2X_3 \rvert$
k_3	$\lvert X_2 + X_3 - 2X_1 \rvert \qquad (7.19)$
k_6	$\lvert X_1 + X_3 - 2X_2 \rvert$

and

Member Stiffness	$g(x)$
k_2	$\lvert X_1 - \min(X_2,\ X_3) \rvert$
k_4	$\lvert X_2 - \min(X_1,\ X_3) \rvert \quad (7.20)$
k_5	$\lvert X_3 - \min(X_1,\ X_2) \rvert$

107

The functions h(x) for the elements in tension are given below.

Member Stiffness	h(x)	
k_2	$\lvert X_1 \rvert$	
k_4	$\lvert X_2 \rvert$	(7.21)
k_5	$\lvert X_3 \rvert$	
k_1	$.707 \lvert X_1 + X_2 + X_3 \rvert$	
k_3	$.707 \lvert X_1 + X_2 + X_3 \rvert$	(7.22)
k_6	$.707 \lvert X_1 + X_2 + X_3 \rvert$	

The variables used in the above stiffness functions in compression were selected such that the model would yield an indefinite strength for the triaxial case of equally applied loads. This is in conformity with test results.

7.4 SOLUTION OF THE MODEL EQUATIONS

The model equations are

$$F = A^T kAX = \overline{\underline{K}}X \qquad (7.23)$$

The matrix $\overline{K}$ is a function of the displacements, hence

$$F = \overline{\underline{K}}(X)X \qquad (7.24)$$

The above equations are easily solved provided that the displacements X are given and the forces F are determined; however, in the development of the stiffness values and control parameters utilized in the model, it was necessary to determine the displacements corresponding to a given set of forces. Inversion of the above equations was difficult if not impossible due to the nonlinear nature of $\overline{\underline{K}}(X)$. This difficulty was avoided by using a procedure suggested by Richard and Goldberg (19). They suggested converting nonlinear equations to a set of linear ordinary first order differential equations. Equations 7.24 are then converted to the differential equations:

$$dF = \overline{\underline{K}}(X)dX \tag{7.25}$$

Methods exist for numerically solving these differential equations. For simplicity, Eulers point-slope method was used. Equation 7.25 then becomes

$$\Delta F = \overline{\underline{K}}(X)\Delta X \tag{7.26}$$

with

$$F_{i+1} = F_i + \Delta F$$

$$\tag{7.27}$$

$$X_{i+1} = X_i + \Delta X$$

where the equations now yield the load and displacement increments instead of the total load and total displacement.

More accurate and sophisticated methods of numerical integration could be used; however, Eulers method is the simplest. Using Eulers method does restrict the size of the increments. They should be kept small to reduce errors in integration. A more accurate integration procedure may be utilized.

7.5 MODEL STIFFNESS CONSTANTS

The initial member stiffness values were selected such that the model would closely simulate the behavior of concrete as observed from a uniaxial test. The relationships between test values and the initial model stiffness values were obtained utilizing the following conditions:

1. Isotropic behavior of model (see Section 7.2).

2. The initial modulus of elastiticy E_o and the initial Poisson's ratio μ are known from a uniaxial test.

3. During the first stress and strain increment, the member stiffnesses are constant.

These conditions are not sufficient to determine the entire stress-strain curves. They control only the initial slopes to the stress-strain curves. The factors which determine the shape of the entire stress-strain curves are presented in Section VIII.

The model equations 7.26 can be written as

$$\begin{Bmatrix} \Delta F_1 \\ \Delta F_2 \\ \Delta F_3 \end{Bmatrix} = \begin{bmatrix} K_{11} & K_{12} & K_{13} \\ K_{12} & K_{22} & K_{23} \\ K_{13} & K_{23} & K_{33} \end{bmatrix} \begin{Bmatrix} \Delta X_1 \\ \Delta X_2 \\ \Delta X_3 \end{Bmatrix} \qquad (7.28)$$

where K_{ij} are the elements of the model stiffness matrix.

For the uniaxial case, $\Delta F_2 = \Delta F_3 = 0$ and $\Delta X_2 = \Delta X_3$. The above equations then reduce to

$$\begin{Bmatrix} \Delta F_1 \\ 0 \\ 0 \end{Bmatrix} = \begin{bmatrix} K_{11} & K_{12} & K_{13} \\ K_{12} & K_{22} & K_{23} \\ K_{13} & K_{23} & K_{33} \end{bmatrix} \begin{Bmatrix} \Delta X_1 \\ \Delta X_2 \\ \Delta X_2 \end{Bmatrix} \quad \begin{matrix} (a) \\ (b) \\ (c) \end{matrix} \qquad (7.29)$$

Now Poisson's ratio is defined as

$$\mu = \frac{\text{lateral strain}}{\text{axial strain}}$$

hence

$$\mu = - \frac{|\epsilon_2|}{|\epsilon_1|} = - \frac{|\Delta X_2|}{|\Delta X_1|} \qquad (7.30)$$

Note that for ΔX_2 to be equal to ΔX_3, the following relationships must be initially satisfied:

111

$$K_{12} = K_{13}$$

<div align="right">(7.31)</div>

$$K_{22} = K_{33}$$

These two conditions are satisfied by the isotropic requirements mentioned earlier. Using the isotropic requirements regarding the element stiffness, the model matrix 7.12 becomes

$$
\begin{bmatrix}
4k_1 + 4k_2 & 2k_1 & 2k_1 \\
\\
2k_1 & 4k_1 + 4k_2 & 2k_1 \\
\\
2k_1 & 2k_1 & 4k_1 + 4k_2
\end{bmatrix}
\qquad (7.32)
$$

remembering that this specialized matrix is valid only for the first stress and strain increment.

The following mathematical development also applies only to the first stress and strain increment.

Recalling Equation 7.29(b).

$$K_{12}\Delta X_1 + (K_{22} + K_{23})\Delta X_2 = 0$$

or

$$\frac{\Delta X_2}{\Delta X_1} = \frac{-K_{12}}{K_{22} + K_{23}}$$

Now

$$\mu = -\frac{|\Delta X_2|}{|\Delta X_1|} = \frac{-K_{12}}{K_{22} + K_{23}} \qquad (7.33)$$

Substituting the values for K_{12}, K_{22}, and K_{23} into the above equation yields

$$\mu = \frac{k_1}{3k_1 + 2k_2} \qquad (7.34)$$

The second relationship is obtained by considering the initial modulus of elasticity as obtained from a uniaxial test. The initial modulus of elasticity is

$$E_o = \frac{\Delta\sigma_1}{\Delta\varepsilon_1} = \frac{\Delta F_1}{2u^2 \Delta X_1/u} = \frac{\Delta F_1}{2u\Delta X_1}$$

or

$$2uE_o = \frac{\Delta F_1}{\Delta X_1} \qquad (7.35)$$

Now recall Equation 7.29(a)

$$\Delta F_1 = K_{11}\Delta X_1 + (K_{12} + K_{13})\Delta X_2$$

or

113

$$\frac{\Delta F_1}{\Delta X_1} = K_{11} + (K_{12} + K_{13}) \frac{\Delta X_2}{\Delta X_1} \qquad (7.36)$$

Recall that

$$\mu = - \frac{|\Delta X_2|}{|\Delta X_1|}$$

therefore,

$$2uE_o = \frac{\Delta F_1}{\Delta X_1} = K_{11} - (K_{12} + K_{13})\mu \qquad (7.37)$$

Substitution of the stiffnesses for K_{11}, K_{12}, K_{13}, K_{22}, and K_{23} yields

$$2uE_o = 4k_1 + 4k_2 - 2k_1\mu$$

or

$$uE_o = 2(k_1 + k_2) - k_1\mu = (2 - \mu)k_1 + 2k_2 \qquad (7.38)$$

Recall

$$\mu = \frac{k_1}{3k_1 + 2k_2}$$

Solving Equations 7.34 and 7.38 for k_1 and k_2 yields:

$$k_1 = \frac{uE_o\mu}{1 - \mu - 2\mu^2} \qquad (7.39)$$

114

$$k_2 = \frac{uE_o(1 - 3\mu)}{2(1 - \mu - 2\mu^2)} \qquad (7.40)$$

The two above relationships yield the initial stiffnesses k_1 and k_2 when given the initial modulus of elasticity and initial Poisson ratio from a uniaxial test.

Again the mathematical development in this section applies only to the first stress and strain increment.

SECTION VIII

MODEL CHARACTERISTICS

8.1 CONTROL PARAMETERS

A number of control parameters are incorporated into the model.
These parameters determine the peak stress values and the strain at the
peak stresses as well as the general shape of the predicted stress-
strain curves. The function of the control parameters is to change the
stiffnesses of the individual members of the model. The parameter
values were determined by the method of successive attempts, that is, for
a given loading proportion, the parameter values were changed until the
model approximately predicted the test results. The model was required
to approximately predict the experimental stress-strain curves for all
loaded axes. Control parameter values were obtained for several loading
proportions. An equation was then fitted to the parameter values. This
empirical equation was then incorporated into the computer program for
the model solution and again verified by comparing the model predicted
results to the test results. In general the control equations were
different for each loading region, that is, a set of control equations
was used for the compression-compression-compression region and a dif-
ferent set of control equations was used for the compression-compression-
tension region.

The control equations (listed later in this section) are functions of
the stress increment ratios $\Delta\sigma_3/\Delta\sigma_1$ and $\Delta\sigma_2/\Delta\sigma_1$. The stress increments are
not initially known for a given set of strain increments; hence, the control

116

parameters are determined from the previous set of stress increments. It is for this reason that several passes through the computer program for model solution must be made to obtain a better result. This difficulty may possibly be lessened by using a more accurate integration procedure.

It would have been more desirable to express the control equations as functions of the strains; however, this was not practicable during the model development stage. The predicted strains changed considerable whenever the control constants were changed.

The control parameters are listed below along with their effect on the model results. The terminology used in conjunction with the parameter descriptions with regard to a typical stress-strain curve is indicated in Figure 36. The parameter names are the same as used in the computer program for the model.

X10 - This parameter controls the stiffness of the exterior diagonal members of the model. It has a pronounced effect on the general slope of the intermediate part of the stress-strain curve and on the magnitude of the lateral deformations. It was used primarily to regulate the lateral deformations.

XOC2 - This parameter partially determines the stiffness of the interior members of the model. Particularly, it controls the stiffness value of the second term of the stiffness function 7.17 listed in Section VII. It determines the strain at which the peak stress occurs. It also affects the magnitude of the peak stress and the range of the intermediate part of a predicted stress-strain curve.

117
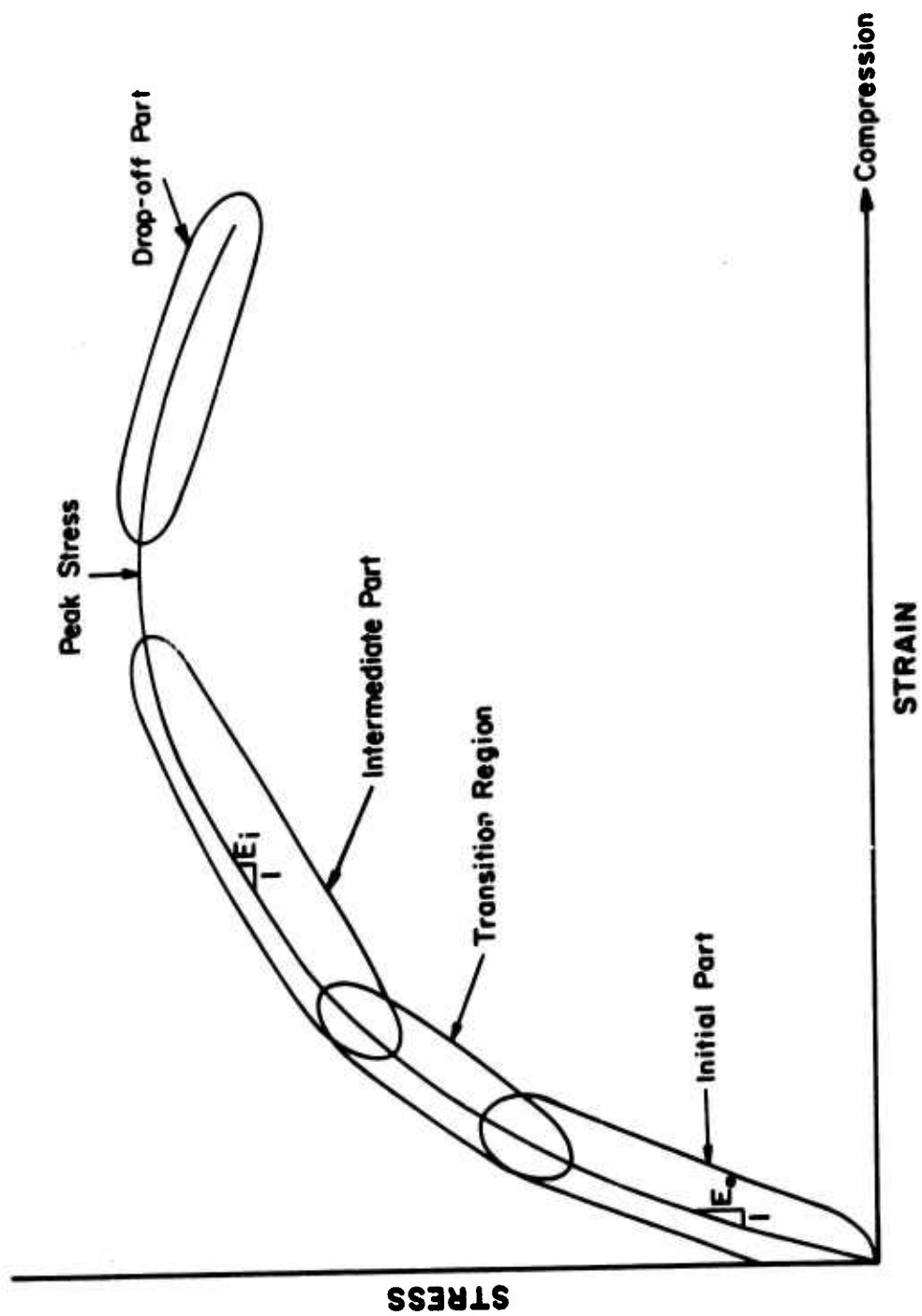
Figure 36. Strain Regions of a Compressive Stress-Strain Curve

DCN - This parameter governs the relative effect of the individual

terms of the stiffness function 7.17. It affects the slope

of the intermediate part as well as the drop-off of the stress-

strain curve. The only stiffness function that can take on

negative values is the second term of the stiffness function

7.17.

X21 - This parameter controls the value of the first term of the

stiffness function 7.17. It determines the strain at which

the interior members decrease in stiffness. The value of this

parameter determines the point at which the stress-strain curve

changes from the initial part to the intermediate part. It

also determines the range of the initial part and influences

the range of the intermediate part of the stress-strain curves.

ET - This parameter governs the strain at which the model members

fail in tension. It controls the maximum tensile strength

that is obtained. Whenever a member fails in tension, the

stress in that member must be set to zero. A zero stiffness

will result in a constant stress level which is not consistent

with actual concrete behavior.

CON - This parameter controls the drop-off part of the stress-strain

curves. It also partially controls the total stress decrease

and the slope of the downward part.

XOT - This parameter has a value equal to or slightly less than ET.

Its function is to provide the slight nonlinear part of a

tension stress-strain curve near the ultimate tensile strength.

The control parameter equations are listed below along with the loading regions they control. The notation

$$B = \Delta\sigma_3/\Delta\sigma_1$$

$$G = \Delta\sigma_2/\Delta\sigma_1$$

is used to simplify the listing of the control equations.

(a) Biaxial compression

X10 = 0.055

XOC2 = 0.0265 + G(0.156 + (G - 0.1)(-0.685 + (G - 0.2)(1.638

  + (G - 0.4)(-2.81 + (G - 0.6)(3.705 + (G - 0.8)(-4.25

  + (G - 0.9)(3.867))))))))

DCN = 1.0 - 0.5G

X21 = 0.03 - 0.0125G

ET = 0.0008

CON = 1.05 + 0.5G

XOT = 0.0008

(b) Triaxial compression

X10 = 0.05 + 0.5B + 3.0B (B - 0.1) + (-0.06 + 1.80B)G

  -(0.05 + 1.50B + 7.50B (B - 0.1))G(G - 0.2)

XOC2 = 0.035 + 1.65B + 3.30B (B - 0.1) + (0.022 - 0.72B + 23.35B

  (B - 0.1))G + 3.75B (B - 0.1)G(G - 0.2) - 50.0B (B - 0.1)

  G(G - 0.2)(G - 0.4)

DCN = 1.0 - 6.95B + 34.75B(B - 0.1) - 4.0BG + 5.0BG(G - 0.2)

X21 = (0.04 - 0.01B - 0.25B(B - 0.1) tanh(G(9.70 - 57.0B + 235.0B

  (B - 0.1)))

ET = 0.008

CON = 1.0

XOT = 0.0008

(c) Uniaxial compression, tension; Biaxial compression-tension;
Triaxial compression-compression-tension, compression-tension-
tension

X10 = 0.055

XOC2 = 0.0265

DCN = 1.0

X21 = 0.055

$ET = ((0.02671 + 0.1668B)G) \exp((-20.383 + 7.773B)G^{(1.25 - 0.5B)})$
$+ 0.0012$

CON = 1.0

XOT = 0.0008

(d) Biaxial tension; Triaxial tension

X10 = 0.055

XOC2 = 0.0265

DCN = 1.0

X21 = 0.055

$ET = 0.0012 - 0.0001G(3 + 3.25B)$

XOT = 0.0008

Two integers, designated NT and NC in the computer program, also have
an influence on the shape of the predicted stress-strain curves. NT and NC
are the names used in the computer program to represent the integers n and
n_1 used in conjunction with the member stiffness functions described in

121

Section VII. The values of these integers affect the quickness or sharpness of the transition zones between the initial and intermediate part and in the vicinity of the peak stresses.

A detailed description of the computer program for the model is presented in Appendix I.

8.2 COMPARISON OF MODEL PREDICTED RESULTS WITH TEST RESULTS

The model predicted results and the test results for several different loading proportions are shown in Figures 37 through 50. Stress-strain curves obtained from tests are shown along with the model predicted results for typical cases. The comparison between model predicted and test results for compressive loads are generally quite good but the model predicted results for the intermediate and minor stresses are usually slightly larger than the test results.

The comparison between model and test results are generally not as good for cases where a tensile stress is applied to an axis. There was also a problem in measuring the smaller strains associated with tensile loading. The extensometers were designed for large strain measurements and may not be very accurate for small strains.

The model does not usually produce lateral deformations as large as those observed from tests. The model geometry is such that a maximum possible ratio of minor strain to major strain is unity. This does not permit the large lateral deformations that were observed in the direction of the minor stress.

The comparison is not always very close after the peak stress had

122

been obtained. The model continues predicting stresses and strains due
to the given loading proportions. In conducting the tests, it was impos-
sible to maintain a given loading proportion once the peak stresses had
been obtained. A comparison of predicted and test values beyond the peak
stresses is therefore not logical.

8.3 MODEL LIMITATIONS

The model was developed in principal stress and strain coordinates;
hence, the model itself predicts principal stresses from principal strains.
For coordinate systems other than principal stress and strain coordinate
systems, the appropriate stress and strain transformation relations must
be used in conjunction with the model.

The control equations were based on a limited number of tests; there-
fore, a limited number of different loading proportions. In triaxial
compression, failure was not accomplished for minor to major stress ratios
above 0.2. The model predicted results are therefore not verified by tests
for minor to major stress ratios above 0.2. The accuracy of predicted
stress-strain values obtained by extrapolation beyond the value of 0.2 is
unknown.

There was a relatively large number of test results available in the
compression region within the limitations mentioned above; however, in the
cases where there was tension on at least one of the axes, the number of
test results was limited. Tension tests were much more difficult and time
consuming than were the compression tests. The region between test points
is greater and not all of these gaps in test results were checked. The

model probably yields results similar to results obtained from tests. During testing, no sudden changes in concrete behavior were detected within a given region.

The testing program utilized essentially one concrete strength; however, there was batch to batch variation. It is believed that the batch to batch variation is small in comparison to the variation that would have been obtained using different concrete strengths. In the model development, the average result was used; hence, this would relate to an average concrete strength.

8.4 OTHER CONCRETE STRENGTHS

The model control parameters were based on experimental stress-strain curves for tests on a single nominal concrete strength. For the model to be of a general use, it would be helpful if it could be easily adjusted to predict stress-strain values for any concrete strength. The effect of different concrete strengths and the effect of different types of aggregate used in the concrete can be determined by additional tests only.

From limited evidence (Part II), it appears that by using the initial tangent modulus for a concrete of any strength, the initial slopes to the predicted stress-strain curves will compare favorably to the initial slopes of experimental stress-strain curves. The peak stresses and the strains at the peak stresses as well as the shape of the predicted stress-strain curves are determined by the control equations. Indications are that the control equations must be altered if the model is to closely predict stress-strain values for different concrete strengths. Adjustments would have to

be made to alter the peak stress, the strain at the peak stress, and the shape of the stress-strain curves. Changing the control equations is no small task. The nature of the control equation alterations for different concrete strengths and possibly different concrete mixes is not known at this time.
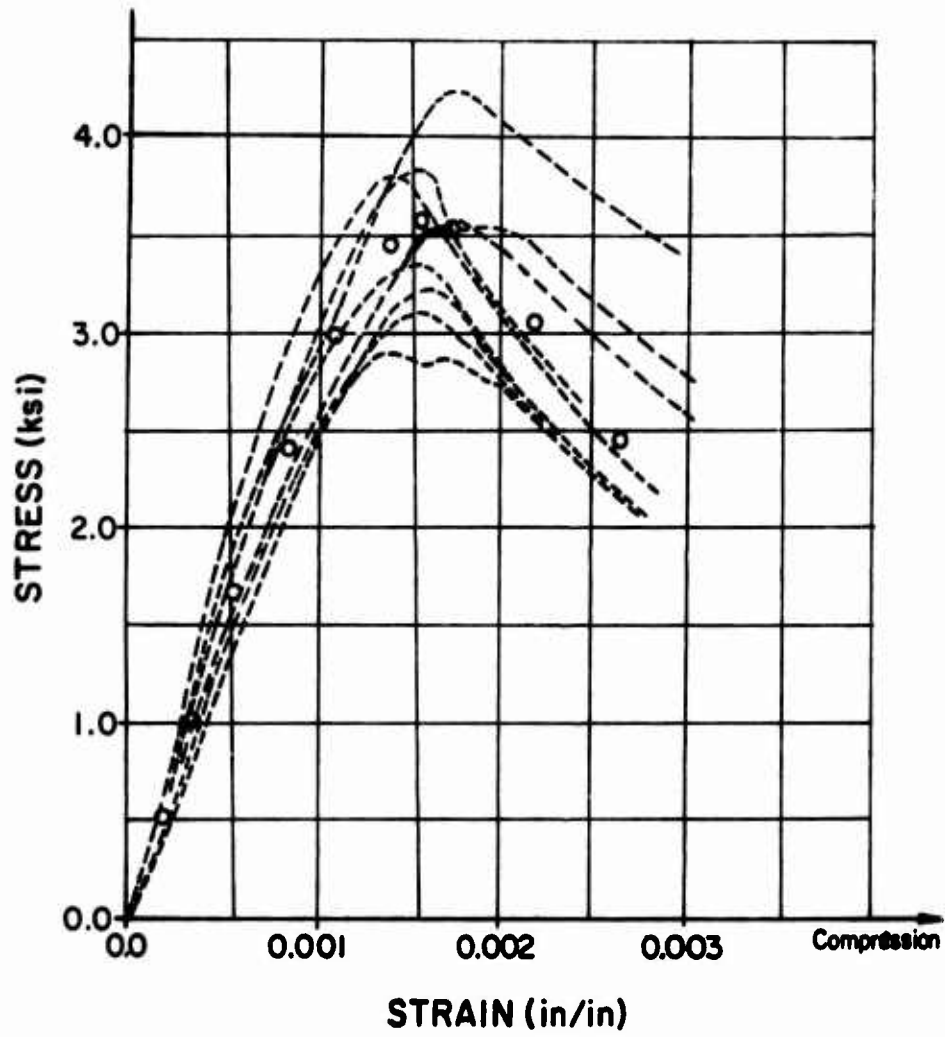
Figure 37. Uniaxial Compressive Stress-Strain Curves

126
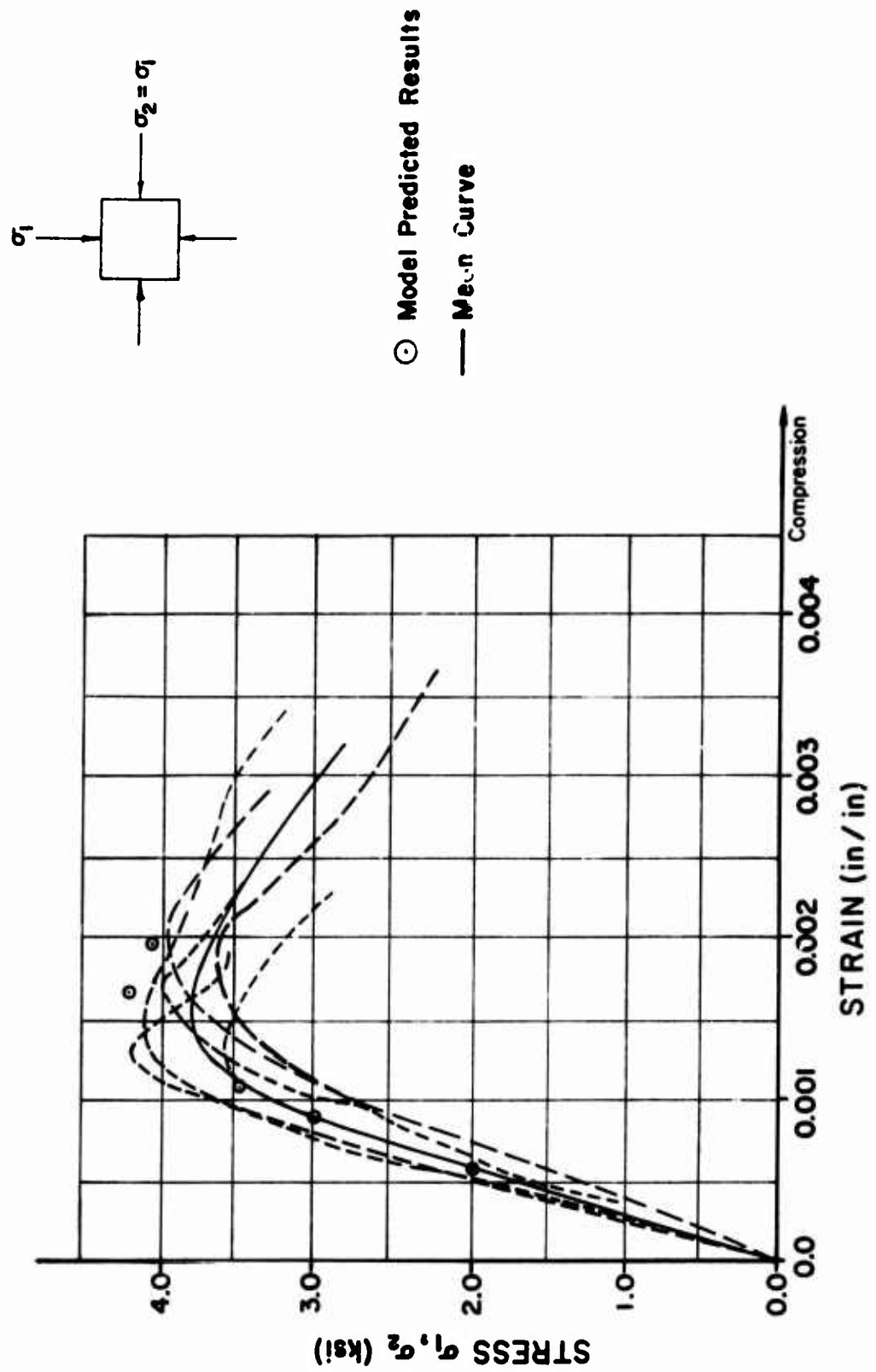
Figure 38. Biaxial Compression Stress–Strain Curves

127
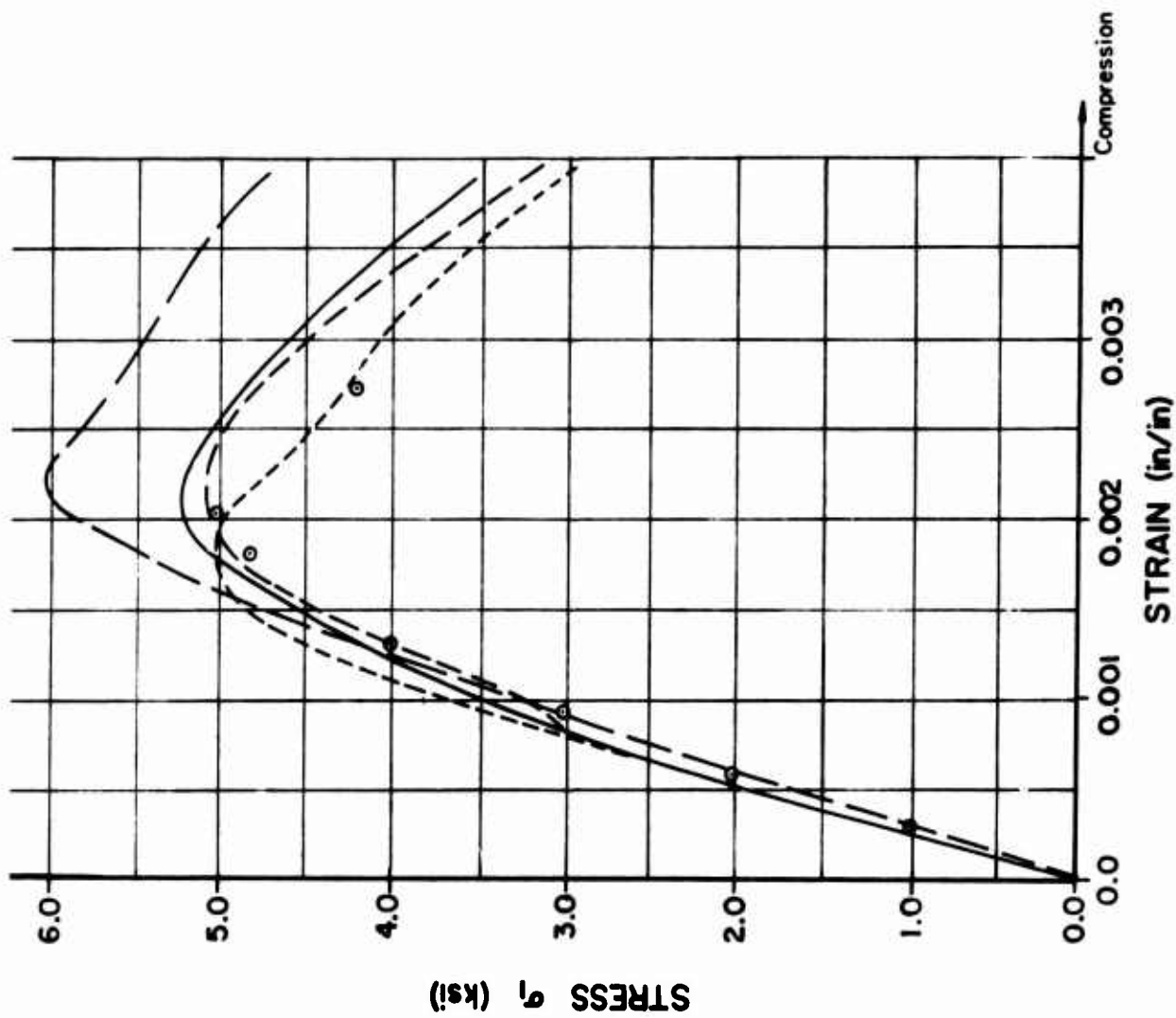
Figure 39. Biaxial Compression Stress-Strain Curves
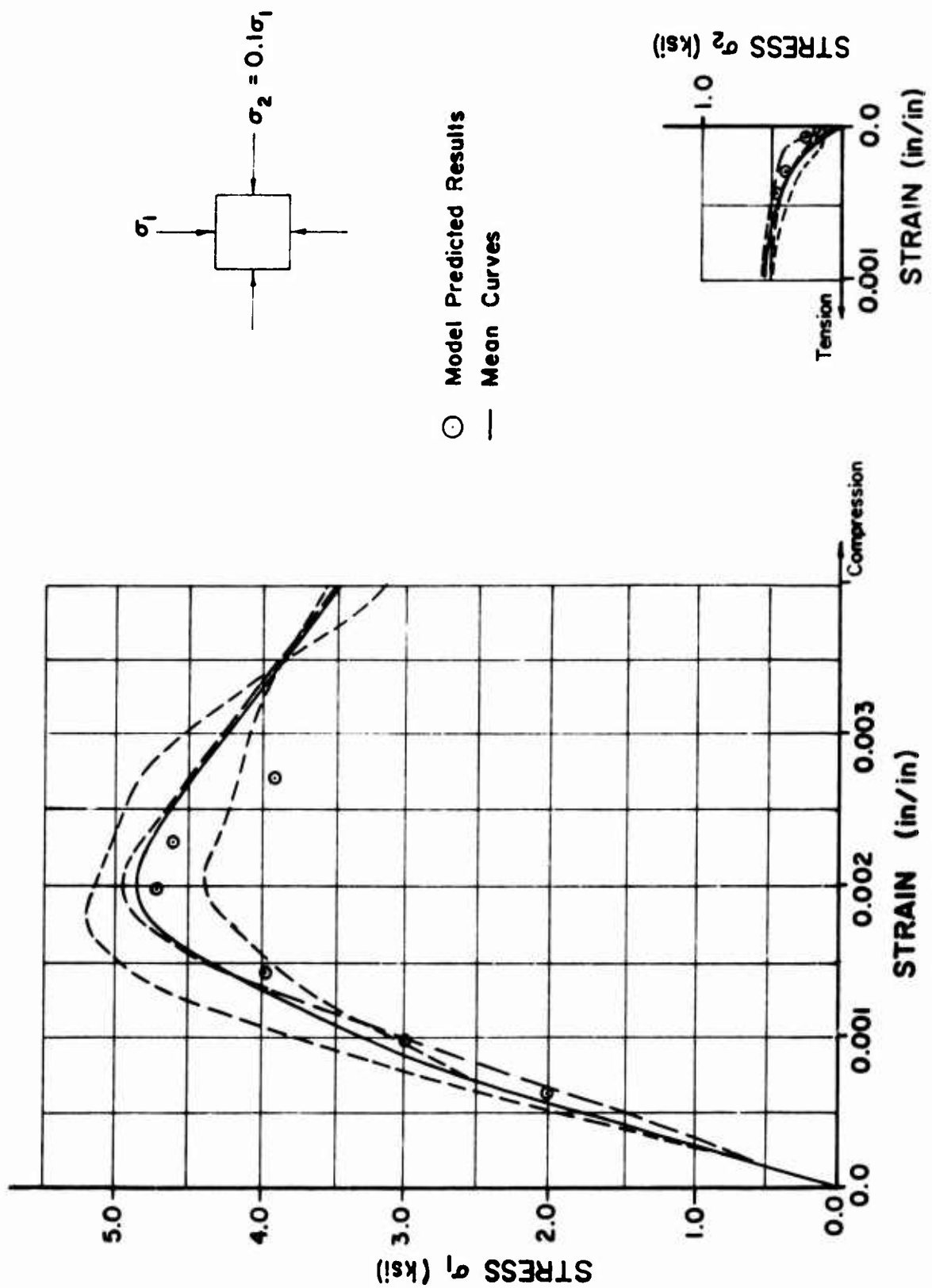
Figure 40. Biaxial Compression Stress-Strain Curves

129
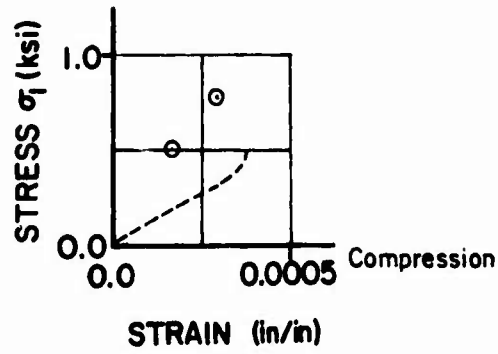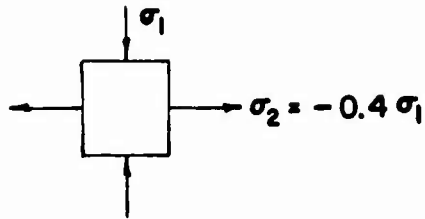
⊙ Model Predicted Results

Figure 41. Biaxial Compression-Tension Stress-Strain Curves

130

Figure 42. Biaxial Tension Stress-Strain Curves

131
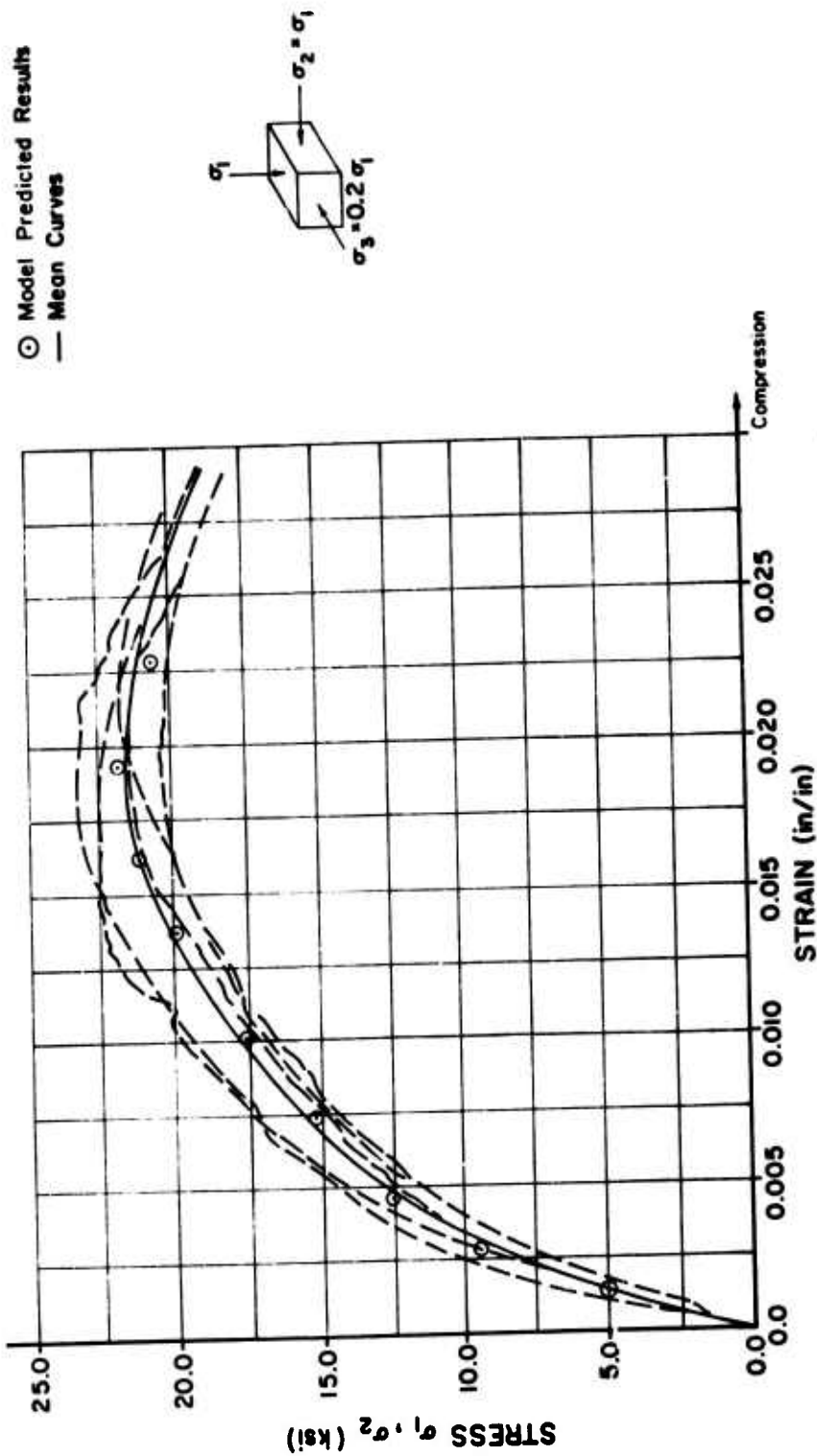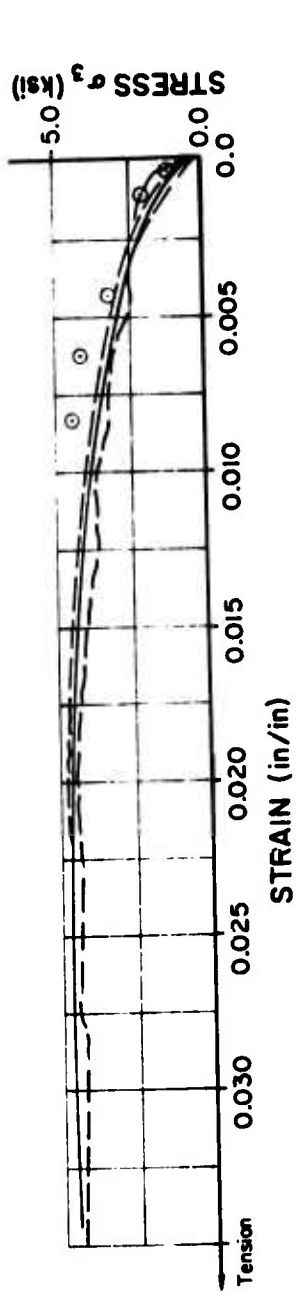
FIGURE 43. TRIAXIAL COMPRESSION STRESS-STRAIN CURVES

132
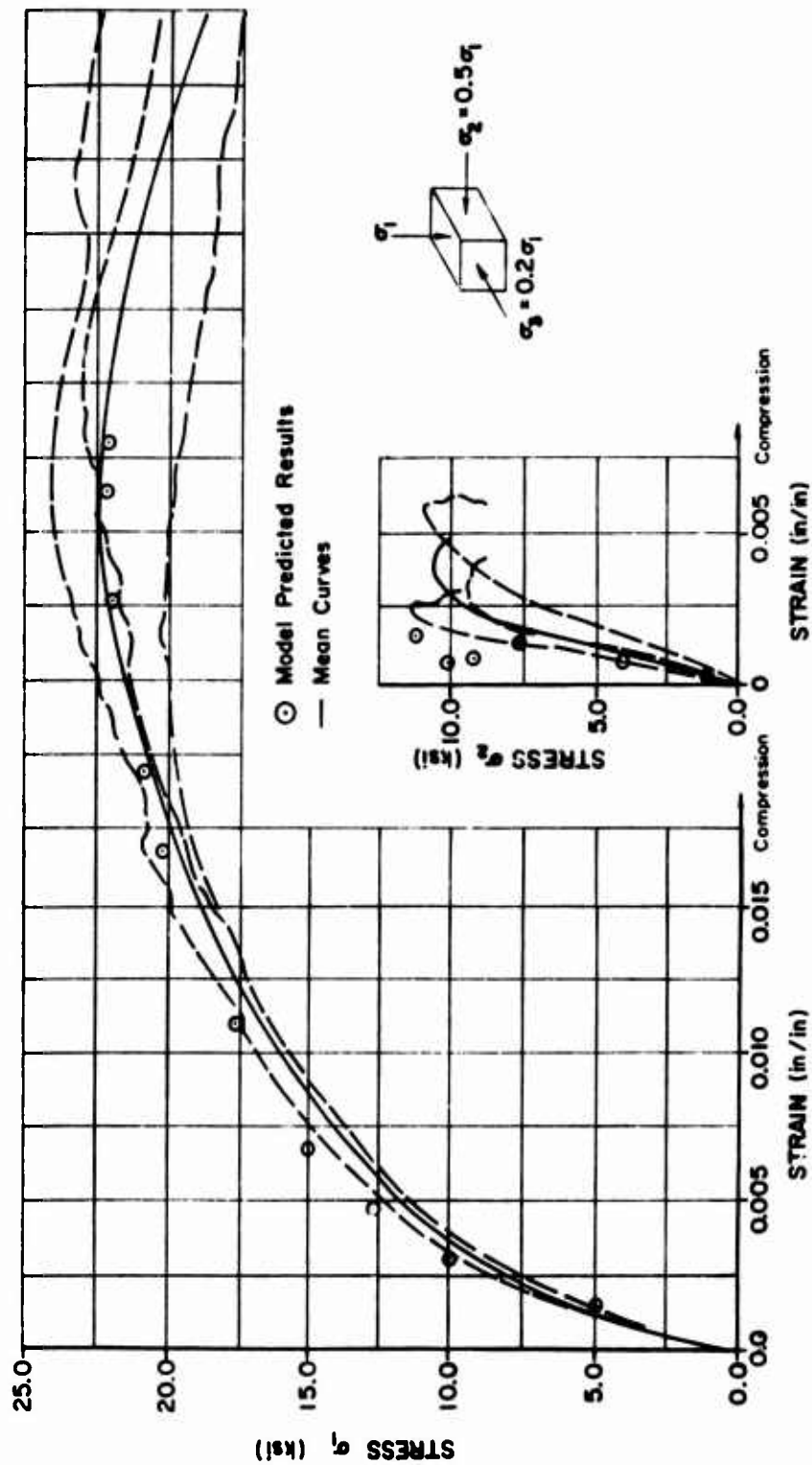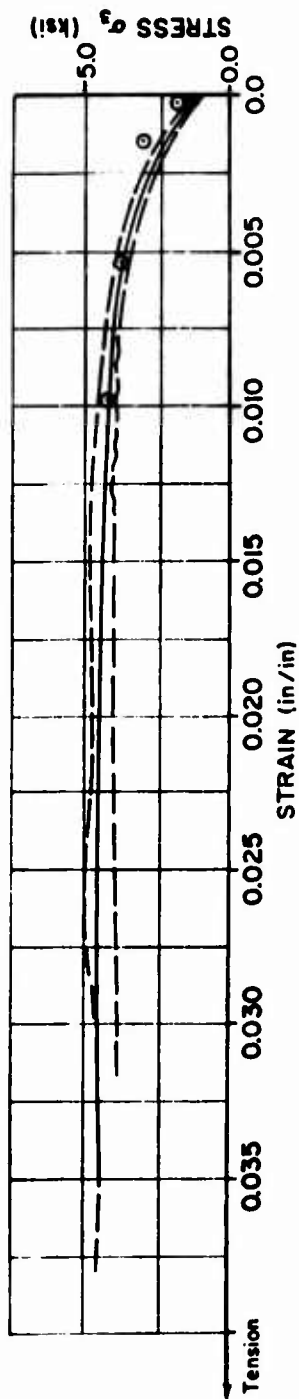
FIGURE 44. TRIAXIAL COMPRESSION STRESS-STRAIN CURVES

133
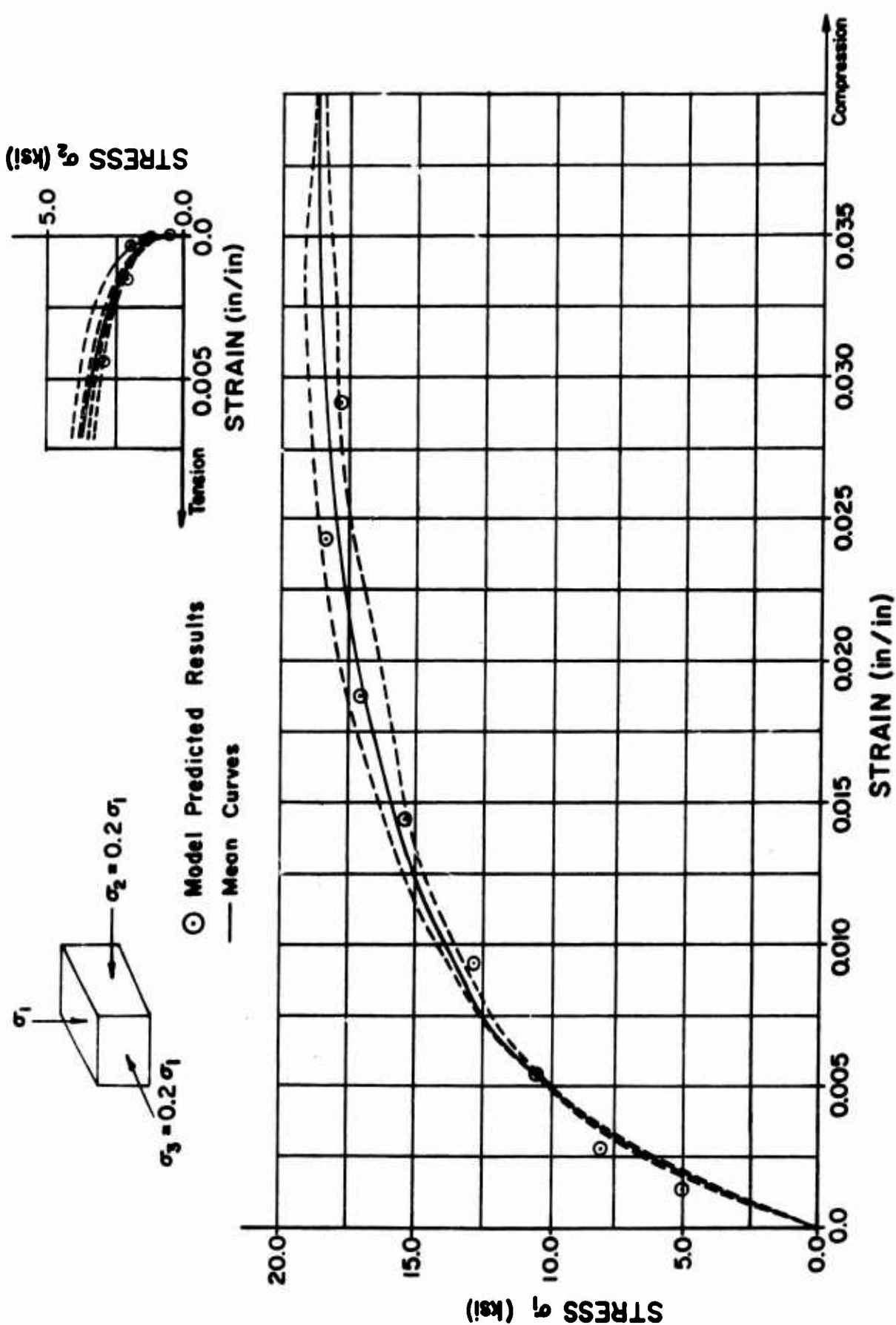
Figure 45. Triaxial Compression Stress-Strain Curves
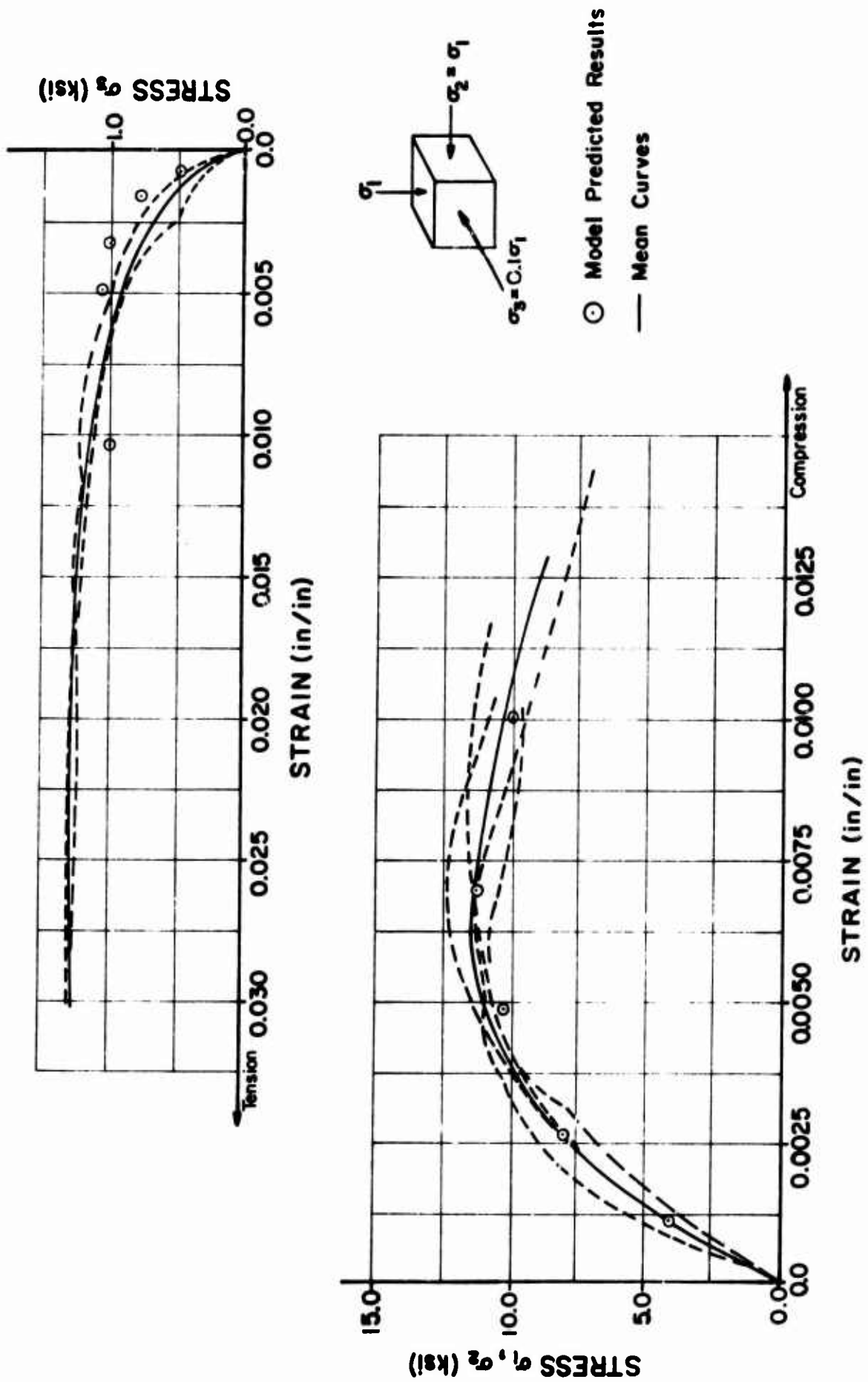
Figure 46. Triaxial Compression Stress-Strain Curves
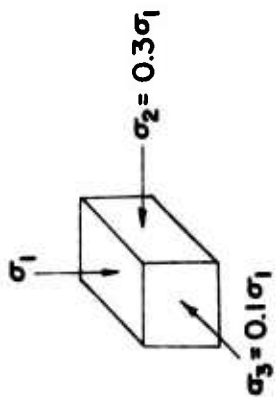
Figure 47. Triaxial Compression Stress-Strain Curves

136
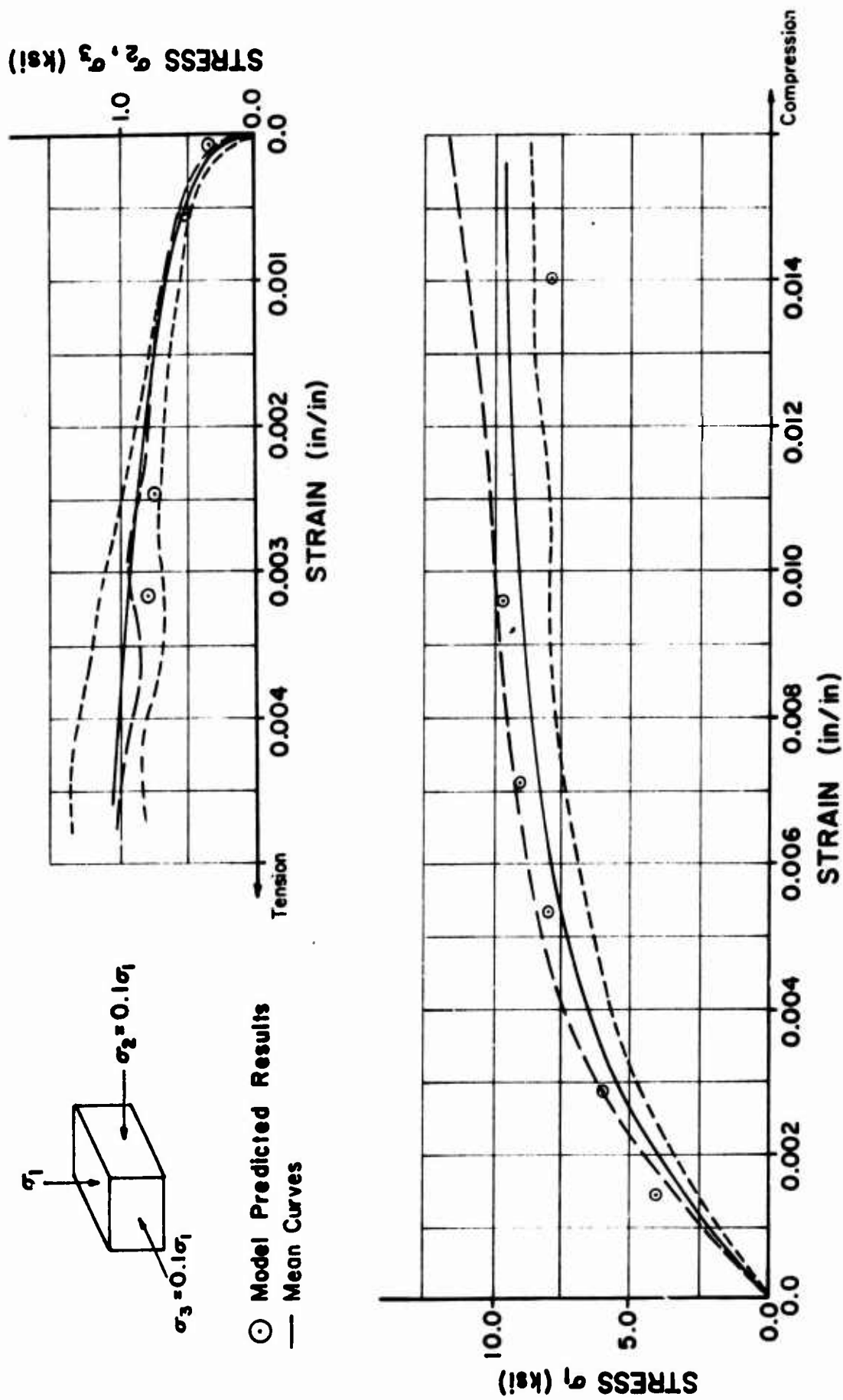
Figure 48. Triaxial Compression Stress-Strain Curves

137
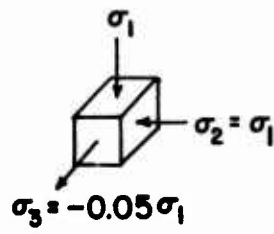
Figure 49. Triaxial Compression-Tension Stress-Strain Curves
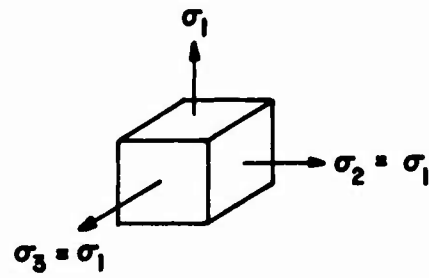
○ Model Predicted Results
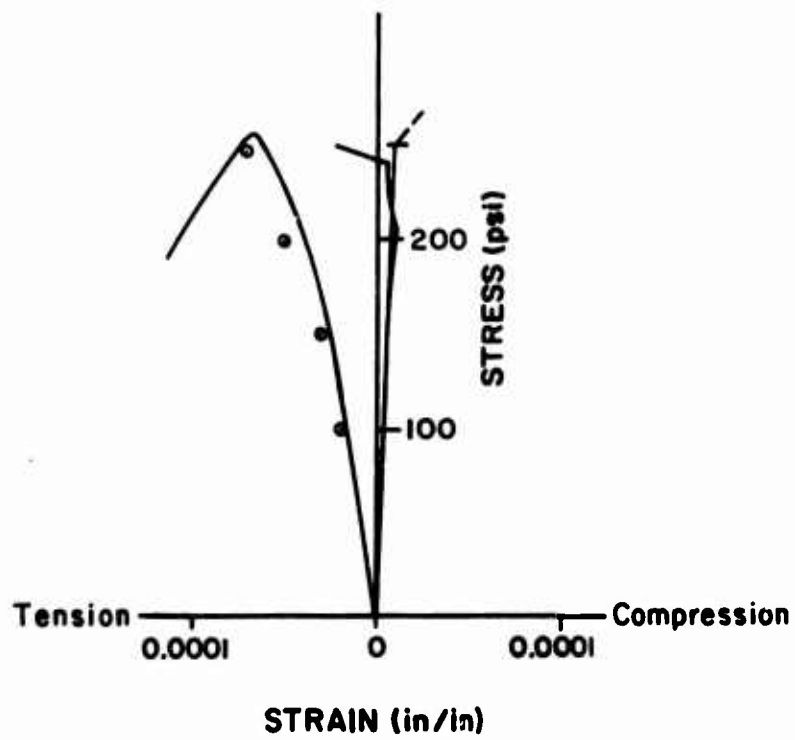
Figure 50.   Triaxial Tension Stress-Strain Curves

139

SECTION IX

CONCLUSIONS AND RECOMMENDATIONS

9.1 CONCLUSIONS

This study was undertaken to determine the behavior of plain concrete under combined stresses and to formulate computer orientated constitutive relations for concrete. One nominal concrete strength was tested under various loading combinations. The loading combinations included the uniaxial, biaxial, and triaxial states of stress with various combinations of compressive and tensile stresses. The test specimens were three-inch cubes. The test information was obtained as stress-strain records for the three principal directions of the cubical test specimens. Generally the loads were applied such that the ratio of the loads relative to each other was constant. In a few cases, an incremental loading was used.

Several items were discovered or observed during the course of the experimental investigation. The effect of friction in testing cubes was considerable. A much higher apparent strength was obtained in tests not utilizing friction reduction methods; consequently, friction reducing pads were utilized throughout the testing program. The friction reducing pads consisted of two polyethelene sheets with grease between them. These pads were placed between the platens and cube surfaces in the compression tests.

During the testing program it was noted that somewhat different strength values were obtained depending upon the orientation of the cube with respect to the applied loads and the direction of casting. The cubes

were not isotropic. Visual examination of the cubes clearly indicated that the orientation of the coarse aggregate was not the same in the direction of casting. It appears that spherical aggregate would have to be used to eliminate the anisotropic condition. The tensile strength in the direction of casting was approximately 30 percent less than the tensile strength in one of the other directions. A similar observation was made by Ash (31) during a study in which specimens were loaded in direct tension. The tensile strength in the direction of casting was approximately 24 percent less than the tensile strength in the direction perpendicular to casting. He attributed the difference in strength to bleeding in concrete which produced weak regions beneath aggregate particles. The uniaxial compressive strength was not greatly affected by the orientation of the cubes; however, the biaxial and triaxial test results were noticeably affected by the cube orientation.

The failure mode of the cubes was identical to that described by several investigators. The cubes split, apparently in tension, in the direction of the lowest compressive stress or the highest tensile stress. The cubes always expanded in those directions. The fracture planes were generally perpendicular to the direction in which the lowest compressive stress or highest tensile stress was applied.

It was noted that the slightest confinement of a test cube in an intended uniaxial test would noticeably affect the maximum strength. Also in a biaxial test, the results would be affected whenever a slight lateral pressure accidently occurred on the "free surfaces." Once discovered,

measures were taken to prevent lateral pressure from developing on the unconfined sides.

In triaxial compressive tests, it was noted that the maximum stress was greatly affected by the magnitude of the minor stress and somewhat affected by the intermediate stress. The strains were generally affected in the same manner. The largest minor stress that could be applied and still obtain failure was approximately 7000 psi. A minor stress above this value would prevent failure of the test specimen before the capacity of the testing machine was reached.

Whenever applicable, the test results from this investigation were compared to the test results reported by other investigators. The scatter in results reported is rather large; however, many of the investigators used different testing procedures, equipment, and different shaped test specimens. The results of this investigation were bounded by the results reported by other investigators.

A model to predict concrete behavior was developed. The mathematical development of the model was theoretical; however, empirical results were incorporated into the model such that the test results were simulated. The model was used to predict the constitutive relations for concrete subjected to combined loads. The loads can be tensile or compressive. The model solution was programmed for use with a computer and written in Fortran IV language.

The model was developed using test results for a concrete strength of 4000 psi. The test results in the compression range were limited by the

minor stress level. The model is controlled by parameters which control the shape of the stress-strain curves and the maximum stresses.

9.2 RECOMMENDATIONS

The model itself can be made to more accurately simulate concrete behavior. The degree of simulation becomes a matter of refinement in the control parameters. The area of doubt with respect to test results was in the tension region. The accuracy of the extensometers should be improved for this region and a testing procedure and machine devised such that bending stresses are not induced into the test specimen during testing.

The model was developed using one concrete strength only; hence, the model predicted results are applicable to the one strength only. The model should be verified for different concrete strengths. This can be done only through a testing program.

The effect of creep and loading rate on concrete under combined stresses is not yet established. The effect of loading and unloading concrete under combined stresses has not been established either. The constitutive relations will not be completely general until all of these effects are known.

APPENDIX I

COMPUTER PROGRAM FOR THE MODEL

1.1 GENERAL

The computer program for the model which was developed and described in Sections VII and VIII is presented in detail in this appendix. Fortran VI was used in the progra ming. The order of presentation is as follows:

(a) Driver Program

(b) Subroutine MATER6

(c) Sample Input

(d) Sample Output

1.2 DRIVER PROGRAM

The purpose of the driver program is to read or compute the information that is transferred into subroutine MATER6. In addition, the driver program prints or writes information computed within the subroutine. Entry into the subroutine is made through a CALL statement. Note that the driver program as presented is self-contained and that it must be modified for use in a more general program. A data card with a strain of unity inserted at the end of a set of strain data cards will reset the program to accept another set of strain data cards. A data card with strains larger than unity will terminate the program. The driver program also equates new stresses and strains to old stresses and strains after a set of new stresses have been computed.

Included in this section is a list of the variables used in the driver program, a flow chart, and a listing of the driver program.

DRIVER PROGRAM

LIST OF VARIABLES AND THEIR DEFINITION

BU   - Initial Poissons' Ratio

E   - Initial Tangent Modulus

SK(I)   - Initial Stiffness of Model Members

SIG1(I) - Old Stresses

SIG(I) - New Stresses

EPS1(I) - Old Strains

EPS(I) - New Strains

FLOWCHART FOR DRIVER PROGRAM

```
                        ┌──────────┐
                        │  Start   │
                        └──────────┘
                             │
                             ▼
                  ╱────────────────────╲
                 ╱ Read Initial Poisson's╲
                │      Ratio and          │
                │   Tangent Modulus       │
                 ╲      BU,E             ╱
                  ╲────────────────────╱
                             │
                             │◄──────────────────────────┐
                             ▼                            │
                  ┌────────────────────┐                 │
                  │  Compute Initial   │                 │
                  │ Member Stiffnesses │                 │
                  │      SK(I)         │                 │
                  └────────────────────┘                 │
                             │                            │
                             ▼                            │
                  ╱────────────────────╲                 │
                 ╱  Read Initial Stress ╲                │
                │     and Strain         │               │
                 ╲   SIG1,EPS1         ╱                 │
                  ╲────────────────────╱                 │
                             │                            │
                             │◄─────────────────────┐     │
                             ▼                       │     │
                  ╱────────────────────╲            │     │
                 ╱   Read New Strains   ╲           │     │
                │        EPS             │          │     │
                 ╲────────────────────╱            │     │
                             │                       │     │
                             ▼                       │     │
                      ╱──────────────╲               │     │
          ┌─────────◄   EPS(1):1      ►──────┐       │     │
          │           ╲──────────────╱       │       │     │
          │                  │                │       │     │
          │                  │ =              ▼       │     │
          ▼                  │          ┌──────────┐  │     │
┌──────────────────────┐    │          │  Exit    │  │     │
│Call Subroutine Mater6(SK,│  │          └──────────┘  │     │
│SIG1,EPS1,SIG,EPS)    │    │                         │     │
└──────────────────────┘    └─────────────────────────┘     │
          │                                                  │
          ▼                                                  │
  ╱────────────────────╲                                    │
 ╱ Write Old Stresses,  ╲                                   │
│ Strains and New        │                                  │
│ Stresses, Strains      │           ┌────────────────────┐ │
│ SIG1,SIG,EPS,EPS1    ╱            │ Set New Strains to Old│◄┘
 ╲────────────────────╱             │ Set New Stresses to Old│
          │                          └────────────────────┘
          └──────────────────────────────────┘
```

147
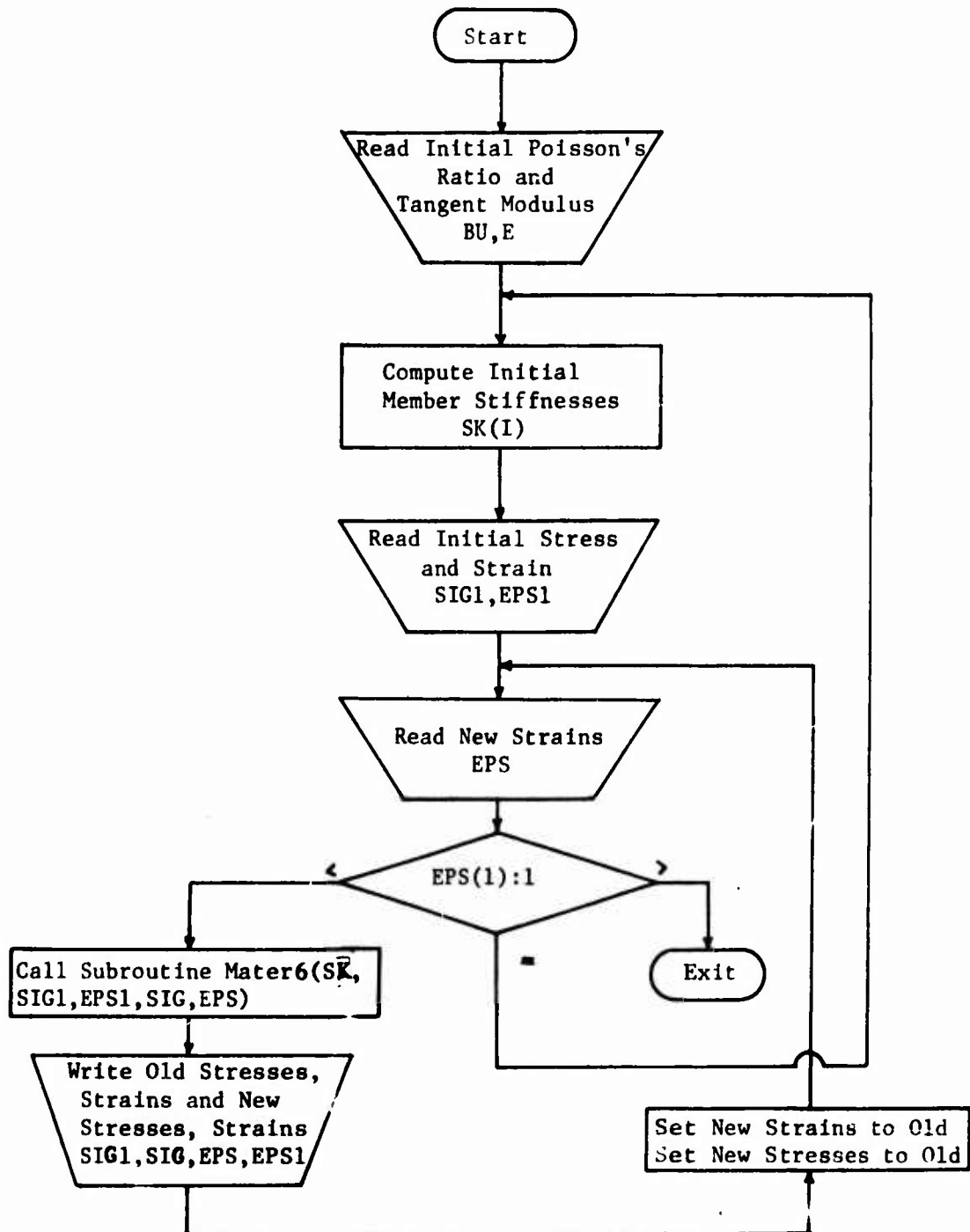
DRIVER PROGRAM LISTING

```
0001          DIMENSION SK(6),SIGI(6),EPSI(6),SIG(6),EPS(6)
0002    C     MATERIAL CONSTANTS FROM UNIAXIAL TEST
         90 READ(5,100)BU,E
0003    100 FORMAT(2F10.0)
        C     COMPUTE INITIAL MEMBER STIFFNESS VALUES
0004    101 SK(1)=10.*BU*E/(1.-BU-2.*BU**2)
0005        SK(2)=SK(1)*(1.-3.*BU)/(2.*BU)
0006        SK(3)=SK(1)
0007        SK(4)=SK(2)
0008        SK(5)=SK(2)
0009        SK(6)=SK(1)
0010        WRITE(6,102)
0011    102 FORMAT(22X,'EPS(1)',5X,'EPS(2)',5X,'EPS(3)',5X,'EPS(4)',5X,
             *'EPS(5)',5X,'EPS(6)')
0012        WRITE(6,103)
0013    103 FORMAT(22X,'SIG(1)',5X,'SIG(2)',5X,'SIG(3)',5X,'SIG(4)',5X,
             *'SIG(5)',5X,'SIG(6)'/)
0014    105 READ(5,110)SIGI,EPSI
0015        READ(5,110)EPS
0016    110 FORMAT(6F10.9)
0017        IF(EPS(1)-1.)140,101,120
0018    120 CALL EXIT
        C     *****************************************************
0019    140 CALL MATER6(SK,SIGI,EPSI,SIG,EPS)
        C     *****************************************************
0020        WRITE(6,800)EPS
0021    800 FORMAT(1X,'STRAINS    (INPUT)',6F11.6)
0022        WRITE(6,810)SIG
0023    810 FORMAT(1X,'STRESSES (OUTPUT)',6F11.0/)
0024        DO 920 J=1,6
0025        SIGI(J)=SIG(J)
0026    920 EPSI(J)=EPS(J)
0027        GO TO 105
0028        END
```

148

1.3 SUBROUTINE MATER6

The purpose of Subroutine MATER6 is to compute a set of stresses from a given set of strains. The subroutine utilizes incremental principal strains from which incremental principal stresses are determined. Converting to principal strains and stresses is a necessity and must be accomplished before strain increments can be computed. Principal strains are determined through the use of the standard subroutine EIGEN. Subroutine EIGEN is also used to determine the directional cosines of the principal new strains. Subroutine EIGEN also sorts the principal stresses or strains from largest to smallest. The principal old stresses are determined using stress transformation equations and the directional cosines obtained from the old strains. The principal incremental stresses are determined and Subroutine MATER6 computes the incremental stresses and total stresses and then converts the stresses back to the original coordinate system. Control is then transferred back to the driver program.

Caution must be exercised in the selection of the strain increments. Subroutine MATER6 utilizes Euler's point-slope integration method; hence, it will become unstable if the strain increments are not kept sufficiently small. The program does contain an accuracy check, and if exceeded, divides the given strain increment. This should not be considered to completely safeguard against an unstable solution.

The list of variables used in Subroutine MATER6 is included in this section along with the flowchart and the computer program listing.

149

SUBROUTINE MATER6 LIST OF VARIABLES

A(I)   Temporary values of stresses and strains

AK(I)   Member stiffness values

ASAT(I,J)   Model stiffness elements

B   Ratio of DDF(3)/DDF(1)

CK   Temporary stiffness value

CON   A control parameter

DC(I)   Directional cosines

DCN   A control parameter

DCP   A fraction of the stiffness of the compressive members

DDF(I)   Sorted absolute values of DF(I), largest to smallest

DF(I)   Principal incremental stresses

DX(I)   Model incremental displacements

EIGEN   Subroutine for computing eigenvalues

G   Ratio of DDF(2)/DDF(1)

G1,G2,G3,

G4   Control equation variables

IP   Counters

NC,NT   Integers used in stiffness functions

NCK   Counter determining the stress condition

NTIME,IQ   Counter determining the number of passes through model computations

O1,O2,O3   Control equation variables

PSNO(I)   Principal strains obtained from old strains

PSNN(I)   Principal strains obtained from new strains

R(I)	Temporary values of directional cosines
SIGP(I)	Principal stresses from old stresses
SIGS(I)	Computed principal stresses
TEF	Temporary principal stress
V	Displacements obtained from new principal strains
XOC	A control parameter
XOC2	A control parameter
XOT	A control parameter
X21	A control parameter
X(I)	Model displacements from old strains

```
                    ( Enter )
                        │
                        ▼
            ┌───────────────────────┐
            │  Set counters to zero │
            │    NQ, NP, NTIME      │
            │  Set variables to zero│
            │      CK, TDF          │
            └───────────────────────┘
                        │
                        ▼
            ┌───────────────────────┐
            │  Set up strain (EPS1) │
            │       matrix          │
            └───────────────────────┘
                        │
                        ▼
            ┌───────────────────────┐
            │ CALL SUBROUTINE EIGEN │
            ├───────────────────────┤
            │Computes principal     │
            │strains, PSNO,         │
            │directional cosine,    │
            │D, and sorts principal │
            │strains largest to     │
            │      smallest         │
            └───────────────────────┘
                        │
                        ▼
            ┌───────────────────────┐
            │  Set up strain (EPS)  │
            │       matrix          │
            └───────────────────────┘
                        │
                        ▼
            ┌───────────────────────┐
            │ CALL SUBROUTINE EIGEN │
            ├───────────────────────┤
            │Compute principal      │
            │strains PSNN,          │
            │directional cosines    │
            │DC, and sorts principal│
            │strains largest to     │
            │      smallest         │
            └───────────────────────┘
                        │
                        ▼
            ┌───────────────────────┐
            │ Compute principal     │
            │ stresses SIGP using   │
            │ stress transformation │
            │ equations, directional│
            │ cosines D, and        │
            │ stresses SIG1.        │
            └───────────────────────┘
```

Right column:

```
            ┌───────────────────────┐
            │   Convert principal   │
            │ strains to displacement│
            │   and incremental     │
            │    displacements      │
            │        X, DX          │
            └───────────────────────┘
                        │
                        ▼
            ┌───────────────────────┐
            │  Initial values of    │
            │  control constants    │
            │ DCN, XOC2, CON, X21,  │
            │      XOC, XOT         │
            └───────────────────────┘
     (C)────────────────┤
                        ▼
            ┌───────────────────────┐
            │  Compute control      │
            │  parameter variables  │
            │     G1, G2, G3,       │
            │     01, 02, 03        │
            └───────────────────────┘
     (G)────────────────┤
                        ▼
            ┌───────────────────────┐
            │  Increase counter     │
            │   NTIME by one        │
            └───────────────────────┘
                        │
                        ▼
            ┌───────────────────────┐
            │ Compute variable DCP  │
            └───────────────────────┘
                        │
                        ▼
            ╱─────────────────────────╲
            │  Compute member stiff-  │
            │  nesses AK  (This is    │
            │  shown in more detail   │
            │      elsewhere)         │
            ╲─────────────────────────╱
                        │
                        ▼
            ┌───────────────────────┐
            │ Compute model stiff-  │
            │ ness elements ASAT    │
            └───────────────────────┘
                        │
                        ▼
                      ( A )
```

152

FLOWCHART FOR DETERMINATION
OF MEMBER STIFFNESSES

```
                        ┌──────┐
                        │  In  │
                        └──────┘
                           │
                    ┌──────────────┐
              <─────│    X(1):0    │─────>
              │     └──────────────┘     │
              │            │  =          │
              │            │             ▼
              │            │       ┌──────────────────────┐
              │            │       │ Compute AK(2) for     │
              ▼            │       │ Compressive Case      │
        ┌──────────────┐  │       └──────────────────────┘
        │ Compute AK(2) for │                │
        │ Tension Case  │                    │
        └──────────────┘                    │
              │                              │
              └────────────┬────────────────┘
                           │
                    ┌──────────────┐
              <─────│    X(2):0    │─────>
              │     └──────────────┘     │
              │            │  =          │
              ▼            │             ▼
        ┌──────────────┐  │       ┌──────────────────────┐
        │ Compute AK(4) for │     │ Compute AK(4) for     │
        │ Tension Case  │         │ Compressive Case      │
        └──────────────┘         └──────────────────────┘
              │                          │
              └──────────┬───────────────┘
                         │
                  ┌──────────────┐
            <─────│    X(3):0    │─────>
            │     └──────────────┘     │
            │          │  =            │
            ▼          │               ▼
      ┌──────────────┐ │       ┌──────────────────────┐
      │ Compute AK(5) for │    │ Compute AK(5) for     │
      │ Tension Case  │        │ Compressive Case      │
      └──────────────┘        └──────────────────────┘
            │                        │
            └──────────┬─────────────┘
                       │
                     ┌───┐
                     │ E │
                     └───┘
```


156

FLOW CHART FOR DETERMINATION OF
MEMBER STIFFNESSES, (contd)

SUBROUTINE MATER6 LISTING

```
0001        SUBROUTINE MATER6(SK,SIGI,EPSI,SIG,EPS)
0002        DIMENSION SK(6),SIGI(6),EPSI(6),SIG(6),EPS(6)
0003        DIMENSION PSND(3),PSNN(3),DF(3),DX(3),DDF(3),X(3)
0004        DIMENSION SIGP(3),SIGS(3),DG(3),ASAT(3,3),A(6),R(9)
0005        DIMENSION AK(5),XOT(6),XOT(6),NC(6),NT(6),D(9),TDF(3)
0006   C
0007        DATA NT(1),NT(2),NT(3),NT(4),NT(5),NT(6)/11,11,11,11,11,11/
           DATA NC(1),NC(2),NC(3),NC(4),NC(5),NC(6)/2,5,2,5,5,2/
     C
     C      INITIALIZE COUNTERS AND VARIABLES
     C
0008        IQ=0
0009        NP=0
0010        NTIMF=0
0011        CK=.0
0012        DO 25 I=1,3
0013   25   TDF(I)=.0
     C
     C      SET UP OLD STRAIN MATRIX
     C
0014        A(1)=-EPSI(1)
0015        A(2)=-EPSI(6)/2.
0016        A(3)=-EPSI(2)
0017        A(4)=-EPSI(4)/2.
0018        A(5)=-EPSI(6)/2.
0019        A(6)=-EPSI(3)
     C
     C      COMPUTE PRINCIPAL STRAINS FROM OLD STRAINS
     C
0020        CALL EIGEN(A,R,3,0)
0021        DO 50 I=1,3
0022        IP=I+(I*I-I)/2
0023   50   PSND(I)=A(IP)
```

158

SUBROUTINE MATER6 LISTING (cont'd)

```
C
C      DIRECTIONAL COSINES FOR DETERMINING PRINCIPAL STRESSES
C
0024          DO 55 I=1,9
0025      55  D(I)=R(I)
C
C      SET UP NEW STRAIN MATRIX
C
0026          A(1)=-EPS(1)
0027          A(2)=-EPS(5)/2.
0028          A(3)=-EPS(2)
0029          A(4)=-EPS(4)/2.
0030          A(5)=-EPS(6)/2.
0031          A(6)=-EPS(3)
C
C      COMPUTE PRINCIPAL STRAINS FROM NEW STRAINS
C
0032          CALL EIGEN(A,R,3,0)
0033          DO 60 I=1,3
0034          ID=I+(I*I-I)/2
0035      60  PSNP(I)=A(ID)
C      DIRECTIONAL COSINES
0036          DO 65 I=1,9
0037      65  DC(I)=-R(I)
C
C      COMPUTE PRINCIPAL STRESSES FROM DIRECTIONAL COSINES
C
0038          SIGP(1)=D(1)**2*SIGI(1)+D(2)**2*SIGI(2)+D(3)**2*SIGI(3)
            *+2.*D(2)*D(3)*SIGI(6)+2.*D(1)*D(3)*SIGI(4)+2.*D(1)*D(2)*SIGI(5)
0039          SIGP(2)=D(4)**2*SIGI(1)+D(5)**2*SIGI(2)+D(6)**2*SIGI(3)
            **+2.*D(5)*D(6)*SIGI(6)+2.*D(4)*D(6)*SIGI(4)+2.*D(4)*D(5)*SIGI(5)
0040          SIGP(3)=D(7)**2*SIGI(1)+D(8)**2*SIGI(2)+D(9)**2*SIGI(3)
            **+2.*D(8)*D(9)*SIGI(6)+2.*D(7)*D(9)*SIGI(4)+2.*D(7)*D(8)*SIGI(5)
C
C      CONVERT STRAINS TO DISPLACEMENTS
C
```

159

SUBROUTINE MATER6 LISTING (cont'd).

```
0041        DO 200 I=1,3
0042        X(I)=PSNU(I)*10.
0043    200 DX(I)=(PSNN(I)-PSNU(I))*10.
C
C       INITIAL VALUES FOR CONTROL PARAMETERS
C
0044        IF(PSNU(I))260,210,260
0045    210 DCN=0.25
0046        X21=0.03
0047        XOC2=0.3
0048        CUN=1.
0049        DO 254 I=1,6
0050        XOC(I)=X21
0051    254 XOT(I)=0.0008
C
C       CONTROL PARAMETER VARIABLES
C
0052    260 G1=ABS(X(1)+X(2)-2.*X(3))
0053        G2=ABS(X(1)+X(3)-2.*X(2))
0054        G3=ABS(X(2)+X(3)-2.*X(1))
0055        G4=ABS(X(1)+X(2)+X(3))*.707
0056        O1=ABS(X(2)-X(3))
0057        O2=ABS(X(1)-X(3))
0058        O3=ABS(X(3)-X(2))
0059    270 NTIMF=NTIME+1
0060        DCP=1.-DCN
C
C       MEMBER STIFFNESS VALUES
C
0061        IF(X(1))500,500,520
0062    500 AK(2)=SK(2)/((1.+(ABS(X(1))/XOT(2))**NT(2))**(1.+1./NT(2))),
0063        GO TO 550
0064    520 AK(2)=SK(2)*(1.+(1.-CON*NC(2))*((G2/(1.*XOC(2)))**NC(2)))**NC(2)))*DCN
0065        AK(2)=AK(2)/((1.+(O2/(1.*XOC(2)))**NC(2))**2)
0066        AK(2)=AK(2)+DCP*SK(2)/((1.+(G2/X21)**4)**(1.250))
0067    550 IF(X(2))570,570,580
```

160

SUBROUTINE MATER6 LISTING (cont'd)

```
0068    570  AK(4)=SK(4)/((1.+(ABS(X(2))/XOT(4))**NT(4))**(1.+1./NT(4)))
0069         GO TO 590
0070    580  AK(4)=SK(4)*(1.+(1.-CON*NC(4))*((O1/XOC(4))**NC(4)))*DCN
0071         AK(4)=AK(4)/((1.+(O1/XOC(4))**NC(4)))
0072         AK(4)=AK(4)+  DCP*SK(4)/((1.+(O1/X21    )**4)**(1.250))
0073    590  IF(X(3,)600,610,610
0074    600  AK(5)=SK(5)/((1.+(ABS(X(3))/XOT(5))**NT(5))**(1.+1./NT(5)))
0075         GO TO 620
0076    610  AK(5)=SK(5)*(1.+(1.-CON*NC(5))*((O3/(1.*XOC(5)))**NC(5)))*DCN
0077         AK(5)=AK(5)/((1.+(O3/XOC(5))**NC(5)))
0078         AK(5)=AK(5)+DCP*SK(5)/((1.+(O3/X21)**4)**(1.250))
0079    620  IF(X(1)+X(2))630,640,640
0080    630  AK(1)=SK(1)/((1.+(G4/XOT(1))**NT(1))**(1.+1./NT(1)))
0081         GO TO 650
0082    640  AK(1)=SK(1)/((1.+(G1/XOC(1))**NC(1))**(1.+1./NC(1)))
0083    650  IF(X(1)+X(3))660,670,670
0084    660  AK(6)=SK(6)/ ((1.+(G4/XOT(6))**NT(6))**(1.+1./NT(6)))
0085         GO TO 680
0086    670  AK(6)=SK(6)/((1.+(G2/XOC(6))**NC(6))**(1.+1./NC(6)))
0087    680  IF(X(3)+X(2))590,690,700
0088    690  AK(3)=SK(3)/((1.+(G4/XOT(3))**NT(3))**(1.+1./NT(3)))
0089         GO TO 710
0090    700  AK(3)=SK(3)/((1.+(G3/XOC(3))**NC(3))**(1.+1./NC(3)))
        C
        C  MODEL STIFFNESS ELEMENTS
        C
0091    710  ASAT(1,1)=2.*AK(1)+2.*AK(6)+4.*AK(2)
0092         ASAT(1,2)= 2.*AK(1)
0093         ASAT(1,3)= 2.*AK(6)
0094         ASAT(2,1) = ASAT(1,2)
0095         ASAT(2,2)= 2.*AK(1)+2.*AK(3)+4.*AK(4)
0096         ASAT(2,3)= 2.*AK(3)
0097         ASAT(3,1) = ASAT(1,3)
0098         ASAT(3,2) = ASAT(2,3)
0099         ASAT(3,3)= 2.*AK(3)+2.*AK(6)+4.*AK(5)
```

161

SUBROUTINE MATER6 LISTING (cont'd)

```
C
C    COMPUTE INCREMENTAL FORCES
C
0100      715 DO 720 I=1,3
0101          DF(I)=0.0
0102          DO 720 J=1,3
0103      720 DF(I)=DF(I)+ASAT(I,J)*DX(J)
C
C    CHECK ACCURACY OF STIFFNESS ELEMENTS
C    IF NOT ACCURATE DIVIDE INTO TEN PARTS
C        EVALUATE MODEL CONSTANTS
C
0104          IF(NTIME-5)731,731,721
0105      721 IF(ABS(CK-ASAT(2,2))-ASAT(2,2)*.005)727,727,722
0106      722 NTIME=0
0107          IF(IQ-1)723,727,727
0108      723 DO 724 I=1,3
0109     .724 DX(I)=DX(I)/10.
0110          IQ=IQ+1
0111          GO TO 260
0112      727 DO 728 I=1,3
0113          X(I)=X(I)+DX(I)
0114      728 TDF(I)=TDF(I)+DF(I)
0115          NP=NP+1
0116          IF(IQ)729,800,729
0117      729 IF(NP-10)730,800,800
0118      730 NTIME=0
0119          GO TO 260
0120      731 CK=ASAT(2,2)
0121          DO 732 J=1,3
0122      732 DDF(J)=ABS(DF(J))
C
C    SORT ABSOLUTE VALUES OF INCREMENTAL FORCES
C
```

162

SUBROUTINE MATER6 LISTING (cont'd)

```
0123        DO 750 I=1,2
0124        IPM=I+1
0125        DO 750 J=IPM,3
0126        IF(DDF(I)-DDF(J))740,740,750
0127    740 TEM=DDF(I)
0128        DDF(I)=DDF(J)
0129        DDF(J)=TEM
0130    750 CONTINUE
0131        G=DDF(2)/DDF(1)
0132        B=DDF(3)/DDF(1)

      C
      C DETERMINE STATE OF STRESS
      C

0133        NCK=0
0134        DO 762 J=1,3
0135        IF(DF(J))754,756,758
0136    754 NCK=NCK+3
0137        GO TO 762
0138    756 NCK=NCK+2
0139        GO TO 762
0140    758 NCK=NCK+1
0141    762 CONTINUE
0142        CON=1.0
0143        DCN=1.0
0144        XOC2=0.0265
0145        X21=0.055
0146        X10=0.055
0147        FT=XOT(2)
0148        GO TO (772,772,772,766,770,770,770,770,774,774),NCK
0149    766 X21=0.030-0.0125*G
0150        DCN=1.0-0.5*G
0151        CON=1.05+0.5*G
0152        XOC2=0.0265+G*(0.1560+(G-.1)*(-0.685+(G-.2)*(1.633+(G-.4)
           1*(-2.91+(G-.6)*(3.705+(G-.8)*(-4.25+(G-.9)*(3.867)))))))
0153        GO TO 774
```

163

SUBROUTINE MATER6 LISTING (cont'd)

```
0154    770 ET=(0.02771+0.1668*B)*G*EXP ((-20.383+7.773*B)*G**(1.25-0.5*B))
             *+0.0012
0155        GO TO 776
0156    772 XOC2=0.025+1.65*B+3.3*B*(B-0.1)+(0.022-0.72*B+23.35*B*(B-0.1))*G
             *+3.75*B*(B-0.1)*G*(G-0.2)-50.*B*(B-0.1)*G*(G-0.2)*(G-0.4)
0157        DCN=1.-6.95*B+34.75*B*(B-0.1)-4.*B*G+5.*B*G*(G-0.2)
0158        X10=0.05+0.5*B+3.0*B*(B-0.1)+G*(-0.06+1.8*B)-G*(     )*(0.05+1.5*B
             *+7.5*B*(B-0.1))
0159        X21=(0.04-0.01*B-0.25*B*(B-0.1)*TANH(G*(9.70-57.      235.*B*(B-0.1)
             *))
0160        GO TO 776
0161    774 ET=0.0012-0.0001*G*(3.+3.25*B)

        C
        C   CHECK IF PARAMETERS ARE WITHIN VALID RANGE
        C   IF OUTSIDE RANGE, RESET TO TYPICAL VALUES
        C
0162    776 IF(XOC2-1.)785,780,780
0163    780 XOC2=.6
0164    785 IF(DCN-1.)790,788,788
0165    788 DCN=.5
0166    790 IF(X21)793,793,795
0167    793 X21=.03
0168    795 XOC(2)=XOC2
0169        XOC(4)=XOC2
0170        XOC(5)=XOC2
0171        XOC(1)=X10
0172        XOC(3)=X10
0173        XOC(6)=X10
0174        GO TO 270
```

```
C
C     CHECK IF TENSILE FAILURE HAS OCCURRED
C     COMPUTE NEW PRINCIPAL STRESSES
C
      800 DO 808 I=1,3
          IF(TDF(I))804,807,807
      804 IF(SIGP(I))807,805,805
      805 V=-10.*PSVN(I)
          IF(ET-V)806,806,807
      806 SIGS(I)=0.0
          GO TO 808
      807 SIGS(I)=SIGP(I)-TDF(I)/200.
      808 CONTINUE
C
C     STRESS TRANSFORMATION-NEW STRESSES TO ORIGINAL COORDINATE SYSTEM
C
      SIG(1)=SIGS(1)*(DC(1))**2+SIGS(2)*(DC(4))**2+SIGS(3)*(DC(7))**2
      SIG(2)=SIGS(1)*(DC(2))**2+SIGS(2)*(DC(5))**2+SIGS(3)*(DC(8))**2
      SIG(3)=SIGS(1)*(DC(3))**2+SIGS(2)*(DC(6))**2+SIGS(3)*(DC(9))**2
      SIG(4)=SIGS(1)*DC(1)*DC(3)+SIGS(2)*DC(4)*DC(6)+SIGS(3)*DC(7)*DC(9)
      SIG(5)=SIGS(1)*DC(1)*DC(2)+SIGS(2)*DC(4)*DC(5)+SIGS(3)*DC(7)*DC(8)
      SIG(6)=SIGS(1)*DC(2)*DC(3)+SIGS(2)*DC(5)*DC(6)+SIGS(3)*DC(8)*DC(9)
      RETURN
      END
```

0175
0176
0177
0178
0179
0180
0181
0182
0183

0184
0185
0186
0187
0188
0189
0190
0191

165

1.4 SAMPLE INPUT

Input to the computer program consists of the following:

(a) Poissons Ratio and Initial Tangent Modulus - BU,E

Both of these values are included on the same data card shown below. Their FORMAT specification is F10.0. Poissons Ratio is dimensionless and the unit for the tangent modulus is psi. This is the first data card in the program.

```
0.15      3282000.0
```

(b) Old Stresses and Old Strains - SIG1, EPS1

These values are read only at the beginning of a

series of given strains and are all zero. Their FORMAT

specification is F10.9. The unit of the strains is in/in

and the unit of the stresses is psi. A sample card is

shown below.

(c) New Strains - EPS

New strains are read in a sequence. The number of cards is variable depending upon the number of strain readings that are available or selected. The FORMAT specification for strains and stresses is Fll.6 and Fll.0, respectively. The units are the same as for the strains in (b) above.

The general strain and stress tensors are, respectively,

$$
\begin{vmatrix}
\epsilon_x & \frac{1}{2}\gamma_{xy} & \frac{1}{2}\gamma_{xz} \\
\frac{1}{2}\gamma_{xy} & \epsilon_y & \frac{1}{2}\gamma_{yz} \\
\frac{1}{2}\gamma_{xz} & \frac{1}{2}\gamma_{yz} & \epsilon_z
\end{vmatrix}
$$

and

$$
\begin{vmatrix}
\sigma_x & \tau_{xy} & \tau_{xz} \\
\tau_{xy} & \sigma_y & \tau_{yz} \\
\tau_{xz} & \tau_{yz} & \sigma_z
\end{vmatrix}
$$

The corresponding order of the input for both stresses and strains is

$$
\begin{vmatrix}
1 & 5 & 4 \\
5 & 2 & 6 \\
4 & 6 & 3
\end{vmatrix}
$$

For example, τ_{xy} would be indicated as SIG(5) or SIG1(5) in the computer program. The strain $\frac{1}{2} \gamma_{xz}$ would be indicated as EPS(4) or EPS1(4) in the computer program.

A sample input card is shown below. Note that the quantities γ_{xy}, γ_{xz}, and γ_{yz} (not the quantities $\frac{1}{2} \gamma_{xy}$, $\frac{1}{2} \gamma_{xz}$, and $\frac{1}{2} \gamma_{yz}$) are used on the input cards.

1.5 SAMPLE OUTPUT

A sample of the output information, which is the new stresses SIG, is shown below. The strains, which are indicated as STRAINS (INPUT), produce the stresses which are indicated as STRESSES (OUTPUT). The strain values shown below may be used as check values to determine if the computer program is functioning properly. The given strains must produce the corresponding stresses. The unit of strains is in/in and the unit of stresses is psi. EPS(5), SIG(5), EPS(6), and SIG(6) are zero and are not always shown.

PRINCIPAL STRESS RATIOS

$$\sigma_1 ; \sigma_2 ; \sigma_3 = 1;1;1$$

		EPS(1) SIG(1)	EPS(2) SIG(2)	EPS(3) SIG(3)	EPS(4) SIG(4)
STRAINS	(INPUT)	0.000010	0.000010	0.000010	0.000000
STRESSES	(OUTPUT)	47.	47.	47.	0.
STRAINS	(INPUT)	0.000021	0.000021	0.000021	0.000000
STRESSES	(OUTPUT)	98.	98.	98.	0.
STRAINS	(INPUT)	0.000034	0.000034	0.000034	0.000000
STRESSES	(OUTPUT)	159.	159.	159.	0.
STRAINS	(INPUT)	0.000054	0.000054	0.000054	0.000000
STRESSES	(OUTPUT)	240.	240.	240.	0.
STRAINS	(INPUT)	0.000065	0.000065	0.000065	0.000000
STRESSES	(OUTPUT)	0.	0.	0.	0.
STRAINS	(INPUT)	0.000076	0.000076	0.000076	0.000000
STRESSES	(OUTPUT)	0.	0.	0.	0.

PRINCIPAL STRESS RATIOS

$$\sigma_1 ; \sigma_2 ; \sigma_3 = 1;1;0$$

		EPS(1) SIG(1)	EPS(2) SIG(2)	EPS(3) SIG(3)	EPS(4) SIG(4)
STRAINS	(INPUT)	0.000006	0.000006	-0.000002	0.000000
STRESSES	(OUTPUT)	23.	23.	0.	0.
STRAINS	(INPUT)	0.000012	0.000012	-0.000004	0.000000
STRESSES	(OUTPUT)	46.	46.	1.	0.
STRAINS	(INPUT)	0.000019	0.000019	-0.000006	0.000000
STRESSES	(OUTPUT)	74.	74.	2.	0.
STRAINS	(INPUT)	0.000025	0.000025	-0.000009	0.000000
STRESSES	(OUTPUT)	96.	96.	-1.	0.
STRAINS	(INPUT)	0.000032	0.000032	-0.000011	0.000000
STRESSES	(OUTPUT)	124.	124.	1.	0.
STRAINS	(INPUT)	0.000038	0.000038	-0.000013	0.000000
STRESSES	(OUTPUT)	147.	147.	1.	0.
STRAINS	(INPUT)	0.000045	0.000045	-0.000015	0.000000
STRESSES	(OUTPUT)	174.	174.	3.	0.
STRAINS	(INPUT)	0.000053	0.000053	-0.000017	0.000000
STRESSES	(OUTPUT)	205.	205.	6.	0.
STRAINS	(INPUT)	0.000062	0.000062	-0.000019	0.000000
STRESSES	(OUTPUT)	240.	240.	9.	0.
STRAINS	(INPUT)	0.000073	0.000073	-0.000019	0.000000
STRESSES	(OUTPUT)	276.	276.	18.	0.
STRAINS	(INPUT)	0.000088	0.000088	-0.000019	0.000000
STRESSES	(OUTPUT)	0.	0.	22.	0.
STRAINS	(INPUT)	0.000091	0.000091	-0.000019	0.000000
STRESSES	(OUTPUT)	0.	0.	0.	0.

PRINCIPAL STRESS RATIOS

$$\sigma_1;\sigma_2;\sigma_3 = -10;4;0$$

		EPS(1) SIG(1)	EPS(2) SIG(2)	EPS(3) SIG(3)	EPS(4) SIG(4)
STRAINS	(INPUT)	-0.000016	0.000008	0.000001	0.000000
STRESSES	(OUTPUT)	-50.	19.	-1.	0.
STRAINS	(INPUT)	-0.000032	0.000016	0.000002	0.000004
STRESSES	(OUTPUT)	-100.	37.	-3.	6.
STRAINS	(INPUT)	-0.000048	0.000025	0.000004	0.000010
STRESSES	(OUTPUT)	-149.	60.	-0.	14.
STRAINS	(INPUT)	-0.000062	0.000033	0.000004	0.000020
STRESSES	(OUTPUT)	-192.	79.	-4.	29.
STRAINS	(INPUT)	-0.000076	0.000041	0.000002	0.000034
STRESSES	(OUTPUT)	-237.	97.	-14.	49.
STRAINS	(INPUT)	-0.000089	0.000050	0.000001	0.000052
STRESSES	(OUTPUT)	-277.	119.	-20.	74.
STRAINS	(INPUT)	-0.000100	0.000058	-0.000004	0.000074
STRESSES	(OUTPUT)	-313.	137.	-40.	106.
STRAINS	(INPUT)	-0.000108	0.000067	-0.000010	0.000098
STRESSES	(OUTPUT)	-339.	159.	-60.	140.
STRAINS	(INPUT)	-0.000114	0.000076	-0.000020	0.000126
STRESSES	(OUTPUT)	-361.	179.	-92.	180.
STRAINS	(INPUT)	-0.000148	0.000078	0.000012	0.000000
STRESSES	(OUTPUT)	-458.	182.	-1.	0.
STRAINS	(INPUT)	-0.000150	0.000080	0.000012	0.000000
STRESSES	(OUTPUT)	-463.	186.	-1.	0.
STRAINS	(INPUT)	-0.000162	0.000088	0.000013	0.000000
STRESSES	(OUTPUT)	-499.	197.	-0.	0.
STRAINS	(INPUT)	-0.000179	0.000106	0.000013	0.000000
STRESSES	(OUTPUT)	-547.	218.	1.	0.
STRAINS	(INPUT)	-0.000187	0.000116	0.000012	0.000000
STRESSES	(OUTPUT)	-570.	225.	-2.	0.
STRAINS	(INPUT)	-0.000190	0.000120	0.000012	0.000000
STRESSES	(OUTPUT)	-577.	229.	-1.	0.

172

PRINCIPAL STRESS RATIOS
$\sigma_1 ; \sigma_2 ; \sigma_3 = -20; -20; 1$

	EPS(1) SIG(1)	EPS(2) SIG(2)	EPS(3) SIG(3)	EPS(4) SIG(4)	EPS(5) SIG(5)	EPS(6) SIG(6)
STRAINS (INPUT)	-0.000090	-0.000104	0.000037	-0.000052	0.0	0.0
STRESSES (OUTPUT)	-394.	-398.	4.	-74.	0.	0.
STRAINS (INPUT)	-0.000122	-0.000130	0.000046	-0.000074	0.0	0.0
STRESSES (OUTPUT)	-474.	-487.	5.	-106.	0.	0.
STRAINS (INPUT)	-0.000144	-0.000156	0.000052	-0.000100	0.0	0.0
STRESSES (OUTPUT)	-562.	-597.	-4.	-143.	0.	0.
STRAINS (INPUT)	-0.000166	-0.000183	0.000058	-0.000128	0.0	0.0
STRESSES (OUTPUT)	-651.	-700.	-15.	-182.	0.	0.
STRAINS (INPUT)	-0.000188	-0.000210	0.000064	-0.000164	0.0	0.0
STRESSES (OUTPUT)	-734.	-801.	-22.	-230.	0.	0.
STRAINS (INPUT)	-0.000232	-0.000238	0.000080	-0.000210	0.0	0.0
STRESSES (OUTPUT)	-894.	-898.	-45.	-282.	0.	0.
STRAINS (INPUT)	-0.000194	-0.000242	0.000075	-0.000236	0.0	0.0
STRESSES (OUTPUT)	-702.	-915.	-79.	-314.	0.	0.
STRAINS (INPUT)	-0.000247	-0.000267	0.000143	0.0	0.0	0.0
STRESSES (OUTPUT)	-934.	-998.	0.	0.	0.	0.

PRINCIPAL STRESS RATIOS
$\sigma_1 ; \sigma_2 ; \sigma_3 = -10 ; -5 ; -2$

		EPS(1) SIG(1)	EPS(2) SIG(2)	EPS(3) SIG(3)	EPS(4) SIG(4)	EPS(5) SIG(5)	EPS(6) SIG(6)
STRAINS	(INPUT)	0.000003	-0.000272	-0.000090	0.000052	0.0	0.0
STRESSES	(OUTPUT)	-211.	-996.	-476.	74.	0.	0.
STRAINS	(INPUT)	-0.000006	-0.000545	-0.000174	0.000126	0.0	0.0
STRESSES	(OUTPUT)	-460.	-1999.	-940.	180.	0.	0.
STRAINS	(INPUT)	-0.000023	-0.000818	-0.000247	0.000220	0.0	0.0
STRESSES	(OUTPUT)	-731.	-2994.	-1370.	314.	0.	0.
STRAINS	(INPUT)	-0.000054	-0.001092	-0.000306	0.000336	0.0	0.0
STRESSES	(OUTPUT)	-1042.	-3998.	-1760.	479.	0.	0.
STRAINS	(INPUT)	-0.000105	-0.001370	-0.000339	0.000473	0.0	0.0
STRESSES	(OUTPUT)	-1422.	-5000.	-2077.	674.	0.	0.
STRAINS	(INPUT)	-0.000268	-0.001654	-0.000266	0.000632	0.0	0.0
STRESSES	(OUTPUT)	-2101.	-6001.	-2101.	900.	0.	0.
STRAINS	(INPUT)	-0.000471	-0.001950	-0.000149	0.000664	0.0	0.0
STRESSES	(OUTPUT)	-2999.	-7002.	-1993.	944.	0.	0.
STRAINS	(INPUT)	-0.000602	-0.002266	-0.000098	0.000675	0.0	0.0
STRESSES	(OUTPUT)	-3519.	-8001.	-2082.	958.	0.	0.
STRAINS	(INPUT)	-0.000722	-0.002611	-0.000043	0.000665	0.0	0.0
STRESSES	(OUTPUT)	-4107.	-8990.	-2124.	43.	0.	0.

PRINCIPAL STRESS RATIOS (cont'd)

$$\sigma_1 : \sigma_2 : \sigma_3 = -10; -5; -2$$

STRAINS (INPUT)	-0.000835	-0.005 13	0.000057	0.000670	0.0	0.	0.
STRESSES (OUTPUT)	-4689.	-9982.	-2295.	999.	0.0	0.	0.
STRAINS (INPUT)	-0.000941	-0.003453	0.000203	0.000660	0.0	0.	0.
STRESSES (OUTPUT)	-5259.	-10956.	-2410.	822.	0.0	0.	0.
STRAINS (INPUT)	-0.001034	-0.004061	0.000396	0.000624	0.0	0.	0.
STRESSES (OUTPUT)	-5795.	-11885.	-2525.	715.	0.0	0.	0.
STRAINS (INPUT)	-0.001117	-0.004704	0.000633	0.000550	0.0	0.	0.
STRESSES (OUTPUT)	-6296.	-12766.	-2640.	575.	0.0	0.	0.
STRAINS (INPUT)	-0.001190	-0.005371	0.000893	0.000426	0.0	0.	0.
STRESSES (OUTPUT)	-6745.	-13570.	-2754.	408.	0.0	0.	0.
STRAINS (INPUT)	-0.001258	-0.006043	0.001162	0.000244	0.0	0.	0.
STRESSES (OUTPUT)	-7136.	-14446.	-2882.	214.	0.0	0.	0.
STRAINS (INPUT)	-0.001321	-0.006721	0.001437	0.0	0.0	0.	0.
STRESSES (OUTPUT)	-7539.	-15397.	-3071.	0.	0.0	0.	0.
STRAINS (INPUT)	-0.001243	-0.007670	0.002143	-0.000340	0.0	0.	0.
STRESSES (OUTPUT)	-7855.	-16208.	-3223.	-233.	0.0	0.	0.
STRAINS (INPUT)	-0.001130	-0.008486	0.002744	-0.000790	0.0	0.	0.
STRESSES (OUTPUT)	-8047.	-16853.	-3369.	-477.	0.0	0.	0.
STRAINS (INPUT)	-0.000968	-0.009295	0.003322	-0.0	0.0	0.	.
STRESSES (OUTPUT)	-8183.	-17491.	-3532.				

PRINCIPAL STRESS RATIOS
$$\sigma_1;\sigma_2;\sigma_3 = -10;-2;0$$

		EPS(1) SIG(1)	EPS(2) SIG(2)	EPS(3) SIG(3)	EPS(4) SIG(4)
STRAINS	(INPUT)	-0.000146	-0.000007	0.000026	0.000018
STRESSES	(OUTPUT)	-494.	-98.	-3.	26.
STRAINS	(INPUT)	-0.000295	-0.000010	0.000057	0.000054
STRESSES	(OUTPUT)	-993.	-195.	-4.	76.
STRAINS	(INPUT)	-0.000442	-0.000013	0.000086	0.000108
STRESSES	(OUTPUT)	-1485.	-294.	-15.	150.
STRAINS	(INPUT)	-0.000597	-0.000014	0.000185	0.000202
STRESSES	(OUTPUT)	-1964.	-394.	-32.	250.
STRAINS	(INPUT)	-0.000761	-0.000013	0.000349	0.000350
STRESSES	(OUTPUT)	-2434.	-494.	-58.	375.
STRAINS	(INPUT)	-0.000920	-0.000013	0.000508	0.000534
STRESSES	(OUTPUT)	-2863.	-593.	-94.	518.
STRAINS	(INPUT)	-0.001075	-0.000016	0.000663	0.000758
STRESSES	(OUTPUT)	-3187.	-694.	-137.	665.
STRAINS	(INPUT)	-0.001233	-0.000019	0.000821	0.001036
STRESSES	(OUTPUT)	-3578.	-772.	-203.	851.
STRAINS	(INPUT)	-0.001410	-0.000021	0.000998	0.001390
STRESSES	(OUTPUT)	-3986.	-871.	-286.	1068.
STRAINS	(INPUT)	-0.001601	-0.000013	0.001189	0.001336
STRESSES	(OUTPUT)	-3546.	-943.	-318.	1062.
STRAINS	(INPUT)	-0.001810	0.000016	0.001398	0.002350
STRESSES	(OUTPUT)	-3126.	-873.	-334.	1022.
STRAINS	(INPUT)	-0.001881	0.000060	0.001469	0.002866
STRESSES	(OUTPUT)	-2906.	-909.	-397.	1073.
STRAINS	(INPUT)	-0.001937	0.000111	0.001525	0.003394
STRESSES	(OUTPUT)	-2744.	-828.	-458.	1121.
STRAINS	(INPUT)	-0.001865	0.000379	0.001453	0.003762
STRESSES	(OUTPUT)	-2610.	-790.	-532.	1178.

APPENDIX II

EXPERIMENTAL DATA

Included in this appendix are the experimental stress-strain curves that were not specifically presented elsewhere in this report. The stress-strain curves are shown in Figures 51 through 67. Also included in this appendix are Tables 8 through 10. These tables contain information used in Section V.
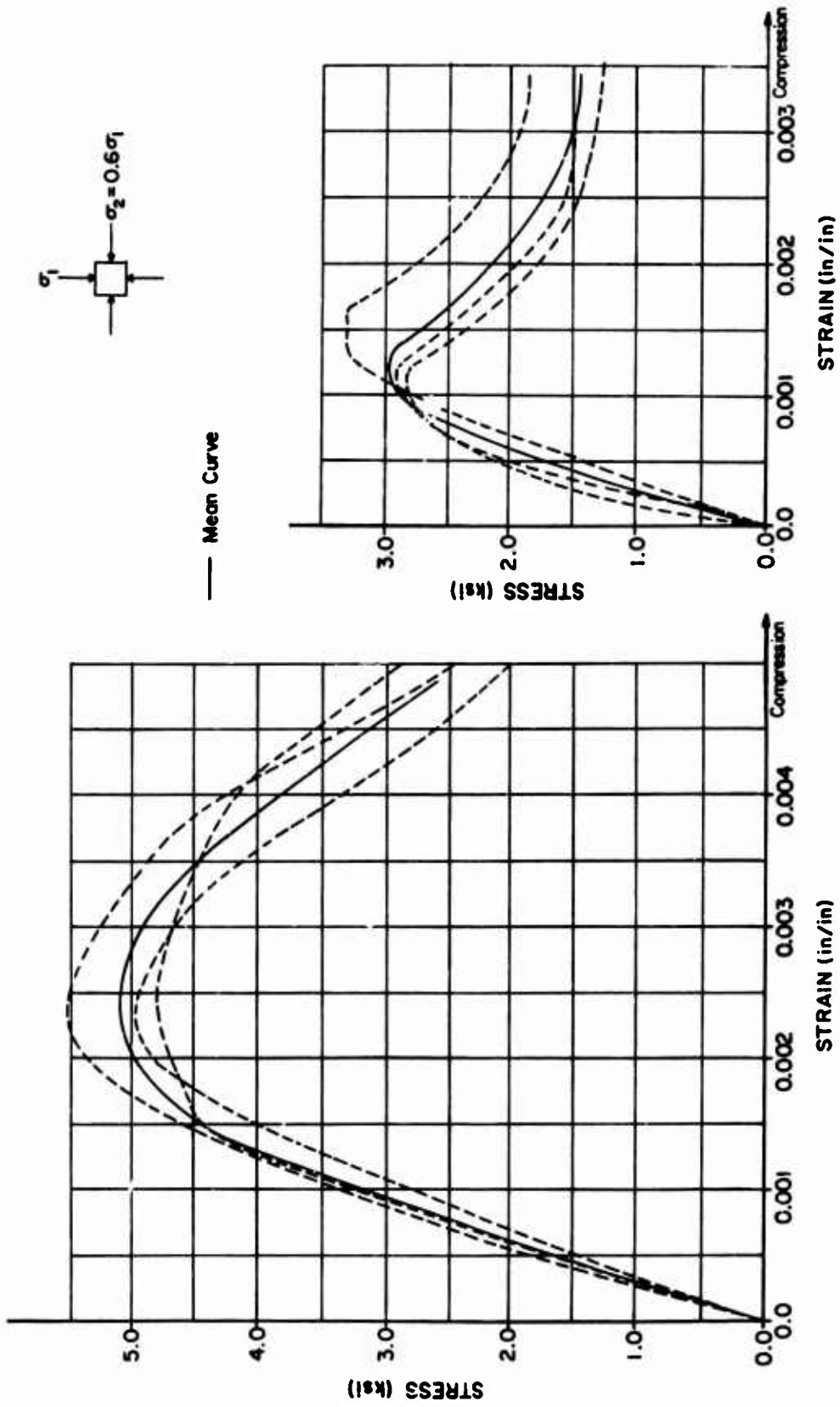
177

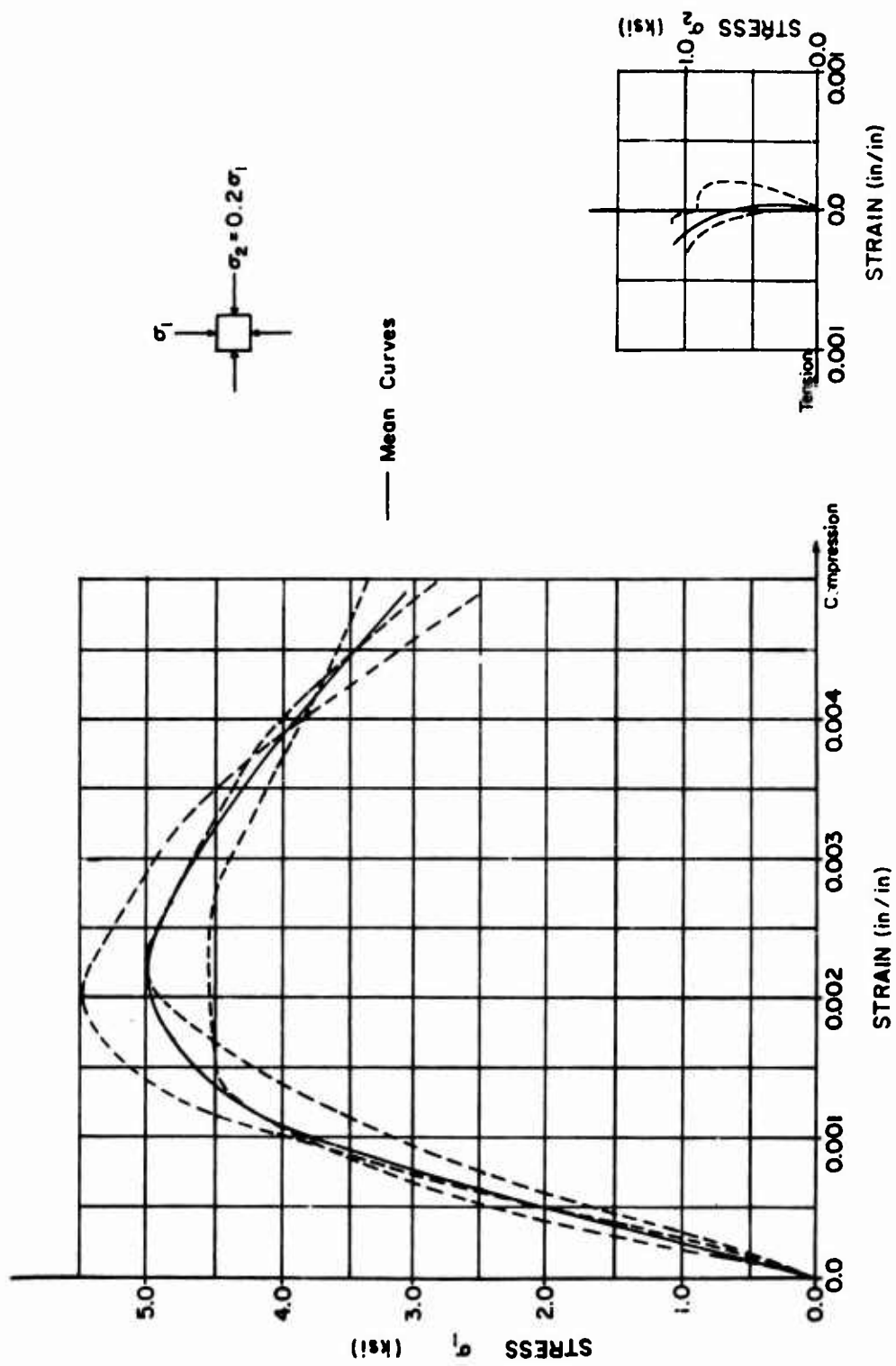FIGURE 51. BIAXIAL COMPRESSION-TENSION STRESS-STRAIN CURVES

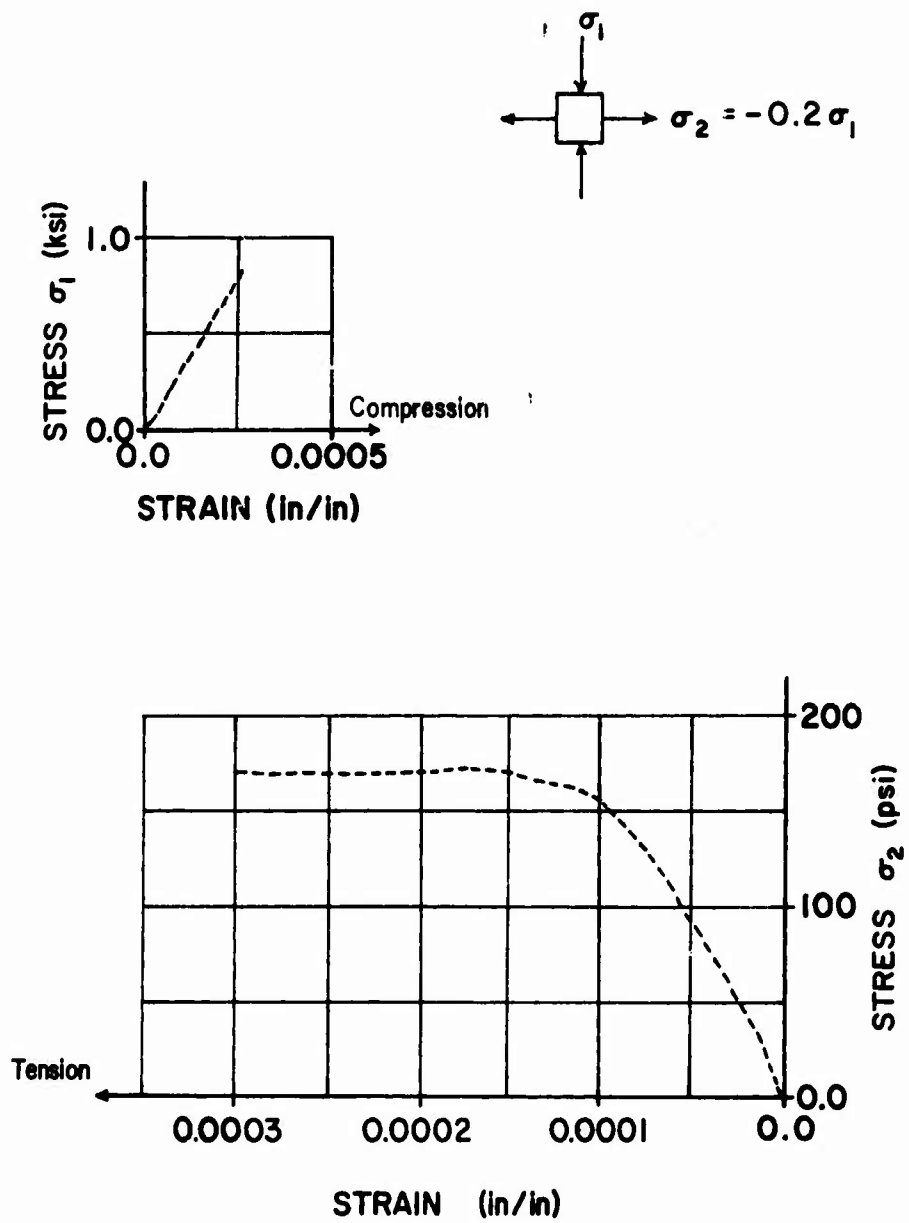FIGURE 52. BIAXIAL COMPRESSION-TENSION STRESS-STRAIN CURVES

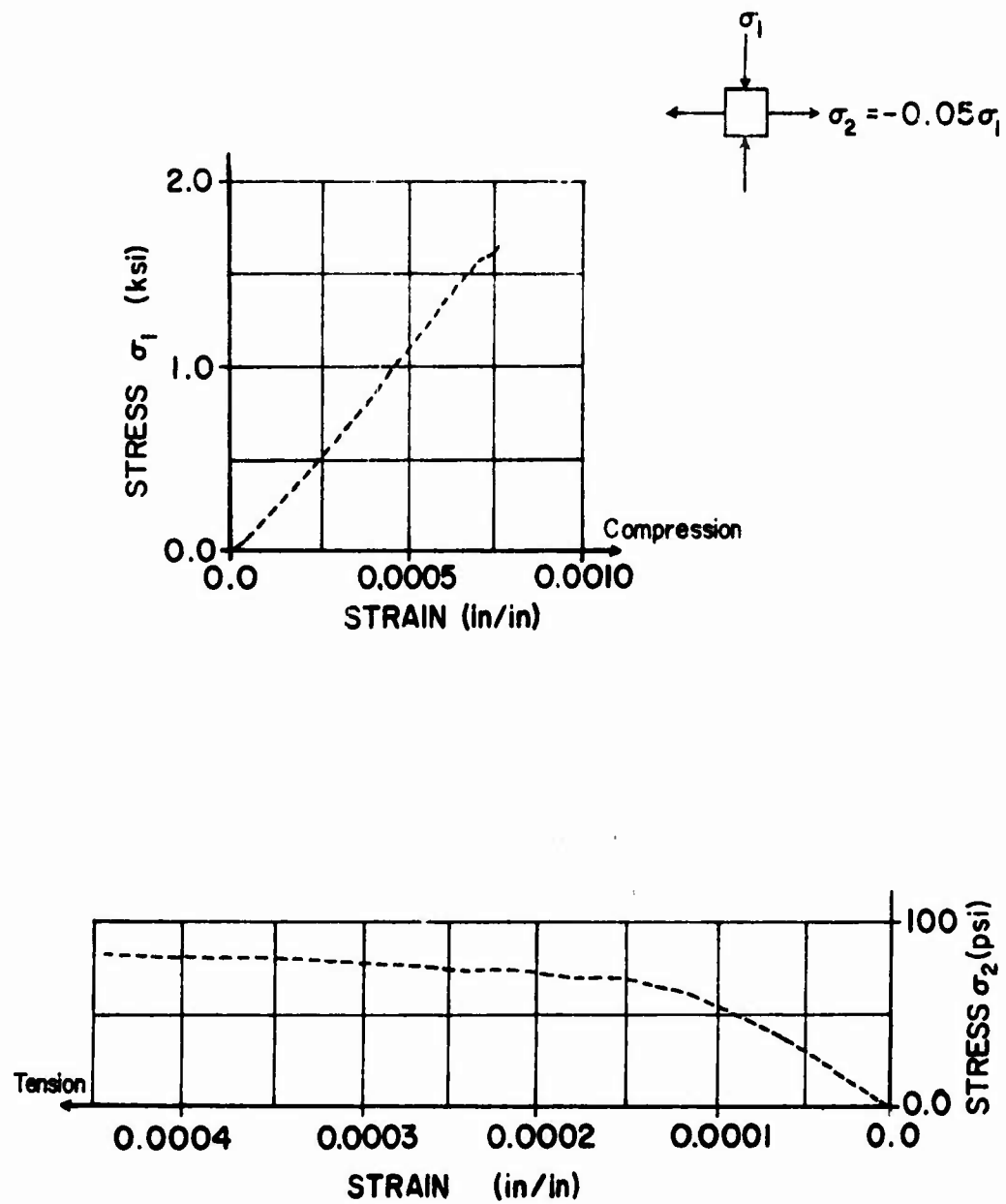Figure 53. Biaxial Compression-Tension Stress-Strain Curves

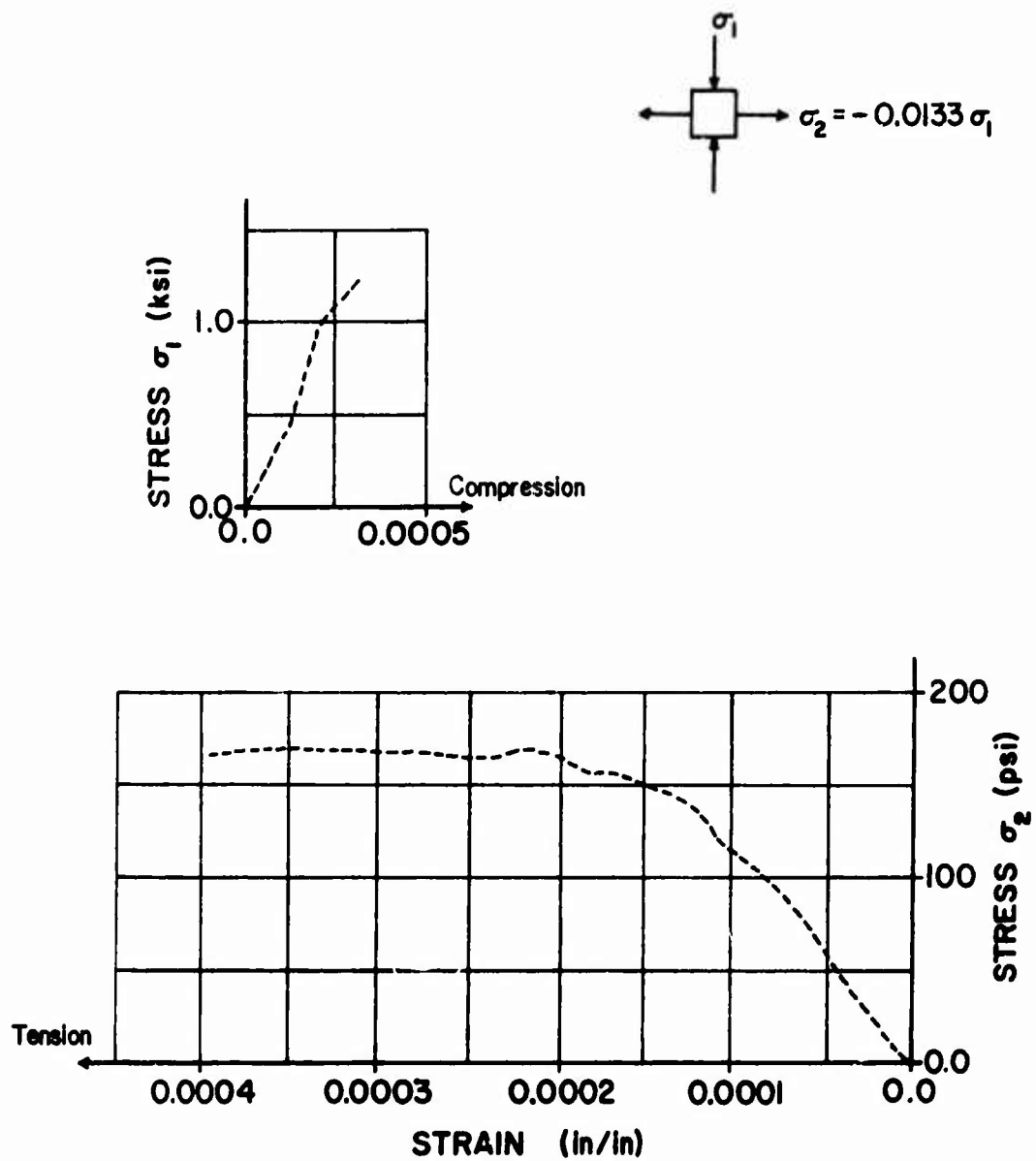Figure 54. Biaxial Compression-Tension Stress-Strain Curves

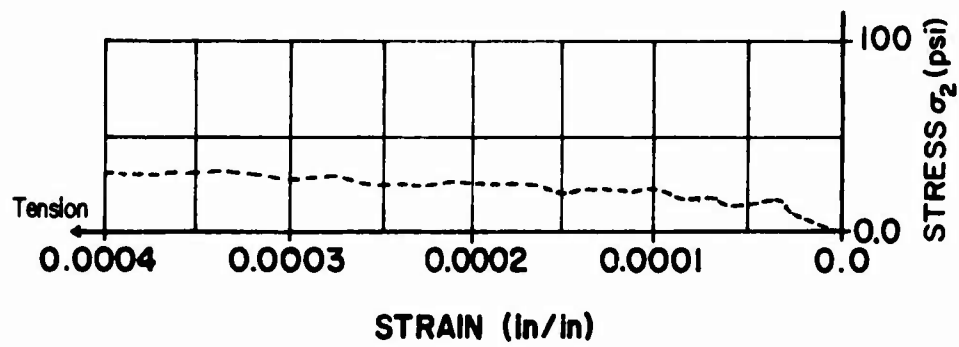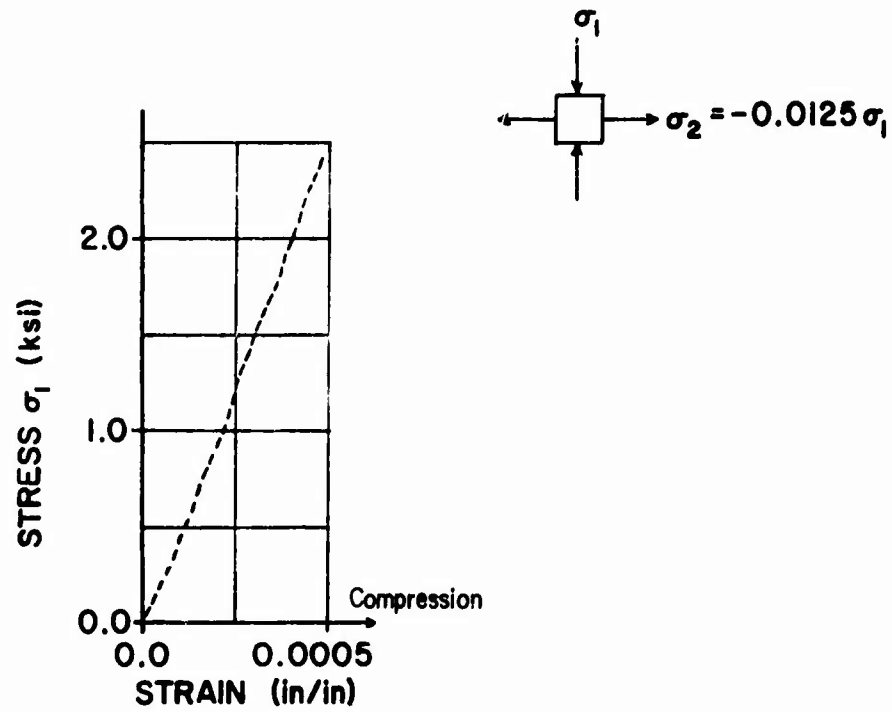Figure 55. Biaxial Compression-Tension Stress-Strain Curves

Figure 56. Biaxial Compression-Tension Stress-Strain Curves

FIGURE 57. TRIAXIAL COMPRESSION STRESS-STRAIN CURVES
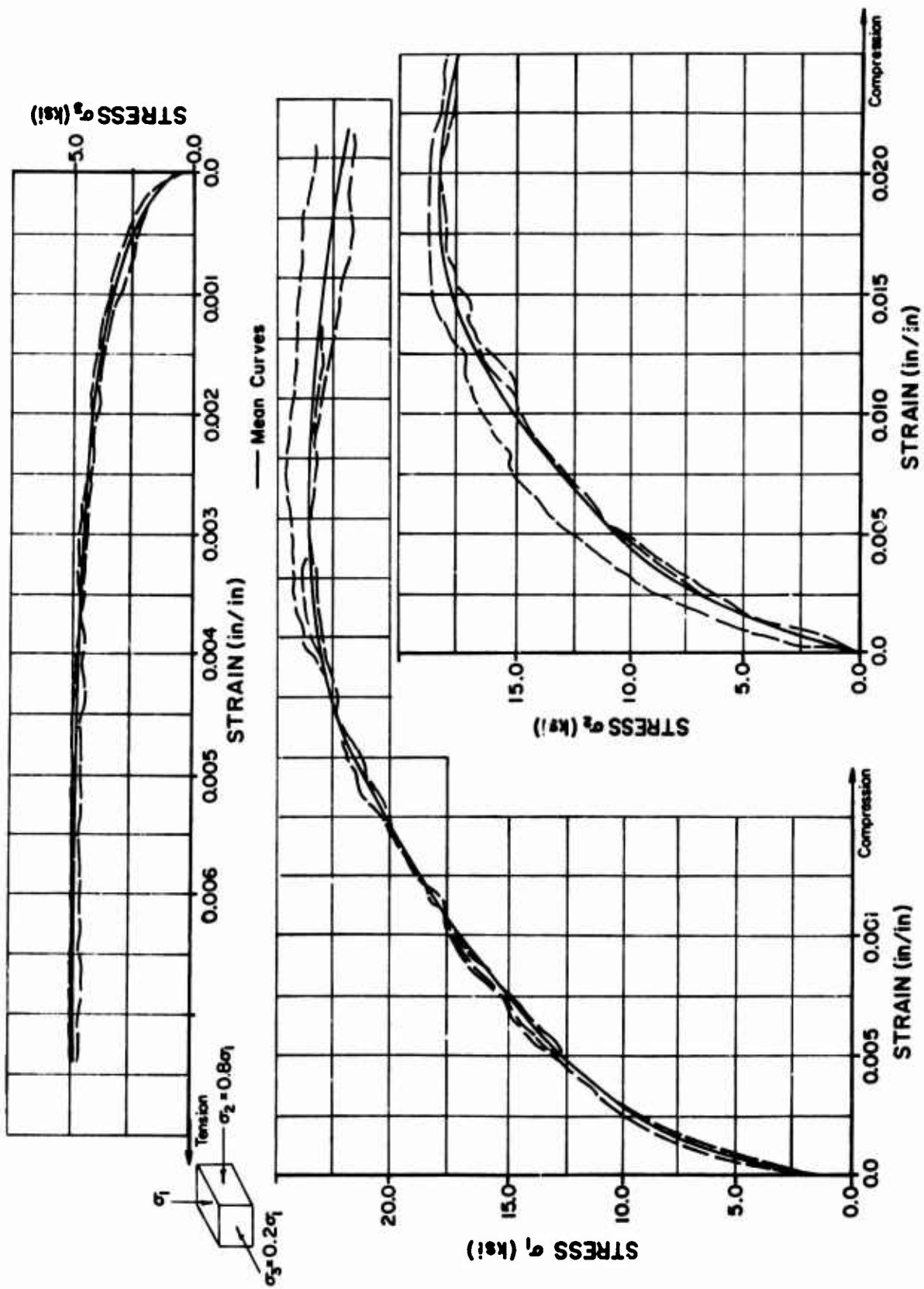
184

Figure 58. Triaxial Compression Stress-Strain Curves

185

FIGURE 59. TRIAXIAL COMPRESSION STRESS-STRAIN CURVES

186

Figure 60. Triaxial Compression Stress-Strain Curves

187
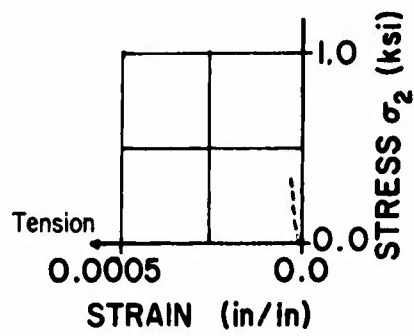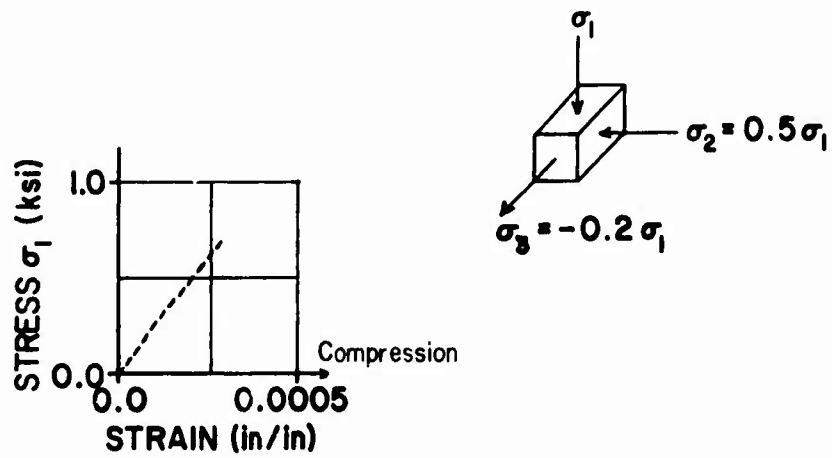
Figure 61. Triaxial Compression-Tension Stress-Strain Curves

188
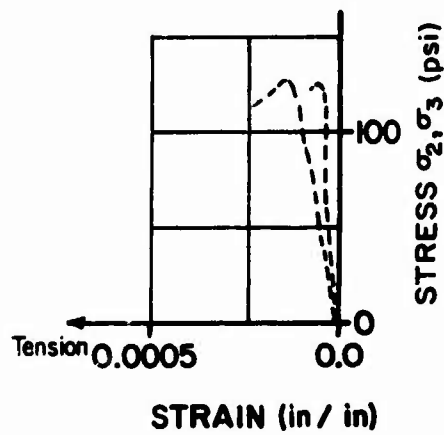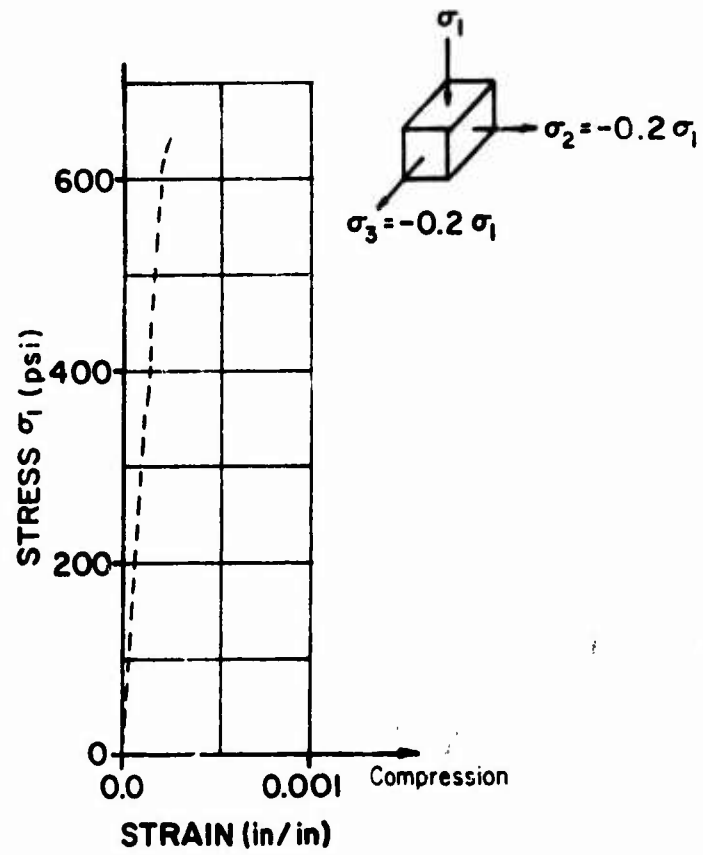
Figure 62.   Triaxial Compression-Tension Stress-Strain Curves
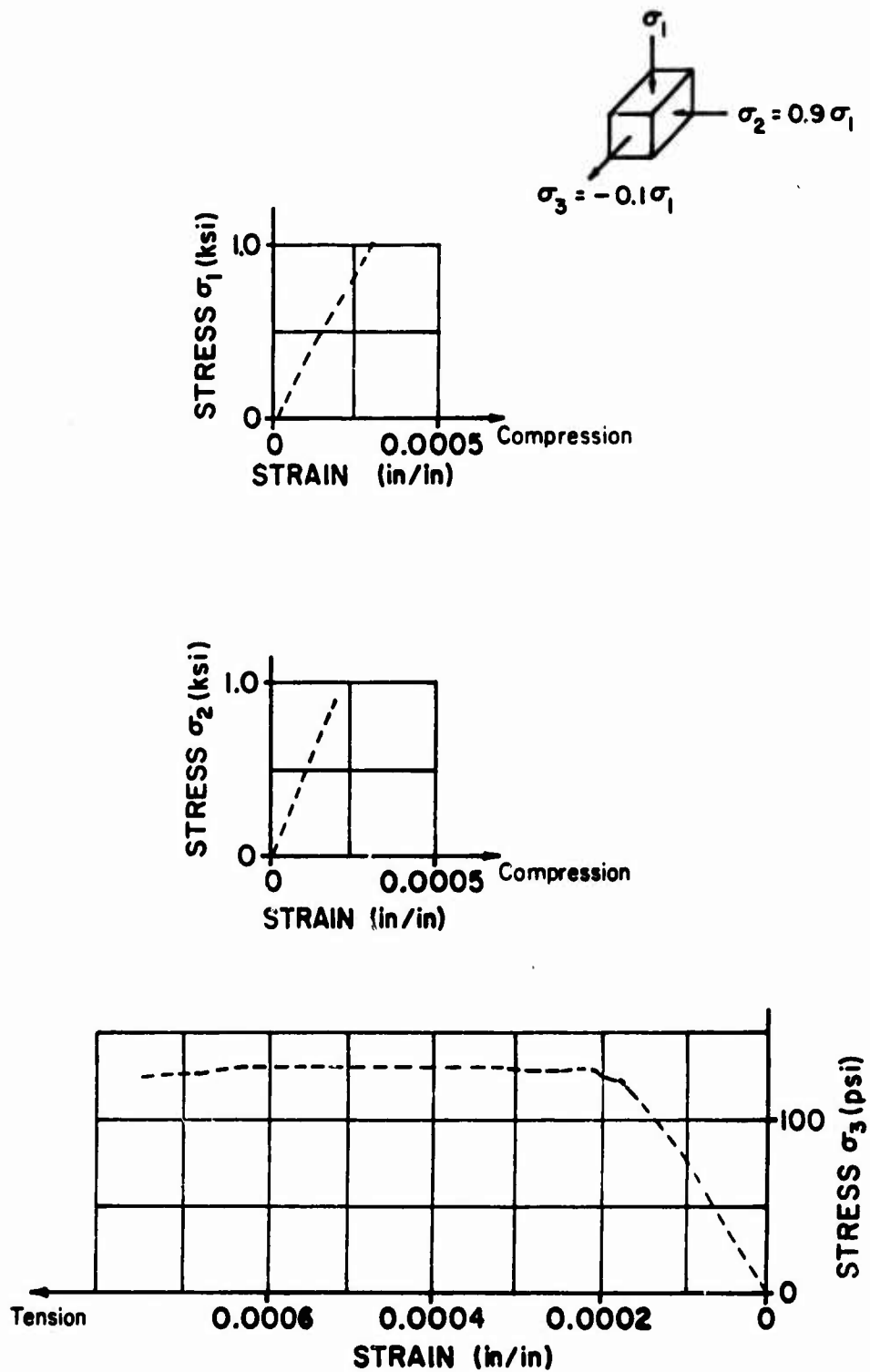
Figure 63. Triaxial Compression-Tension Stress-Strain Curves
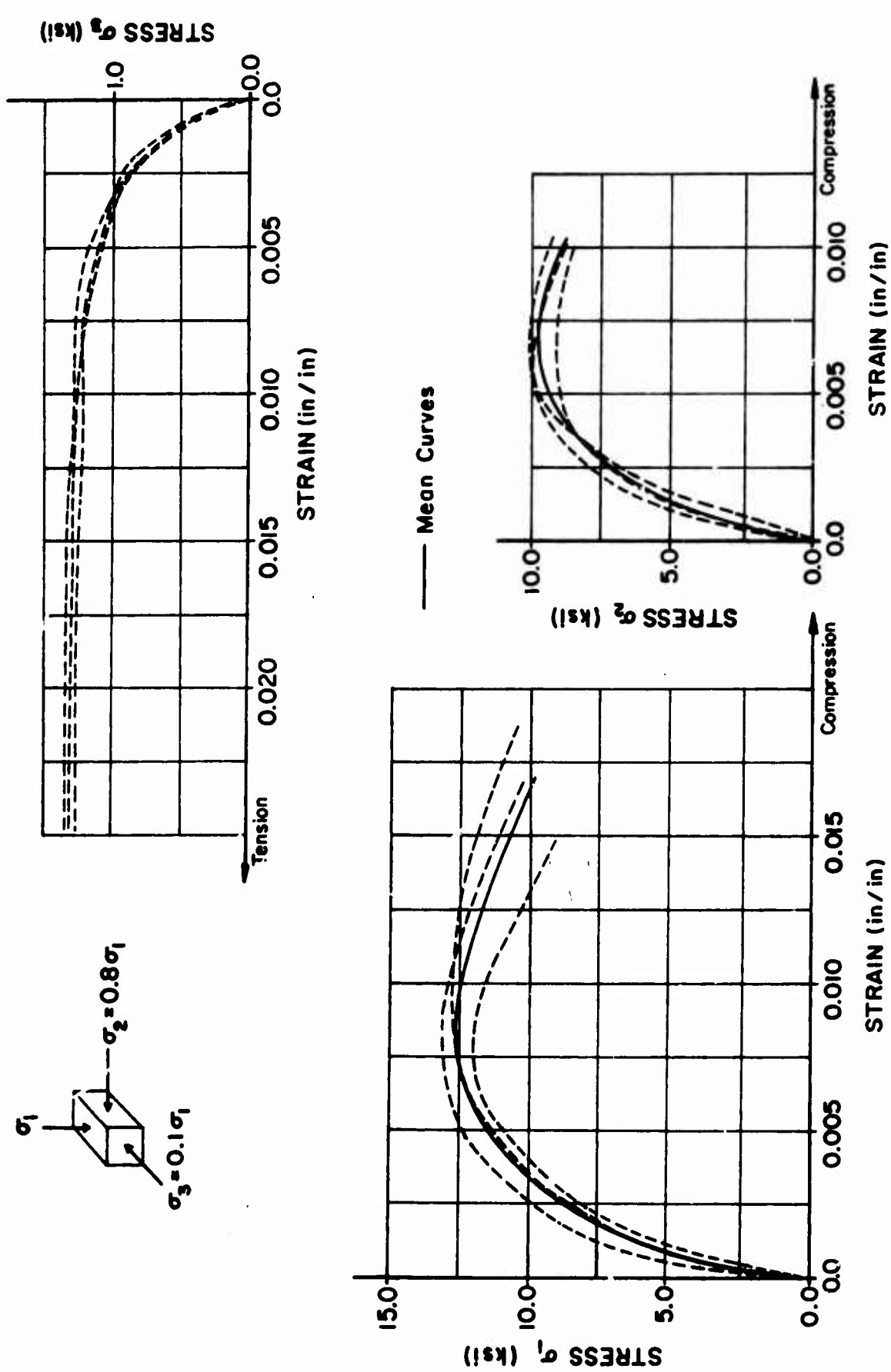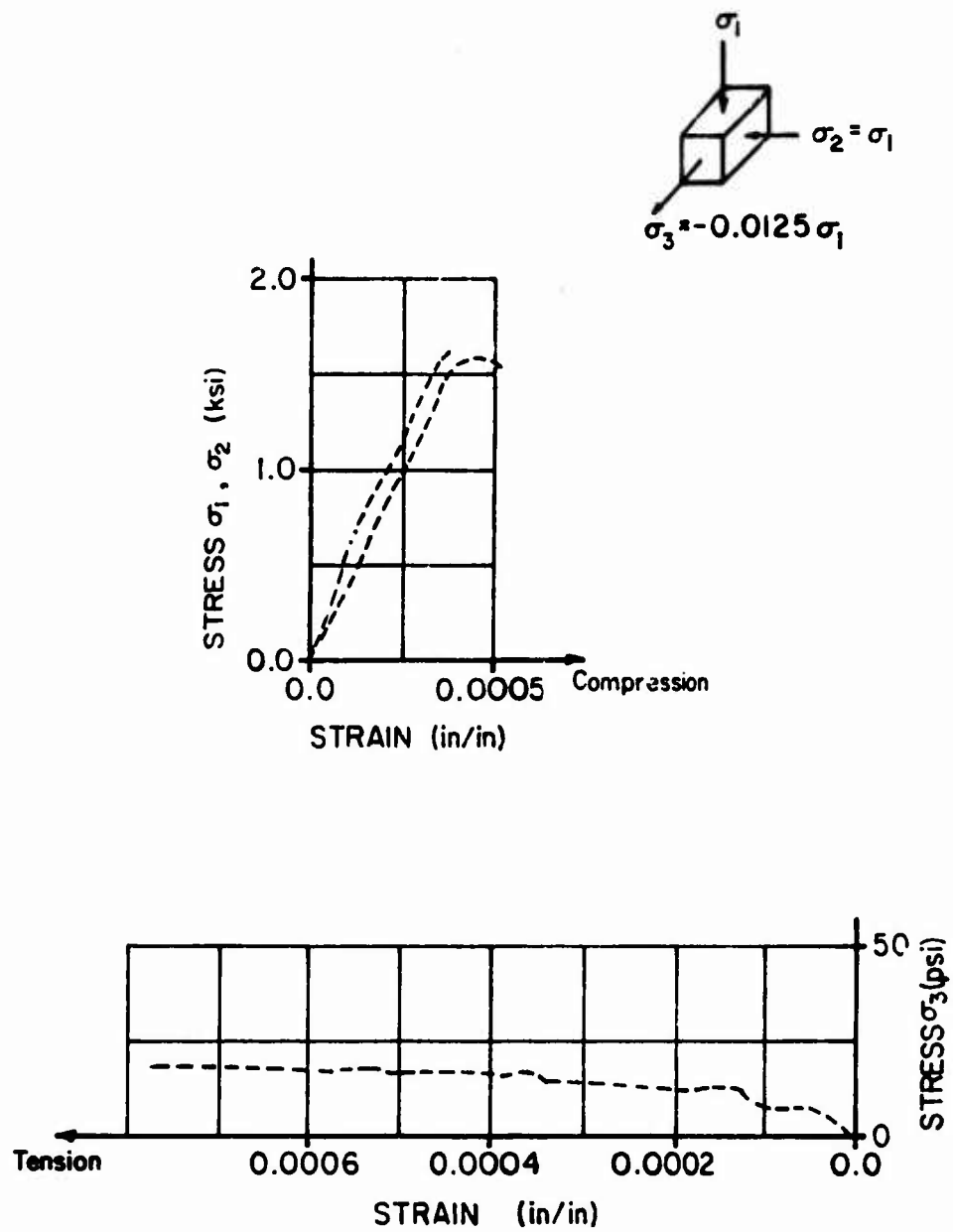
Figure 64. Triaxial Compression-Tension Stress-Strain Curves
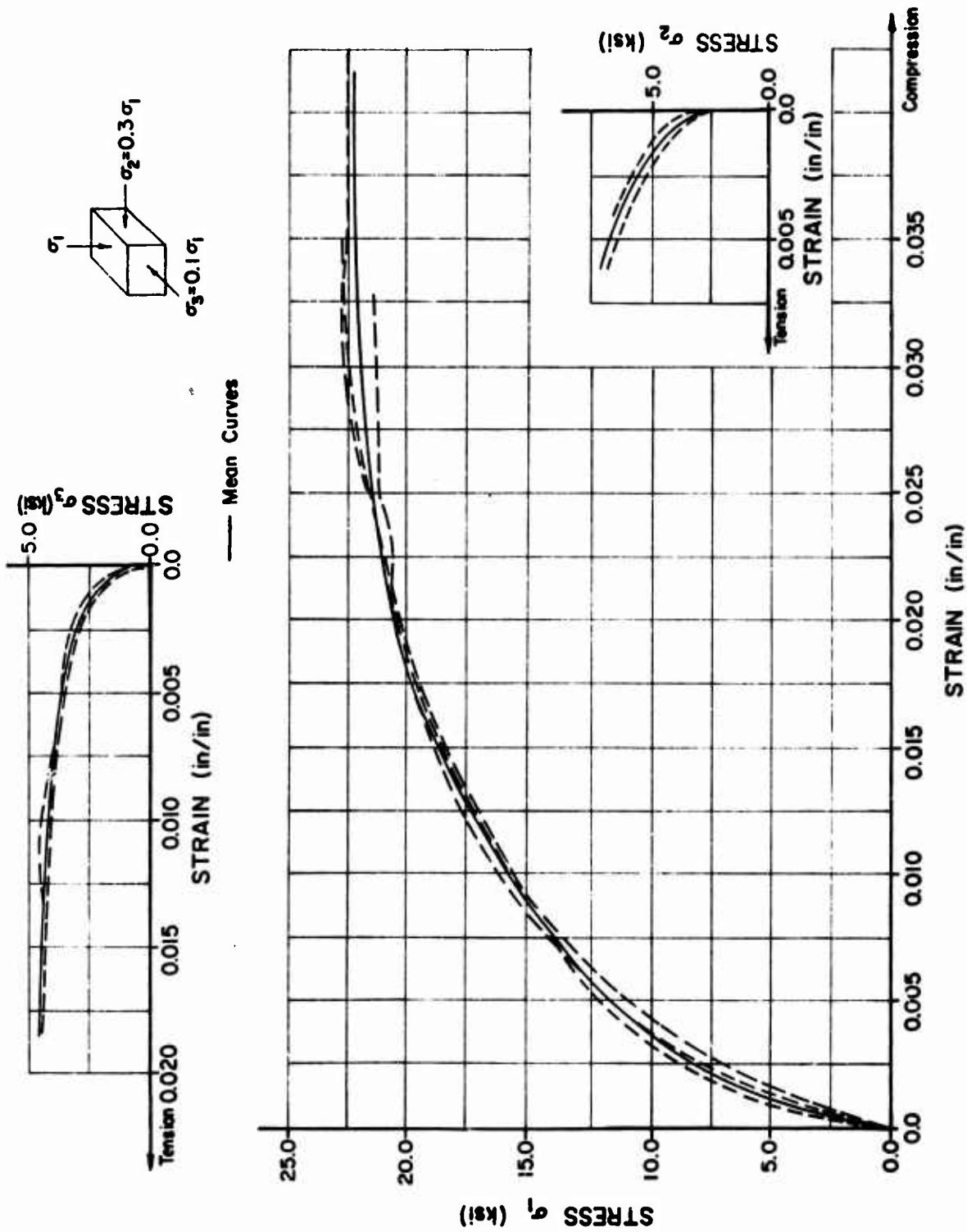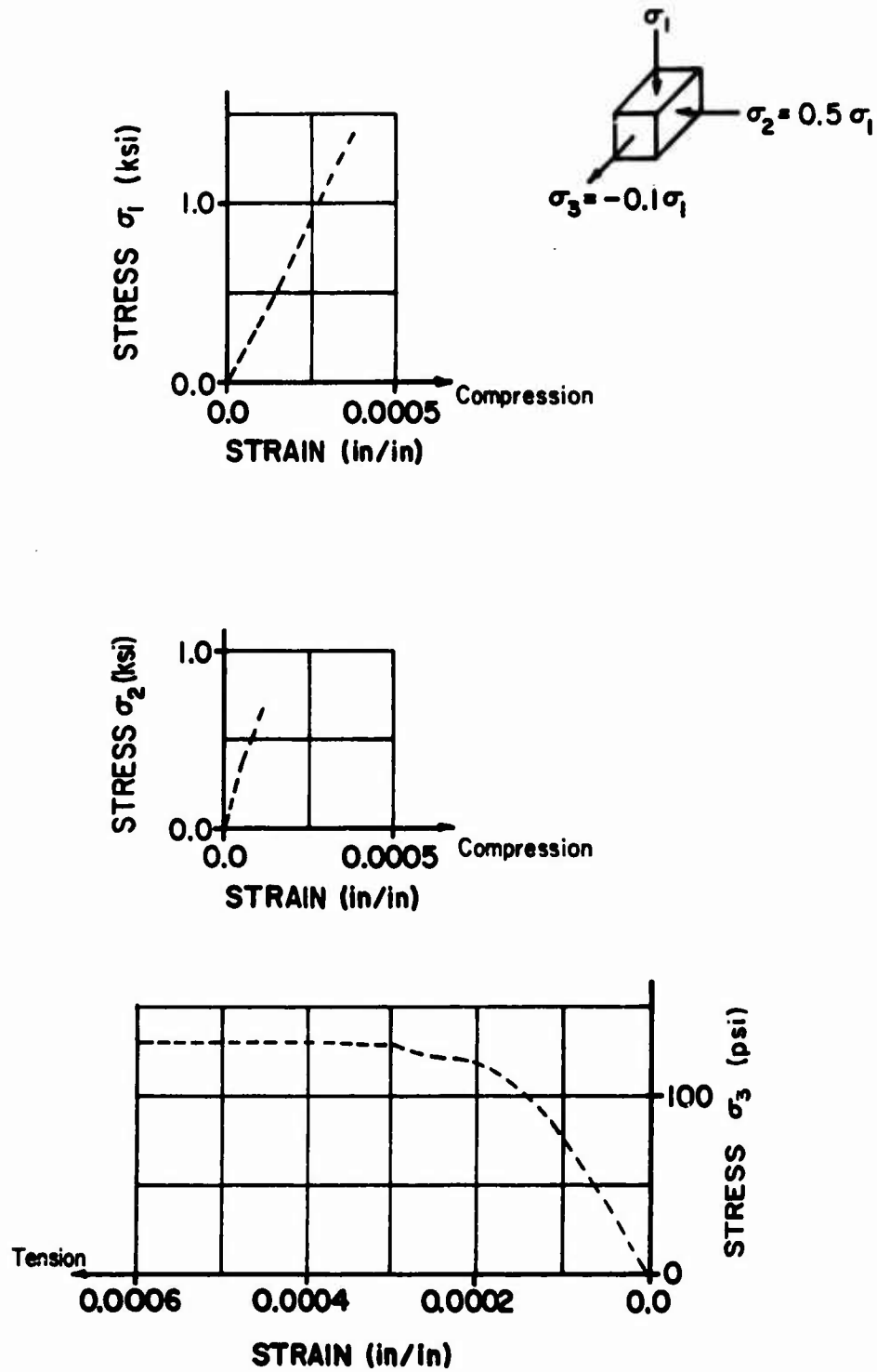
Figure 65.   Triaxial Compression-Tension Stress-Strain Curves
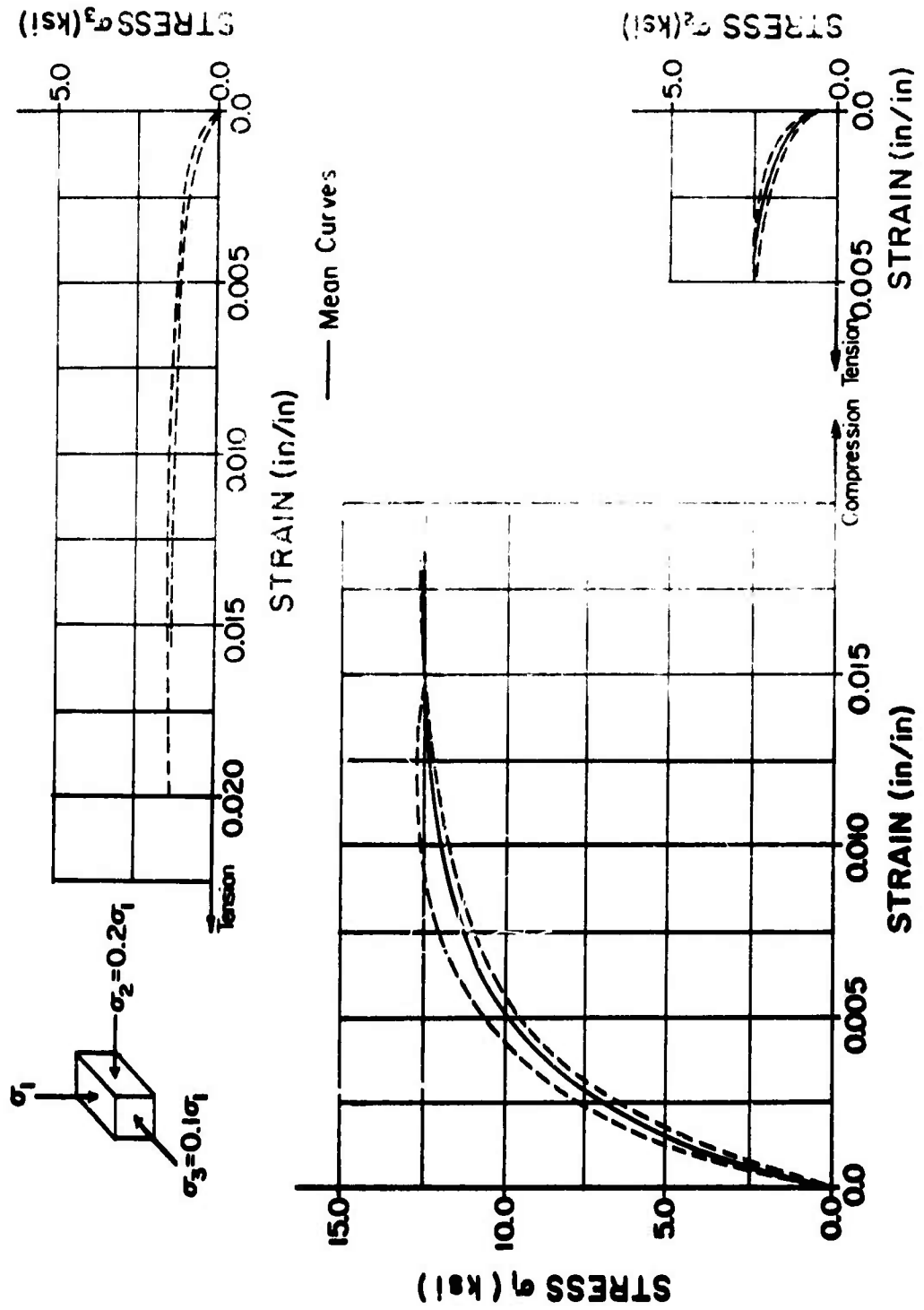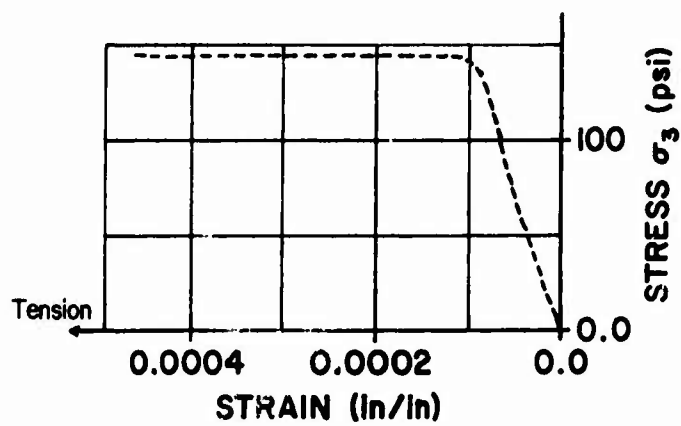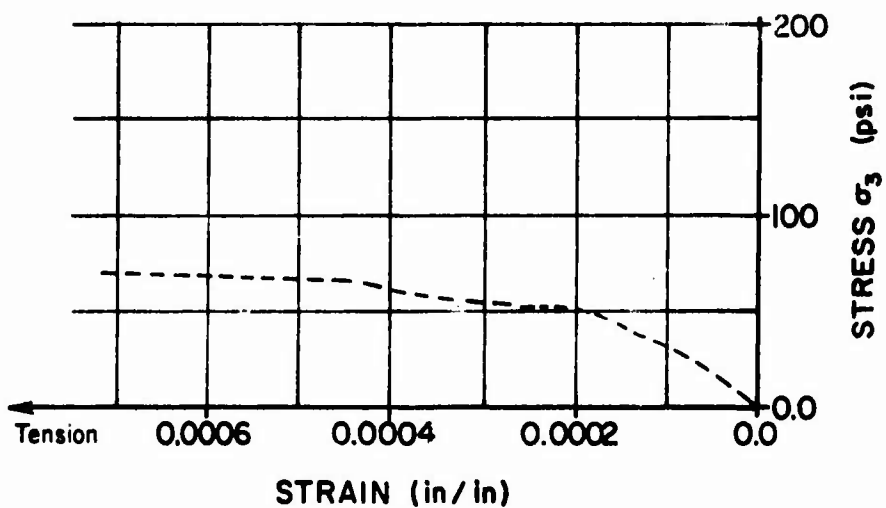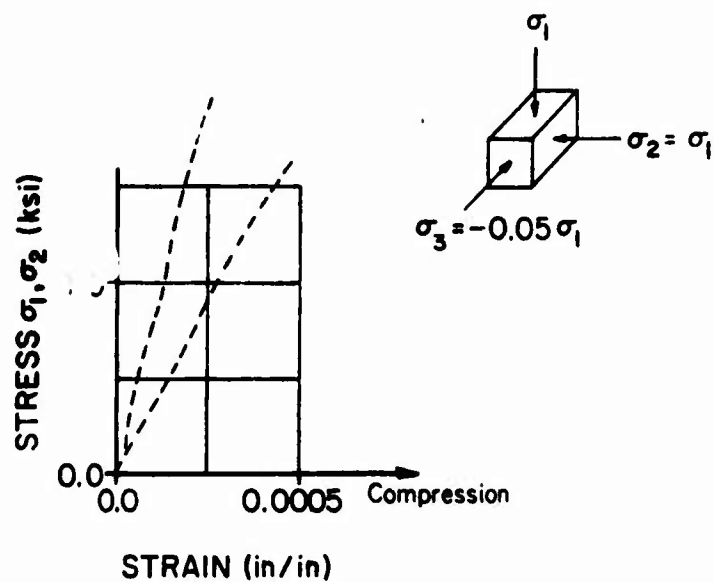
Figure 66.   Triaxial Compression-Tension Stress-Strain Curves
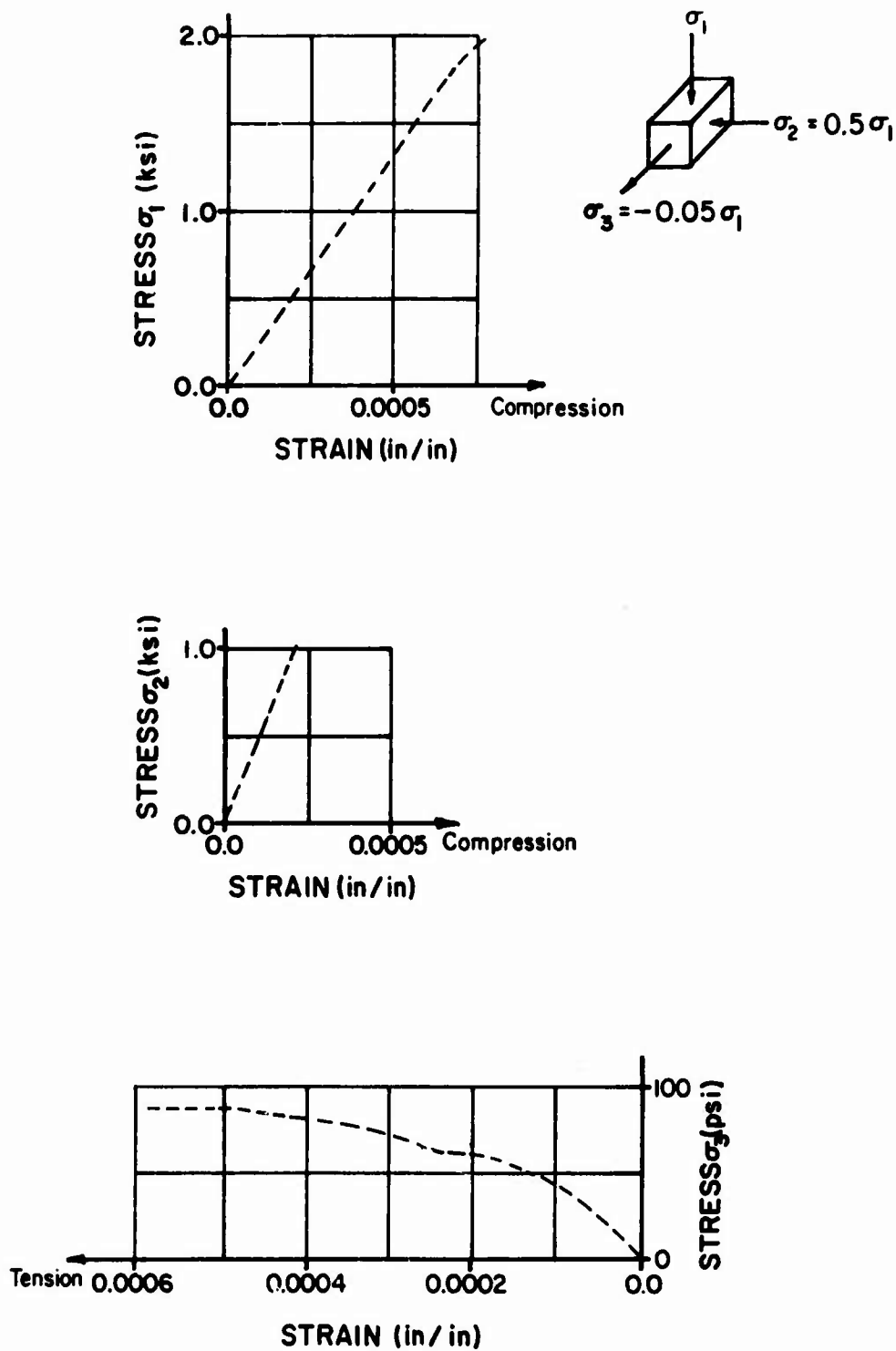
Figure 67. Triaxial Compression-Tension Stress-Strain Curves

194

TABLE 8

BIAXIAL COMPRESSION STRENGTH DATA

σ_1/σ_r	σ_2/σ_r	Nominal Ratio σ_1/σ_2	Average σ_1/σ_r	σ_2/σ_r
1.20	1.17			
1.14	1.13			
1.03	1.03			
1.07	1.05			
1.05	1.05	10/10	1.15	1.14
1.24	1.23			
1.26	1.24			
1.17	1.16			
1.14	1.14			
1.21	1.04			
1.21	0.98			
1.39	1.11			
1.36	1.06			
1.20	0.97			
1.20	0.96	10/8	1.25	1.00
1.39	1.11			
1.21	1.04			
1.23	0.97			
1.11	0.83			
1.24	0.93			
1.24	0.94			
1.29	0.81			
1.18	0.71	10/6	1.29	0.78
1.20	0.72			

TABLE 8 (Continued)

σ_1/σ_r	σ_2/σ_r	Nominal Ratio σ_1/σ_2	Average σ_1/σ_r	σ_2/σ_r
1.51	0.91			
1.36	0.80			
1.31	0.77	10/6	1.29	0.78
1.30	0.81			
1.21	0.71			
1.20	0.64			
1.31	0.66			
1.21	0.61	10/5	1.26	0.64
1.31	0.66			
1.33	0.52			
1.32	0.53			
1.33	0.52	10/4	1.33	0.53
1.35	0.53			
1.31	0.26			
1.30	0.26			
1.28	0.26			
1.33	0.25			
1.20	0.24			
1.33	0.27	10/2	1.29	0.28
1.45	0.29			
1.33	0.27			
1.25	0.24			
1.16	0.29			
1.19	0.31			
1.27	0.33			

TABLE 8 (Continued)

σ_1/σ_r	σ_2/σ_r	Nominal Ratio σ_1/σ_2	Average σ_1/σ_r	σ_2/σ_r
1.33	0.12			
1.18	0.12			
1.32	0.13			
1.31	0.14	10/1	1.29	0.13
1.40	0.16			
1.18	0.14			
1.27	0.07			
1.14	0.06	20/1	1.20	0.07
1.20	0.07			

197

TABLE 9

TRIAXIAL COMPRESSION DATA

Nominal Ratio σ_1-σ_2-σ_3	σ_1 (psi)	σ_2 (psi)	σ_3 (psi)	σ_1/σ_r	σ_2/σ_r	σ_3/σ_r	σ_2/σ_1	σ_3/σ_1
(10-1-1)	10,040	1,360	1,270	3.006	0.407	0.380	0.135	.120
	12,060	1,460	1,090	3.611	0.437	0.326	0.121	.090
	8,990	1,100	1,000	2.692	0.329	0.299	0.122	.111
(10-2-1)	12,500	2,600	1,500	3.750	0.780	0.450	0.208	.120
	12,200	2,500	1,400	3.660	0.750	0.420	0.205	.115
	12,900	2,560	1,350	3.870	0.770	0.405	0.198	.105
	13,000	2,700	1,300	2.997	0.622	0.300	0.207	.100
(10-3-1)	13,400	4,300	1,400	4.020	1.290	0.420	0.321	.104
	12,500	3,800	1,300	3.750	1.140	0.390	0.304	.104
	13,300	4,100	1,300	3.990	1.230	0.390	0.308	.098
(10-5-1)	13,700	7,000	1,370	3.159	1.614	0.316	0.511	.100
(10-8-1)	12,000	9,500	1,200	3.653	2.892	0.365	0.792	.100
	12,700	10,400	1,280	3.866	3.166	0.390	0.819	.101
	13,000	10,400	1,300	3.957	3.166	0.396	0.800	.100
	13,500	10,800	1,350	3.113	2.490	0.311	0.800	.100
(10-10-1)	10,500	10,500	1,050	3.000	3.000	0.300	1.000	.100
	10,500	10,500	1,050	3.000	3.000	0.300	1.000	.100
	12,500	12,400	1,250	2.880	2.870	0.288	0.996	.100
	10,000	10,000	1,000	3.164	3.164	0.316	1.000	.100
	10,600	10,380	1,010	2.900	2.840	0.275	0.979	.095
	9,420	9,350	780	2.570	2.560	0.213	0.996	.083
	11,600	11,500	1,200	2.670	2.660	0.277	0.991	.103

TABLE 9 (Continued)

Nominal Ratio σ_1-σ_2-σ_3	σ_1 (psi)	σ_2 (psi)	σ_3 (psi)	σ_1/σ_r	σ_2/σ_r	σ_3/σ_r	σ_2/σ_1	σ_3/σ_1
(10-2-2)	18,080	4,150	3,960	5.413	1.243	1.186	0.230	.219
	18,300	4,250	3,870	5.479	1.270	1.159	0.232	.211
	19,700	4,120	4,010	5.898	1.234	1.201	0.209	.203
	20,800	4,150	4,150	6.580	1.313	1.316	0.199	.200
(10-3-2)	21,400	6,750	4,500	6.421	2.025	1.350	0.315	.210
	22,500	7,000	4,500	6.751	2.100	1.350	0.311	.200
	22,500	7,000	4,500	6.751	2.100	1.350	0.311	.200
(10-5-2)	24,000	12,000	4,800	7.306	3.653	1.461	0.500	.200
	20,400	10,000	4,000	6.210	3.044	1.218	0.490	.196
	23,200	11,600	4,500	7.062	3.531	1.370	0.500	.194
	27,300	13,700	5,450	8.637	4.334	1.727	0.502	.200
(10-8-2)	24,500	19,700	4,800	7.458	5.997	1.461	0.804	.196
	23,500	19,000	4,700	7.154	5.784	1.431	0.808	.200
	23,600	19,000	4,700	7.184	5.784	1.431	0.805	.199
	25,200	20,500	5,040	7.972	6.485	1.594	0.813	.200
(10-10-2)	18,180	17,730	3,680	5.443	5.308	1.102	0.975	.202
	18,060	17,500	3,380	5.392	5.240	1.132	0.972	.210
	19,060	18,590	4,410	5.707	5.566	1.240	0.975	.217
	20,500	20,000	4,000	5.857	5.714	1.143	0.976	.195
	19,300	19,000	3,800	5.514	5.529	1.086	0.985	.197
	21,700	21,700	4,500	6.200	6.200	1.286	1.000	.207
	20,300	20,300	4,000	5.800	5.800	1.143	1.000	.197

199

TABLE 9 (Continued)

Nominal Ratio σ_1-σ_2-σ_3	σ_1 (psi)	σ_2 (psi)	σ_3 (psi)	σ_1/σ_r	σ_2/σ_r	σ_3/σ_r	σ_2/σ_1	σ_3/σ_1
	20,450	20,250	4,075	5.840	5.780	1.162	0.990	.199
	22,200	22,000	4,450	7.023	6.960	1.408	0.991	.200
	20,200	19,600	4,350	5.510	5.350	1.185	0.971	.215
(10-10-2)	22,900	22,500	4,665	5.280	5.187	0.999	0.982	.193
	22,500	22,500	4,500	5.190	5.190	1.048	1.000	.202
	23,300	23,300	4,680	5.370	5.370	1.079	1.000	.201
	10,620	4,410	960	3.180	1.320	0.287	0.415	.090
	10,800	4,120	1,110	3.234	1.234	0.332	0.381	.103
(10-4-1)	9,010	3,600	1,030	2.698	1.078	0.308	0.400	.114
	10,070	4,452	890	2.750	1.220	0.245	0.443	.089
	6,800	6,800	340	2.151	2.151	0.107	1.000	.050
(10-10-$\frac{1}{2}$)	9,250	9,250	500	2.133	2.133	0.115	1.000	.054
	8,800	8,700	500	2.029	2.006	0.115	0.989	.057
	13,300	13,300	2,000	4.208	4.208	0.631	1.000	.150
	17,550	17,500	2,460	4.790	4.780	0.671	1.000	.140
(10-10-$1\frac{1}{2}$)	15,400	15,400	2,300	3.551	3.551	0.530	1.000	.149
	16,000	15,800	2,380	3.689	3.643	0.549	0.987	.149

TABLE 10

TRIAXIAL TENSION-COMPRESSION DATA

$\dfrac{\sigma_1}{\lvert\sigma_r\rvert}$	$\dfrac{\sigma_2}{\lvert\sigma_r\rvert}$	$\dfrac{\sigma_3}{\lvert\sigma_r\rvert}$	$\dfrac{\lvert\sigma_3\rvert}{\lvert\sigma_1\rvert}$
-0.664	-0.614	+0.008	0.012
-0.924	0	+0.013	0.014
-0.759	0	+0.013	0.017
-0.498	-0.498	+0.012	0.025
-0.498	+0.020	+0.016	0.033
-0.465	-0.465	+0.026	0.057
-0.579	-0.299	+0.029	0.050
-0.616	0	+0.031	0.050
-0.661	0	+0.032	0.049
-0.465	-0.232	+0.042	0.091
-0.332	-0.305	+0.043	0.130
-0.462	0	+0.063	0.136
-0.265	-0.265	+0.050	0.187
-0.282	-0.282	+0.056	0.200
-0.133	-0.133	+0.027	0.200
-0.232	-0.116	+0.048	0.207
-0.279	0	+0.056	0.200
-0.289	0	+0.057	0.200
-0.240	+0.048	+0.048	0.200
-0.204	0	+0.081	0.396

(-) Compressive

(+) Tensile

REFERENCES

1. Krishnaswamy, K. T., "Strength and Microcracking of Plain Concrete Under Triaxial Compression," ACI JOURNAL Proceedings, V. 65, No. 10, Oct. 1958, pp. 856-862.

2. Gardner, Noel J., "Triaxial Behavior of Concrete," ACI JOURNAL, Proceedings, V. 66, No. 2, Feb. 1969, pp. 136-146.

3. Robinson, George S., "Behavior of Concrete in Biaxial Compression," Journal of the Structural Division, ASCE, Vol. 93, No. ST1, Proc. Paper 5090, Feb. 1967, pp. 71-86.

4. Kupfer, Helmut; Hilsdorf, Hubert K.; and Rusch, Hubert, "Behavior of Concrete Under Biaxial Stresses," ACI JOURNAL, Proceedings, V. 66, No. 8, Aug. 1969, pp. 656-666.

5. Iyengar, K. T. Sundara Raja; Chandrashekhara, K.; and Krishnaswamy, K. T., "Strength of Concrete Under Biaxial Compression," ACI JOURNAL, V. 62, No. 2, Feb. 1965, pp. 239-250.

6. Smith, G. M., "Failure of Concrete Under Combined Tensile and Compressive Stresses," ACI JOURNAL, Proceedings, V. 50, No. 2, Oct. 1953, pp. 137-140.

7. Bresler, B. and Pister, K. S., "Strength of Concrete Under Combined Stresses," ACI JOURNAL, Proceedings, V. 30, No. 3, Sept. 1958, pp. 321-345.

8. McHenry, D. and Karni, J., "Strength of Concrete Under Combined Tensile and Compressive Stress," ACI JOURNAL, Proceedings, V. 29, No. 10, April 1958, pp. 829-839.

9. Akroyd, T. N. W., "Concrete Under Triaxial Stress," Magazine of Concrete Research, V. 13, No. 39, Nov. 1961, pp. 111-118.

10. Goode, C. D. and Helmy, M. A., "The Strength of Concrete Under Combined Shear and Direct Stress," Magazine of Concrete Research, V. 19, No. 59, June 1957, pp. 105-112.

11. Bellamy, C. J., "Strength of Concrete Under Combined Stresses," ACI JOURNAL, Proceedings, V. 58, No. 4, Oct. 1961, pp. 367-381.

12. Krishnaswamy, K. T., "Strength of Concrete Under Combined Tensile-Compressive Stresses," MATERIALS AND STRUCTURES RESEARCH AND TESTING (Paris), V. 2, No. 9, May-June 1969, pp. 187-194.

REFERENCES (cont'd)

13. Balmer, G. G., "Shearing Strength of Concrete Under High Triaxial Stress," Laboratory Report No. SP-23, U.S. Department of the Interior, Bureau of Reclamation, Oct. 1949.

14. Campbell-Allen, D., "Strength of Concrete Under Combined Stresses," Construction Review, Sydney, Australia, V. 35, No. 4, April 1962. pp. 29-37.

15. Richart, F. E. and Brandtzaeg, A. and Brown, R. L., "A study of the Failure of Concrete Under Combined Compressive Stresses," Engineering Experiment Station Bulletin No. 185, University of Illinois, 1928.

16. Glucklich, J., "Fracture of Plain Concrete," Journal of the Engineering Mechanics Division, ASCE, V. 89, No. #M6, Dec. 1963, pp. 127-137.

17. Reeves, J. S., "The Strength of Concrete Under Combined Direct and Shear Stresses," London, Cement and Concrete Association, Nov. 1962, pp. 10, Technical Report TRA/365.

18. Tsuboi, Y. and Suenaga, Y., "Experimental Study on Failure of Plain Concrete Under Combined Stresses," Part 3, Transaction of the Architectural Institute of Japan, No. 64, Feb. 1960, pp. 25-36.

19. Goldberg, J. E. and Richard, R. M., "Analysis of Nonlinear Structures," Journal of the Structural Division, ASCE, V. 89, No. ST4, Proc. Paper 3604, August 1963, pp. 333-351.

20. Laursen, Harold I., Matrix Analysis of Structures, McGraw-Hill Book Company, Inc., New York, N. Y., 1966.

21. Mill, L. L. and Zimmerman, R. M., "Compressive Strength of Plain Concrete Under Multiaxial Loading Conditions," ACI JOURNAL, Proceedings, V. 67, No. 10, Oct. 1970, pp. 802-807.

22. Rosenthal, Israel and Glucklich, Joseph, "Strength of Plain Concrete Under Biaxial Stress," ACI JOURNAL, Proceedings, V. 67, No. 11, Nov. 1970, pp. 903-914.

23. Anson, M., "An Investigation into a Hypothetical Deformation and Failure Mechanism for Concrete," MAGAZINE OF CONCRETE RESEARCH, V. 16, No. 47, June 1964, pp. 73-82.

24. Levy, H. and Boggott, E. A., Numerical Solutions of Differential Equations, Dover Publications, Inc., New York, N. Y., 1950.

REFERENCES (cont'd)

25. Mills, L. L., "A Study of the Strength of Concrete Under Combined Compressive Loads," Ph.D. Thesis, New Mexico State University, Dec. 1967.

26. Vile, Gerald W. D., "The Strength of Concrete Under Short-Term Static Biaxial Stress," International Conference on the Structure of Concrete, Paper F2, Sept. 1965.

27. Weigler, H. and Becker, G., "Investigation into Strength and Deformation Properties of Concrete Subjected to Biaxial Stresses," Proceedings, V. 157, Deutscher Ausschuss fur Stahlbeton, Berlin, 1963.

28. Chinn, J. and Zimmerman, R., "Behavior of Plain Concrete Under Various High Triaxial Compression Loading Conditions," AIR FORCE WEAPONS LABORATORY, Technical Report No. WL-TR-64-163, Kirtland AFB, New Mexico, August 1965.

29. Zimmerman, R. M., "The Effects of Various Types of Lateral Restraint on the Triaxial Behavior of Plain Concrete," Doctoral Thesis, University of Colorado, 1965.

30. Butters, S. W. and Green, S. J., "Concrete Cube Test Specimens," AIR FORCE WEAPONS LABORATORY, Kirtland AFB, New Mexico (soon to be published).

31. Ash, John E., "Bleeding in Concrete-A Microscopic Study," ACI JOURNAL, Proceedings, V. 69, No. 4, Apr. 1972, pp. 209-211.

32. Buyukozturk, Oral; Nilson, Arthur H.; and Slate, Floyd O.; "Stress-Strain Response and Fracture of a Concrete Model in Biaxial Loading," ACI JOURNAL, Proceedings, V. 68, No. 8, Aug. 1971, pp. 590-599.